AEDC-TR-74-76

ARCHIVE COPY
DO NOT LOAN

cy.1

AN INVESTIGATION OF THREE-DIMENSIONAL WALL INTERFERENCE IN A VARIABLE POROSITY TRANSONIC WIND TUNNEL

T. W. Binion, Jr.
ARO, Inc.

PROPULSION WIND TUNNEL FACILITY
ARNOLD ENGINEERING DEVELOPMENT CENTER
AIR FORCE SYSTEMS COMMAND
ARNOLD AIR FORCE STATION, TENNESSEE 37389

October 1974

Final Report for Period March 5 – July 5, 1973

Approved for public release; distribution unlimited.

AEDC TECHNICAL LIBRARY
5 0720 00033 7313

Property of U. S. Air Force
AEDC LIBRARY
F40600-75-C-0001

Prepared for

DIRECTORATE OF TECHNOLOGY (DY)
ARNOLD ENGINEERING DEVELOPMENT CENTER
ARNOLD AIR FORCE STATION, TENNESSEE 37389

NOTICES

When U. S. Government drawings specifications, or other data are used for any purpose other than a definitely related Government procurement operation, the Government thereby incurs no responsibility nor any obligation whatsoever, and the fact that the Government may have formulated, furnished, or in any way supplied the said drawings, specifications, or other data, is not to be regarded by implication or otherwise, or in any manner licensing the holder or any other person or corporation, or conveying any rights or permission to manufacture, use, or sell any patented invention that may in any way be related thereto.

Qualified users may obtain copies of this report from the Defense Documentation Center.

References to named commercial products in this report are not to be considered in any sense as an endorsement of the product by the United States Air Force or the Government.

APPROVAL STATEMENT

This technical report has been reviewed and is approved.

Carlos Tirres

CARLOS TIRRES
Captain, USAF
Research and Development
Division
Directorate of Technology

Robert O Dietz

ROBERT O. DIETZ
Director of Technology

UNCLASSIFIED

REPORT DOCUMENTATION PAGE		READ INSTRUCTIONS BEFORE COMPLETING FORM
1. REPORT NUMBER AEDC-TR-74-76	2. GOVT ACCESSION NO.	3. RECIPIENT'S CATALOG NUMBER
4. TITLE (and Subtitle) AN INVESTIGATION OF THREE-DIMENSIONAL WALL INTERFERENCE IN A VARIABLE POROSITY TRANSONIC WIND TUNNEL		5. TYPE OF REPORT & PERIOD COVERED Final Report - March 5 - July 5, 1973 6. PERFORMING ORG. REPORT NUMBER
7. AUTHOR(s) T. W. Binion, Jr. - ARO, Inc.		8. CONTRACT OR GRANT NUMBER(s)
9. PERFORMING ORGANIZATION NAME AND ADDRESS Arnold Engineering Development Center (DYFS) Arnold Air Force Station Tennessee 37389		10. PROGRAM ELEMENT, PROJECT, TASK AREA & WORK UNIT NUMBERS Program Element 65802F
11. CONTROLLING OFFICE NAME AND ADDRESS Arnold Engineering Development Center (DYFS) Arnold Air Force Station, Tennessee 37389		12. REPORT DATE October 1974 13. NUMBER OF PAGES 82
14. MONITORING AGENCY NAME & ADDRESS (if different from Controlling Office)		15. SECURITY CLASS. (of this report) UNCLASSIFIED 15a. DECLASSIFICATION/DOWNGRADING SCHEDULE

16. DISTRIBUTION STATEMENT (of this Report)

Approved for public release; distribution unlimited.

17. DISTRIBUTION STATEMENT (of the abstract entered in Block 20, if different from Report)

1. Porous wall wind tunnels -- PWT
2. " " " -- Interference
3. [illegible]

18. SUPPLEMENTARY NOTES

Available in DDC

19. KEY WORDS (Continue on reverse side if necessary and identify by block number)

wind tunnels
porous walls
test facilities
upwash interference
transonic flow
transonic wind tunnel wall interference

20. ABSTRACT (Continue on reverse side if necessary and identify by block number)

This report presents the results of an experimental program to measure the wall interference effects on an idealized lifting model in the Mach number range from 0.6 to 1.3. The interference phenomena were evaluated by direct comparisons of data obtained in the Propulsion Wind Tunnel (16T) and the Aerodynamic Wind Tunnel (4T) at identical test conditions. The results show that a flow angularity which is apparently a function of model attitude and configuration can be induced into the tunnel flow field and

DD FORM 1 JAN 73 1473

UNCLASSIFIED

20. ABSTRACT (Continued)

be misconstrued as an upwash interference. The porosity schedule currently used in Tunnel 4T is shown to result in negligible blockage interference. The data indicate that the available subsonic theory will provide reasonable upwash and pitching-moment corrections provided one knows the "right" value of the boundary condition and the flow is everywhere subsonic. At Mach numbers less than unity, with moderate to large regions of supercritical flow over the model, the interference is characterized by an apparent distortion of the supercritical portion of the flow field which is not alleviated by porosity variations. At supersonic Mach numbers, the interference is caused by wave reflections.

AFSC
Arnold AFS Tenn

PREFACE

The work reported herein was conducted by the Arnold Engineering Development Center (AEDC), Air Force Systems Command (AFSC), under Program Element 65802F. The results presented were obtained by ARO, Inc. (a subsidiary of Sverdrup & Parcel and Associates, Inc.), contract operator of AEDC, AFSC,. Arnold Air Force Station, Tennessee. The tests were conducted under ARO Project Nos. PF222 and PF422. The manuscript (ARO-PWT-TR-74-49) was submitted for publication on June 18, 1974.

CONTENTS

		Page
1.0	INTRODUCTION	5
2.0	APPARATUS	
	2.1 Wind Tunnels	6
	2.2 Experimental Model	7
	2.3 Instrumentation	8
3.0	PROCEDURE	
	3.1 Experimental Procedure	8
	3.2 Determination of Model Incidence	8
	3.3 Precision of Measurements	9
4.0	RESULTS AND DISCUSSION	
	4.1 Flow Angularity	10
	4.2 Blockage Interference	12
	4.3 Lift Interference at the Wing Position	15
	4.4 Interference at the Tail Position	18
	4.5 Interference Effects on Pressure Drag and Pitching Moment	21
5.0	CONCLUDING REMARKS	22
	REFERENCES	23

ILLUSTRATIONS

Figure		
1.	Location of the Model in the Tunnel	25
2.	Model Installation	27
3.	Model Dimensions	30
4.	Solid Blockage Distribution in Tunnel 4T	31
5.	Pressure Orifice Locations	32
6.	Flow Angularity in Tunnel 4T	34
7.	Effect of Flow Angularity on Correlation of Lift Data	36
8.	Theoretical Blockage Corrections in Tunnel 4T	37
9.	Pressure Distribution on the Wing Centerbody, $M_\infty = 0.95$	38

Figure		Page
10.	Comparison of Experimental and Theoretical Blockage Corrections, $M_\infty = 0.95$	39
11.	Pressure Distributions on the Wing Centerbody at Angle of Attack, $M_\infty = 0.95$	40
12.	Wing Centerbody Pressure Distributions, $\alpha_{WB} = 6$ deg	41
13.	Wing Lift Coefficient	43
14.	Experimentally Determined Upwash Interference Factor	44
15.	Wing Pressure Distributions, Tail Forward	45
16.	Effect of Porosity on the Wing Pressure Distribution, Tail Aft, $M_\infty = 0.9$, $\alpha_{WB} = 6$ deg	54
17.	Wall Interference on the Three Configurations at Supercritical Flow Conditions, $\alpha_{WB} \approx \alpha_{TB} \approx 6$ deg	55
18.	Interference Angle at the Tail Centerbody Position	58
19.	Comparison of Theoretical and Experimental Upwash Interference Factors	63
20.	Effect of Porosity on Tail Lift Coefficient	64
21.	Tail Pressure Distributions, $\alpha_{WB} = 6$ deg	65
22.	Effect of Porosity on Pressure Drag	68
23.	Effect of Porosity on Pitching Moment	71
24.	Porosity Schedule for Zero Blockage Correction	80
NOMENCLATURE		81

1.0 INTRODUCTION

Wall interference has affected wind tunnel data to some degree since the Wright brothers tested their first airfoil. Fortunately, in most instances, wall effects were either correctable or negligible. With the recent interest in investigating transonic phenomena, however, it has become increasingly clear that wall interference at transonic speeds is neither correctable by available theory nor negligible except for extremely small model-to-tunnel size ratios (Ref. 1). A great deal of effort has been expended in recent years to determine Reynolds number effects on various phenomena associated with aircraft development. Yet, it has been shown (Ref. 2) that wall interference can overshadow the effects of Reynolds number variations. Thus, ways must be found to compensate for wall interference before other problems may be effectively resolved.

A theoretical and experimental effort has been undertaken at AEDC to fully understand transonic wall interference phenomena and to devise means to remove its effects from wind tunnel data. A portion of the theoretical work has been published in Refs. 3 to 5. Reported herein are the results of an experimental program to measure wall interference effects on a three-dimensional lifting model in the Mach number range from 0.6 to 1.3. Jacocks has shown (Ref. 6) that, while it is possible to obtain correct lift data on an aircraft configuration by changing wall porosity with Mach number, the drag and pitching moment thus obtained are not interference free. A primary goal of the experimental effort reported herein was to provide additional insight into the degree and mechanism of the drag and pitching-moment discrepancies. The interference on pitching moment was thought to arise from axial gradients of interference. Therefore, the model was designed with a metric horizontal tail which could be tested in two axial positions to investigate the axial interference variations. In addition, data were obtained with the tail-alone configuration to provide information on the effect of model size.

The interference phenomena are evaluated by direct comparisons of data obtained in the Propulsion Wind Tunnel (16T) and the Aerodynamic Wind Tunnel (4T). In order to remove as many data anomaly producing factors as possible, the tests in the two tunnels were conducted on the same model and support combination at identical test conditions, using the same instrumentation, data reduction, and testing procedures. The model boundary layers were tripped with carborundum grit to remove transition Reynolds number effects. The pressure difference across the model forebody was calibrated versus the flow stream angle in

Tunnel 16T so that data were obtained at the same angle of attack with respect to the flow stream to within ±0.05 deg in each instance. The only identifiable effects not accounted for, other than the wall interference, is the influence of the different acoustical/turbulent environments in the two tunnels on turbulent boundary layer growth with its inherent effect on separation and the effect of the tunnel flow dynamics on the pneumatic damping/amplification within the pressure tubing. Neither of these factors is thought to seriously affect the results.

The tests were conducted in two phases - a force phase and a pressure phase. Analysis of the force data revealed several inconspicuous instrumentation difficulties which affected the data such that only qualitative wall interference effects could be ascertained. Unfortunately, the models had been converted to measure pressure distributions before the instrumentation problems were discovered. Thus, although the results of the two phases are in general agreement, only the pressure data will be presented.

2.0 APPARATUS

2.1 WIND TUNNELS

2.1.1 Tunnel 16T

The AEDC Propulsion Wind Tunnel (16T) is a variable-density, continuous-flow tunnel capable of operation at Mach numbers from 0.2 to 1.6 at stagnation pressures up to 4000 psfa. The test section is 16 ft square by 40 ft long and is enclosed by perforated walls of fixed 6-percent porosity. The general arrangement of the test section and wall geometry is shown in Fig. 1a.

2.1.2 Tunnel 4T

The AEDC Aerodynamic Wind Tunnel (4T) is a variable-density, continuous-flow tunnel capable of operation at Mach numbers from 0.2 to 1.3 at stagnation pressures up to 3700 psfa. The test section is 4 ft square by 12.5 ft long and is equipped with variable-porosity (0- to 10-percent) walls. The general arrangement of the test section and wall geometry is shown in Fig. 1b.

2.2 EXPERIMENTAL MODEL

The wall interference model, shown installed in the wind tunnels in Fig. 2, consists of a rectangular planform wing and horizontal tail, each separately sting mounted. The rectangular planform was selected for two reasons. First, the variation of wall interference with position becomes increasingly severe as Mach number increases toward unity. A rectangular planform minimizes the necessity to account for the interference gradients. In fact, the tail was made separately metric in an attempt to separate the axial interference gradients. Secondly, it is currently not known how sophisticated the mathematical representation of the model must be to theoretically calculate wall interference effects in the transonic regime. Therefore, it was considered desirable to keep the model configuration as simple as possible to facilitate its mathematical representation. Each airfoil has the symmetrical NACA 63A006 profile which was selected because of its smooth and continuous variation of aerodynamic coefficients with angle of attack throughout the Mach number range and its slightly higher drag than some other candidates. The wing was sized such that the upwash interference angle of attack would be about one deg at $C_L = 1$ in a solid-wall tunnel with the constraint that the span to Tunnel 4T width ratio be less than 0.7. The axisymmetric model centerbody radii were calculated from

$$R = R_{max}\left[1 - \left(1 - \frac{2x}{L}\right)^2\right]^{3/4}$$

where the maximum radii (R_{max}) are 1.24 and 0.925 in. and the reference body lengths (L) are 20.87 and 12.98 in. for the wing and tail, respectively. The size of each centerbody was minimized, based on constraints established by the balance size and anticipated loads. The tail was designed to be tested in two axial positions by reversing the tail support strut. The distances between the wing and tail 1/4-chord lines were 14 and 28 in. for the forward and aft positions, respectively. In addition, the wing and its sting could be removed leaving the tail alone in the tunnel (Fig. 2c). Pertinent model dimensions are shown in Fig. 3. The solid-blockage distributions for the three model configurations in Tunnel 4T are shown in Fig. 4.

Both wing and tail models are equipped with rows of pressure orifices along the top and bottom rays of each centerbody and along the upper surface of the right airfoil and the lower surface of the left airfoil at mid-semispan. The location of the pressure orifices are shown in Fig. 5.

2.3 INSTRUMENTATION

The steady-state pressures were measured by individual 15-psid transducers in Tunnel 16T. In Tunnel 4T, 24-port scannivalves equipped with 15-psid transducers were used. The gravimetric angle of attack was measured with a damped-pendulum angle-of-attack sensor located just behind the tail support (see Fig. 3).

3.0 PROCEDURE

3.1 EXPERIMENTAL PROCEDURE

The tests were conducted at a constant unit Reynolds number of 4×10^6 per ft at Mach numbers from 0.60 to 1.3. The tunnel total temperature was maintained at 110 ± 5°F in each tunnel. Thus, except for flow angularity and the acoustic/turbulent environment, all free-stream flow parameters were equal in the two facilities. The wall porosity in Tunnel 4T was varied from 1 to 7 percent open as a test parameter.

After the desired tunnel free-stream conditions were established in Tunnel 16T, the model was positioned to discrete gravimetric angles of attack from -4 to +6 deg and in some cases to +10 deg in 2-deg increments. The model was then rolled 180 deg, and data were obtained in the angle-of-attack range of ±4 deg to establish the flow angularity in Tunnel 16T. After the establishment of the desired free-stream test conditions and wall porosity in Tunnel 4T, the model was set to the same angle of attack with respect to the flow stream as established in Tunnel 16T by the procedure discussed below. In each tunnel, the instrumentation readings were recorded by an on-line computer system which reduced the raw data to engineering units, computed pertinent parameters, and tabulated and plotted the results.

The force and moment coefficients for the wing and tail were obtained by integration of the section pressure distributions and by assuming a uniform spanwise loading. The model pitching moment was computed about the wing 1/4-chord line.

3.2 DETERMINATION OF MODEL INCIDENCE

The upright and inverted data obtained in Tunnel 16T were used to establish the relation,

$$\alpha_{WB} = \sum_{i=0}^{5} A_i(\Delta C_{PWB1})^i \tag{1}$$

where, $A_i = f_i(M_\infty)$ and ΔC_{PWB1} is the difference between the pressure coefficients of the first upper and lower orifices on the wing centerbody. Thus, the model centerbody was, in effect, calibrated as a flow angularity probe. During the Tunnel 4T tests, not only was Eq. (1) used to determine model incidence with respect to the flow stream but the model was positioned such that

$$(\Delta C_{PWB1})_{16T} = (\Delta C_{PWB1})_{4T} \pm 0.003$$

at each test condition. The rather laborious and time consuming procedure was followed so that pressure distributions obtained in the two tunnels could be compared directly rather than as a function of incidence angle.

The same procedure was used with the tail-only configuration. Fortunately, the calibration established for the tail in Tunnel 16T is a very weak function of Mach number, thereby allowing an approximate determination of the downwash angle at the position of the tail centerbody nose when the tail was tested in conjunction with the wing.

The angle measurements in Tunnel 16T were made with respect to the angle sensor location (see Fig. 3) and do not include the deflection of the sting forward of that point. For the purposes of the present investigation, the sting deflections are of no consequence since any convenient reference would suffice.

3.3 PRECISION OF MEASUREMENTS

Uncertainties (bands which include 95 percent of the calibration data) of the basic tunnel parameters (P_{t_∞} and M_∞) were estimated from repeat calibrations of the instrumentation and from the repeatability and uniformity of the test section flow during tunnel calibrations. Uncertainties of the instrumentation systems were estimated from repeat calibrations of the systems against secondary standards whose precisions are traceable to the National Bureau of Standards calibration equipment. The uncertainties were combined using the Taylor series method of error propagation to determine the precision of the reduced parameters presented in the following table:

M_∞	Tunnel 16T					Tunnel 4T				
	$\pm\Delta M$	$\pm\Delta C_P$	$\pm\Delta C_L$	$\pm\Delta C_D$	$\pm\Delta C_M$	$\pm\Delta M$	$\pm\Delta C_P$	$\pm\Delta C_L$	$\pm\Delta C_P$	$\pm\Delta C_M$
0.60	0.002	0.016	0.005	0.005	0.004	0.002	0.014	0.004	0.004	0.004
0.80	0.003	0.012	0.004	0.004	0.003	0.002	0.009	0.003	0.003	0.002
0.85	0.004	0.012	0.004	0.004	0.003	0.002	0.009	0.003	0.003	0.002
0.90	0.004	0.011	0.003	0.003	0.003	0.002	0.008	0.002	0.002	0.002
0.95	0.005	0.012	0.004	0.004	0.003	0.002	0.008	0.002	0.002	0.002
1.00	0.005	0.011	0.003	0.003	0.003	0.002	0.010	0.003	0.003	0.003
1.10	0.007	0.011	0.004	0.004	0.004	0.005	0.011	0.003	0.003	0.003
1.20	0.008	0.011	0.003	0.003	0.003	0.006	0.013	0.004	0.004	0.004
1.30	0.010	0.010	0.003	0.003	0.003	0.010	0.016	0.005	0.005	0.005

The gravimetric angle of attack and model incidences have uncertainties of ±0.03 and 0.05 deg, respectively.

4.0 RESULTS AND DISCUSSION

In general, the data presented herein are a comparison at identical test conditions of measurements obtained in Tunnel 16T with those obtained in Tunnel 4T with various values of wall porosity. In many cases, the data from Tunnel 16T are presented as a line with the data points omitted. In those cases, the lines have been constructed to pass exactly through the data points rather than as an indication of smoothed values.

4.1 FLOW ANGULARITY

Evaluation of wind tunnel wall effects must be preceded by a procedure to remove the effects of flow angularity, which is present in nearly all tunnels. It has generally been tacitly assumed that it was sufficient to correct the data by adjusting the gravimetric angle of attack by an amount equal to half the difference between upright and inverted data at zero lift. The tests reported herein offered an opportunity to test that rather basic assumption. Generally, model inverted data are obtained over a small angle range, say ±4 deg, to establish the flow angularity increment. Small differences in $\partial C_L/\partial\alpha$ between the upright and inverted data have been attributed to instrumentation or procedural inexactness. Since it was deemed imperative that the model incidence with respect to the flow stream be known as exact as possible in the present investigation, the procedure outlined in Section 3.2 was devised which allowed the model incidence to be established for every data point. The difference between the model incidence and the gravimetric angle of attack versus model incidence is presented in Fig. 6 for

the three model configurations at various combinations of Mach number and wall porosity. If the above assumption is correct, the "flow angle" will be constant for each test condition although its magnitude may reasonably be expected to vary with Mach number and wall porosity. Data are shown for 81 combinations of model, Mach number, and wall porosity. Only 16 of the combinations have a "flow angle" which is constant within ±0.1 deg, and of those, 9 occur with the low-blockage tail-only configuration.

It could be argued that the model incidence measurement, particularly subsonically, contains, to some degree, an increment caused by upwash interference. The upwash interference angle to a first-order approximation is directly proportional to the lift coefficient, hence to α_{WB}, since C_L is essentially linear with α_{WB} as shown in Section 4.3. The data in Fig. 6, however, are very nonlinear. Also the fact that the "flow angle" is, in general, not constant at supersonic Mach numbers, where the wing is entirely within the shock rhombus, tends to further negate the argument that the measured interference angle is substantially affected by upwash interference.

The center of rotation of the model system (see Fig. 3) is such that the vertical movement of the wing-body nose is 0.5 in. at 6-deg incidence. Tunnel-empty surveys in Tunnel 4T do not indicate spatial gradients of flow angle in the model vicinity greater than ±0.1 deg.

Evidence that the incidences inferred from the pressure measurements are correct is indicated in Fig. 7, wherein the wing lift coefficients from Tunnels 16T and 4T are compared versus α_{WB} and α_G for two representative Mach numbers. It is evident that the data correlation is excellent on the basis of α_{WB}, whereas, adjustment of α_G by any constant would not result in as good an agreement. It is recognized that the incidence measurement is with respect to the Tunnel 16T flow field and may not represent an absolute measurement of the actual incidence. However, because of the small model size with respect to Tunnel 16T and for the purposes of the present investigation any anomalies in the Tunnel 16T flow field are not considered large enough to significantly affect the results. Thus, all subsequent analyses have been accomplished on the basis of model incidence defined by the nose pressure measurements rather than a "corrected" gravimetric angle of attack.

It is seen from Fig. 6 that the "flow angle" variation appears to be dependent on Mach number, wall porosity, and model configuration in addition to model attitude. However, there are many other factors,

both fluid dynamic and operational, which may be responsible for the nonconstancy of the flow angularity. While it is tempting to speculate on probable causes, final understanding must await additional information. Two particularly disturbing questions arise, however. Does the phenomena exist in other ventilated tunnels? And, if so, how does one determine a priori the model incidence with reasonable precision?

4.2 BLOCKAGE INTERFERENCE

4.2.1 Interference at Zero Incidence

Application of theoretical wall interference corrections have evolved from an assumption of a small model with respect to the wind tunnel so that the influence of the wall may be considered linear over the length of the model. As Mach number increases toward unity, however, compressibility effects cause, in general, a nonlinear variation of the perturbation velocities over the model length. The wind tunnel model is in effect tested in a flow field whose "local equivalent free-stream Mach number" is given by

$$M = M_\infty \left[1 + \left(1 + \frac{\gamma - 1}{2} M_\infty^2\right)\epsilon\right] \tag{2}$$

where M_∞ is the tunnel calibration Mach number and ϵ is the local value of the blockage factor defined in Ref. 3. In general, since ϵ is a function of position, each point in the flow field has a different "equivalent free-stream Mach number" which is dependent on the model configuration, its support system, and the tunnel wall configuration. From isentropic relations, the change in pressure produced by a small change in Mach number is given by

$$\frac{\Delta P}{P_t} = -\gamma M_\infty \left(1 + \frac{\gamma - 1}{2} M_\infty^2\right)^{-\frac{2\gamma - 1}{\gamma - 1}} \Delta M \tag{3}$$

Equations (2) and (3) may be combined with the definition of the pressure coefficient to obtain

$$(C_P)_\infty = (C_P)_m + \frac{2\epsilon\left(1 + \frac{\gamma - 1}{2} M_\infty^2\right)^{\frac{2\gamma - 1}{\gamma - 1}} \left[1 + \left(1 + \frac{\gamma - 1}{2} M_\infty^2\right)\epsilon\right]}{\left\{1 + \frac{\gamma - 1}{2} M_\infty^2 \left[1 + \left(1 + \frac{\gamma - 1}{2} M_\infty^2\right)\epsilon\right]^2\right\}^{\frac{2\gamma - 1}{\gamma - 1}}} \tag{4}$$

which expresses the pressure coefficient referred to the undisturbed free-stream conditions in terms of the measured pressure coefficient, the tunnel calibration Mach number, and the blockage factor. The blockage factor may be determined, using the superposition principle, by representing the model, its support system, and the wake by appropriate distributed singularities.

Solutions for blockage interference factors for singularities located away from the tunnel centerline in a perforated tunnel have not yet been calculated. An estimate of blockage interference was made for the present investigation by representing the model and its support system as an area-equivalent body-of-revolution at zero incidence. The body-of-revolution was described by distributed source-sink surface elements whose strengths were obtained by the method of Ref. 7. The interference factors as a function of x were then obtained by superposition of the solutions presented in Ref. 3 for each singularity describing the model. The resulting theoretical corrections, from Eq. (4), to the pressure coefficients measured on the model in Tunnel 4T are presented in Fig. 8. The corrections were calculated using a value of 0.6 for the porosity parameter (Q)(Ref. 3) which yielded reasonable agreement with the experiment in Ref. 2 for porosities greater than 3 percent. In the present case, it can be seen by comparing Fig. 8 with the table in Section 3.3 that, except in the vicinity of the wing at $M_\infty = 0.95$, the blockage corrections are within the precision of measurement.

Since the data from the two tunnels may be compared at essentially the same incidence and free-stream conditions, it seems reasonable to presume that any differences in the pressure distributions obtained in the two tunnels along the model centerbodies, particularly forward of the wing, can be attributed to blockage effects. Typical pressure distributions on the wing centerbody at $M_\infty = 0.95$, zero incidence, are presented in Fig. 9. The data from Tunnels 16T and 4T at 5-percent porosity are in excellent agreement except for a slight displacement of the terminal shock. The data obtained at $\tau = 1.5$ do show a deviation from the Tunnel 16T data. A comparison of the difference between the pressure distributions from Tunnels 16T and 4T at $\tau = 1.5$ with the theoretical solutions described above for three values of the porosity parameter is shown in Fig. 10. While the solution for Q = 0.6 predicts the observed differences very well near the nose of the body, the axial interference variation does not conform to theory. Several factors could contribute to the descrepancy. First, the true wall boundary condition is unknown. However, an empirical determination of the boundary value could be made if that were the only problem, provided the assumption of boundary homogeneity is applicable. Second, the theory is

applicable only to subcritical flow, whereas the case under consideration contains a supercritical region. Theoretical solutions using the transonic equations may be expected to modify the predicted interference distribution. Finally, the model is represented as a body of revolution rather than a three-dimensional winged body. It is felt that the model representation may be the most serious factor contributing to the disagreement between theory and experiment. Thus, it appears that, while subsonic theory can be used to predict the approximate magnitude of blockage interference at rather high Mach numbers, the theoretical treatment must be more complex if detailed data corrections are required.

4.2.2 Interference at Angles of Attack

The discussion above pertains to data taken near zero incidence. Pressure distributions along the upper ray of the wing centerbody at angle of attack are presented in Fig. 11 for $M_\infty = 0.95$ and porosities of 1.5 and 5 percent. These data, while not necessarily typical, are representative of the data at lower Mach numbers. The pressure distributions obtained at 5-percent porosity in Tunnel 4T are in excellent agreement with the 16T data except in the region of the terminal shock. The pressure distribution in that region is influenced by the flow over the wing as discussed below. Thus, only the measurements ahead of the wing may be used to indicate blockage effects if the flow is supercritical. It is evident that blockage interference is essentially zero at $\tau = 5$ percent. At $\tau = 1.5$ percent, however, the difference between Tunnel 4T and 16T data forward of the wing increases with increasing inclination as may be expected because of the increase in wake blockage with incidence. Theoretical treatment of blockage interference for models at angle of attack at high subsonic Mach numbers is beyond the present state-of-the-art.

Typical upper-ray wing centerbody pressure distributions at 6-deg incidence are presented for the range of Mach numbers and porosities of the tests in Fig. 12. The effect of blockage at 6-deg incidence is greater than at lower angles at all Mach numbers. Therefore, the data in Fig. 12 indicate the maximum deviation of the centerbody pressures obtained in Tunnel 4T from those in 16T. Consider first the data at subsonic Mach numbers (Figs. 11 and 12a). The interference over the forebody ($x/c < 0$) with $\tau = 5$ percent is less than the precision of measurement for all subsonic Mach numbers. The effect of varying porosity, if the local velocity is subcritical, is, in general, small in comparison with its effect on the supercritical portion of the flow field.

It is supposed that, if the appropriate model representation and wall boundary condition were known, classical theory would provide an exact correction if the flow were subcritical. For supercritical flow, however, it appears that the tunnel boundary can distort the flow field to such an extent as to render treatment with small perturbation theory inappropriate at rather low Mach numbers (0.8) and relatively small model blockage (0.9 percent). This point will be illustrated further when the wing flow field is considered below.

The pressure distribution along the wing centerbody at supersonic Mach numbers is presented in Fig. 12b. Where the flow over the forebody is subsonic, $M_\infty = 1.0$ and 1.1, the pressure distribution is a function of porosity in Tunnel 4T with the measurements taken at low values of porosity agreeing well with the 16T data. At $x/c > 0$, the flow is entirely supersonic and independent of porosity except near the trailing edge of the wing where the shock locus may be changed slightly by its interaction with the tunnel boundary. At $M_\infty = 1.2$, the wing centerbody is entirely within the shock rhombus, and therefore, the agreement between the two tunnels is excellent. The tunnel-empty calibration at $M_\infty = 1.3$ (Ref. 8) indicates a Mach number gradient of -0.0014/in. from the leading edge location ($x = 0$) forward caused by the fact that Tunnel 4T has a fixed sonic nozzle, and therefore, the flow is still accelerating at the location of the wing forebody. Correction of the data to account for the Mach number gradient results in excellent agreement with the measurements from Tunnel 16T as shown.

Theory indicates that the blockage interference at the tail position is negligible (Fig. 8b). However, because of upwash and wave interference and because the tail could not be deflected with respect to the wing, the theoretical calculations for the blockage at the tail cannot be substantiated by the present experiment. The interference at the tail positions, as will be seen, is dominated by other factors which are not associated with blockage interference per se. Therefore, for the purpose of the present report, it will be assumed that blockage interference at the tail positions does not significantly affect the data.

4.3 INTERFERENCE AT THE WING POSITION

The lift coefficients obtained by integrating the pressure distributions on the wing are presented in Fig. 13 for the tail-forward and tail-aft configurations. The data indicate that the wing lift coefficient is relatively insensitive to porosity at Mach number 0.6 and Mach numbers above 1.1.

However, a more definitive measure of the agreement of lift on the wing in the two tunnels may be obtained if it is assumed that the low-speed upwash correction equation,

$$\Delta\alpha = (\alpha)_{16T} - (\alpha)_{4T} = \delta \frac{S}{C} C_L \tag{5}$$

is applicable over the entire Mach number range. Values for the upwash interference factor (δ), determined in the least-squares sense from the experimental data in the -4 to +6 deg incidence range, are presented in Fig. 14 for constant values of porosity throughout the Mach number range. The size of the symbols in Fig. 14 corresponds to a $\Delta\alpha$ of ±0.1 deg at a C_L of unity. At Mach numbers less than 0.9 and above 1.1, the interference factor at a given porosity is essentially the same (within experimental error) for the two models. At Mach numbers 0.95 and 1.0, however, the interference factor is model-configuration dependent. It is somewhat surprising that the wing experiences larger values of interference with the tail in the aft position than in the forward position. The wall interference resulting from the distrubance caused by the tail in the aft position should be negligible at the location of the wing. Thus, it would appear that the wall interference caused by the tail in the forward position has an offsetting effect on the interference at the wing. It is shown below, however, that the effect may be fortuitous.

The fact that the upwash interference factor is zero at the wing is a necessary but not sufficient condition to indicate an interference-free flow field. Pressure data obtained in the two tunnels on the wing with the tail forward are compared in Fig. 15. The data were selected such that the upwash factor is near zero or, in case of $M_\infty = 1$, a minimum. Only the upper surface pressures are shown for $\alpha_{WB} = 0$ for clarity. The pressure distributions at Mach number 0.6 from the two tunnels are essentially identical except for $\alpha_{WB} = 6$ deg where the flow expands a little more over the leading edge and the terminal shock is slightly farther forward in Tunnel 4T than in Tunnel 16T. In the Mach number range from 0.8 to 0.95, there is, in general, a compressive disturbance on the upper surface with the terminal shock farther aft in Tunnel 4T. The lower surface is also affected by the wall constraint but to a lesser extent than the upper surface. At Mach number 1, the data over the forward portion of the wing are essentially the same in the two tunnels except at $\alpha_{WB} = 6$ deg where the upper surface flow field is more expanded in Tunnel 4T than in Tunnel 16T, and the terminal shock is further forward. Beyond $M_\infty = 1.0$, the wing is within the shock

rhombus, and the data from the two tunnels are in excellent agreement. It is evident that, at Mach numbers below unity when the region of supercritical flow reaches an as yet undefined state, the wall interference can cause compensating effects which result in interference-free values of the lift coefficient with incorrect pressure distributions.

4.3.1 Effect of Wall Porosity

The effect of varying porosity at a constant Mach number is illustrated in Fig. 16. It can be seen that both the upper and lower surface pressures are affected by porosity changes. In the illustrated case, the lower surface pressure distribution obtained in Tunnel 4T is in agreement with the interference-free data at τ = 7 percent (Fig. 16d). However, the compressive disturbance on the upper surface was never completely eliminated by porosity variations. The same effects are observed at all Mach numbers and angles of attack where a moderate to large region of supercritical flow exists.

4.3.2 Effect of Model Size

An indication of the effect of model configuration and size on the interference field may be seen in Fig. 17, wherein the pressure distributions on the wing with the tail forward and aft and the tail alone are presented for various Mach numbers. The maximum solid-blockage ratios in Tunnel 4T are 0.90 percent for the wing configuration and 0.26 percent for the tail-alone configuration. While there are discernible differences in the wing pressure distributions at Mach numbers above 0.6, the tail-alone data from the two tunnels agree well at Mach numbers below 0.85. The compressive disturbance over the forward portion of the airfoil's upper surface is generally more severe on the wing with the tail forward than aft which, in regard to the lift coefficients, compensates for the shock position change, thereby appearing to result in less interference with the former configuration. The compressive disturbance does not appear on the tail-alone configuration until M_∞ = 0.95 and disappears at M_∞ = 1.0. Above M_∞ = 1.0, the data on the tail-alone configuration from the two tunnels are identical and are not presented herein.

Comparing the interference effects on the three models, particularly at Mach numbers 0.9 to 1.0, shows that the variation of the interference over the airfoil is a strong function of the model configuration. It is relevant to recall that in Ref. 2 a compressive disturbance was observed over the forward portion of a supercritical body of revolution (blockage

ratio 1.5 percent) which had a pressure distribution similar to the wing in the present investigation. In that case, the data were partially corrected by blockage theory. In the same paper, a two-dimensional wing between end plates (blockage ratio 0.69 percent) showed no effect of porosity variations on pressure distributions over the first 30 percent of the chord, but it did show a strong dependence of shock position on wall porosity. The pressure distribution in the latter case indicated a slower acceleration of the flow than with either the body of revolution or the present airfoils. These results suggest that the influence of the tunnel walls on the supercritical flow field is not only dependent on model size but may also be dependent on the pressure gradient or some other characteristic of the field. If this is true, theoretical computation of wall interference must be much more complex than the present state-of-the-art allows. Further, to obtain completely valid data at moderate incidences in the Mach number range from 0.85 to 1.0, wind tunnel models should be smaller than 1/4-percent blockage.

4.4 INTERFERENCE AT THE TAIL POSITION

Distortion of the flow field over the wing caused by wall interference, particularly that which causes changes in the terminal shock strength, obviously affects the flow field at the tail. Since it appears that wall interference effects are configuration dependent in the transonic regime, it seems impossible to experimentally separate the effects at the tail caused by the wall interference at the wing from an additional increment caused by the presence of the tail itself. However, if the effects can be decoupled to the extent that the wall interference on the tail-alone configuration may be considered indicative of the interference on the tail in the presence of the wing, some qualitative separation may be attained. The data presented in Fig. 17 indicate that the tunnel walls appreciably affect the tail data only at Mach numbers from 0.85 to 1.0. Further, the interference effect is seen primarily as a change in location of the terminal shock on the tail surface. When the tail is in the presence of the wing, either in the forward or aft position, the flow over the tail is supercritical at $M_\infty = 0.9$ and above. Thus, it is argued that, as far as the present data are concerned, the interference at the tail results almost entirely from disturbances caused by the presence of the wing except possibly at $M_\infty = 0.9$ and 0.95.

The change in local flow angle between the two tunnels at the location of the first two orifices on the tail centerbody is presented in Fig. 18 as a function of the wing lift coefficient. The fact that $\Delta\alpha_I$ is nonzero at

$C_{LW} = 0$ is attributed to differences in the flow angle gradient between the two facilities except at $M_\infty = 0.9$ and 0.95 with the tail forward. The large variation in $\Delta\alpha_I$ at Mach number 0.95 with the tail forward (Fig. 18c) is caused by the wing's trailing shock system. Schlieren photographs taken in Tunnel 16T show that the terminal shock system from the wing passes just in front of the tail centerbody in the forward position. A slight change in the shock system would cause a significant change in the nose pressures used to indicate the flow angle. The data in Fig. 15 indicate that shock position does change significantly at $M_\infty = 0.95$ and to a lesser extent at $M_\infty = 0.90$. Thus, it is concluded that the measurement of $\Delta\alpha_I$ is not valid above $M_\infty = 0.9$ with the tail in the forward position.

At a given porosity in the 0.6 to 0.85 Mach number range, portions of the $\Delta\alpha_I$, C_{LW} curves are linear. Those portions which are linear coincide with the condition of subcritical or very little supercritical flow over the wing. As the extent of the supercritical flow increases, whether caused by Mach number or incidence increases, the variation of the interference angle with the wing lift coefficient becomes nonlinear. Sufficient data are not available to determine the mechanism producing the nonlinear behavior. At supersonic Mach numbers, the flow approaching the tail in the aft position is obviously affected by wave reflections at some conditions. The effect of wave reflections are more readily seen by examining the tail lift coefficients and pressure distributions presented below.

4.4.1 Comparison of Experiment and Theory

The linear portions of the $\Delta\alpha_I$, C_{LW} curves at subsonic Mach numbers (Figs. 18a, b, and c) were used in conjunction with Eq. (5) to compute a value of the upwash interference factor at the measurement position. The results of the calculations, performed in the least-squares sense, along with the upwash interference factor at the wing averaged over the 0.6 to 0.85 Mach number range from Fig. 14 are compared with the theory of Ref. 3 in Fig. 19. The wing 1/4-chord is taken as $x = 0$. Values of the porosity parameter (Q) were selected such that the theoretical curves passed through the upwash interference factors determined for the wing. Since the theory is calculated only along the tunnel centerline, whereas the measurement positions were above the centerline ($z/b = 0.21$), the interference factors from the tail would be expected to be greater than predicted. Also, as $x/\beta b$ increases, either because of increases in x or Mach number (decreasing β), the increment of interference caused by being off the centerline should increase. Both of these expectations are reflected in the experimental data, although

the data from the tail in the aft position is lower than expected. It should be noted that the slope ($d\Delta\alpha_I/dC_{LW}$) from which δ was computed was evaluated from only three or four points. Thus, its accuracy is questionable. Nevertheless, it appears that small perturbation theory using the small span model assumption provides a reasonable prediction of the upwash interference provided the flow is everywhere subcritical and the porosity parameter (Q) is known. Thus, under those conditions, one could calculate corrections to aircraft pitching moment by employing a simple angle-of-attack correction for the tail.

4.4.2 Effect of Wall Porosity

The effect of porosity variations in Tunnel 4T on the tail lift coefficient is presented in Fig. 20. Representative pressure distributions on the tail airfoil are presented in Fig. 21 for selected values of the wall porosity which result in the best agreement with the data from Tunnel 16T. At Mach number 0.90 and below, porosity variations have little effect on the lift coefficient whether the tail is in the forward or aft position. However, the lift data from the two tunnels, in general, agree better with the tail forward. As with the wing, attainment of "correct" lift data does not ensure an interference-free flow field. Examination of Fig. 21 shows that the pressure distributions obtained in Tunnel 4T are significantly affected by the presence of the walls. As with the wing, agreement of the lift data from the two tunnels is, in most instances, fortuitous. The mechanism of the interference at the tail at high subsonic Mach numbers appears to be associated with reflections of portions of the wing's supercritical flow field from the tunnel wall. The interference is particularly severe at $M_\infty = 0.95$ where the location of the free-air sonic line is far beyond the tunnel boundary and the wing trailing edge shock is almost normal to the wall.

Unlike conditions at the wing, the interference effects at the tail extend well into the supersonic speed range. At a given supersonic speed, waves of different strengths are generated along the wing centerbody and between the wing's leading and trailing edges. The waves reflect from the tunnel boundary with strengths dependent on the strength of the incident wave and the boundary crossflow characteristics. It is evident from Fig. 20 that the interference is very severe at $M_\infty = 1.0$, particularly at the tail's aft position. Not only is there no value of porosity which will yield interference-free data, the variation of the interference (as indicated by ΔC_L) is not monotonic with porosity. As Mach number increases, the advantage of a variable porosity tunnel is clearly evident as the value of porosity producing minimum interference is a

function of Mach number. It should be noted, however, that the value of porosity needed to reproduce the interference-free tail lift coefficient is also dependent on tail location. This dependency arises because the waves, which have the possibility of reflecting onto the tail at a given position, require different values of porosity for their "cancellation" because of their different strengths and incidence angles. While it has been shown that the 60-deg inclined hole wall has good wave attenuation properties for a cone-cylinder model above a Mach number of about 1.1 (Ref. 9), there have been little data acquired to assess the cancellation requirements for waves produced by winged models. The "wave interference pattern" for a winged model is dependent on model-attitude, Mach number, and porosity and is currently impossible to predict for general configurations at low supersonic Mach numbers because of the lack of detailed knowledge concerning the "wave reflectance" properties of the porous walls.

4.5 INTERFERENCE EFFECTS ON PRESSURE DRAG AND PITCHING MOMENT

The variation of the pressure drag coefficient obtained in Tunnel 16T and at various values of porosity in Tunnel 4T is presented in Fig. 22 for the wing and wing plus tail. It should be noted that the integration of the pressure measurements does not result in very accurate values of the axial force because of the lack of a sufficient number of orifices near the airfoil's leading edges. Comparison of the data from the two facilities is reasonable, however, since both data sets suffer the same limitations. For the most part, the differences between the drag polars obtained at a given Mach number are within the data precision (see Section 3.3). This arises because the interference affects the pressure distributions in regions of small area change. Hence, a relatively large interference on the pressure distribution is not appreciably reflected in the axial force. Thus, with a notable exception at $M_\infty = 0.95$ where the shock position on the wing changed significantly at low incidences in Tunnel 4T (see Fig. 15c), the data are not precise enough to detect meaningful results. Had skin friction been included the data differences would possibly have been greater.

The effect of porosity on the pitching moment about the wing 1/4-chord is presented in Fig. 23. The differences between the data obtained in Tunnels 4T and 16T are primarily the result of disturbances at the tail position. With the tail forward, particularly at low Mach numbers, the effect of porosity variations in Tunnel 4T are relatively minor. Except for Mach numbers 0.95 and 1.0, the agreement of the data from the two facilities is satisfactory for many test programs. Most of the pitching-moment data taken in Tunnel 4T with the tail in the aft position show large interference effects for the reasons indicated in Section 4.4.

5.0 CONCLUDING REMARKS

The experimental program reported herein was designed to minimize, in as much as possible, the effect of all factors, except wall interference, which may cause discrepancies in wind tunnel data. It was shown that a flow angularity can be induced into the tunnel flow which is an apparent function of model configuration, model attitude, and tunnel configuration and not associated with wall interference in the normal sense of the term. An effect of the flow angularity phenomena, while small, could nevertheless be construed as an upwash interference. Unless its cause can be identified and eliminated where it exists, application of strictly theoretical corrections for ventilated wind tunnels is impossible.

The model was purposely made small in cross-sectional area to minimize blockage interference. Theoretical computations, with the model represented as an area equivalent body of revolution at zero incidence, indicated the blockage interference to be within the precision of the data except at Mach number 0.95. At that Mach number, the experimental corrections did not entirely agree with theory even though the flow was locally subcritical. The disagreement is believed to stem from the model representation. As sonic Mach number is approached, the three-dimensional area distribution becomes an increasingly important factor affecting the flow field. Thus, it is felt that a three-dimensional model representation will be required for blockage interference calculations in the transonic speed range.

The data at angles of attack other than zero indicate blockage effects which increase with increasing incidence and Mach number. At each Mach number, however, a value of wall porosity was found which resulted in negligible amount of blockage interference at all incidences. The variation of the "zero blockage interference" porosity with Mach number (shown in Fig. 24) agrees with the porosity schedule currently used in Tunnel 4T which has evolved from the analysis of a number of investigations.

Unhappily, the influence of porosity on upwash interference is not as straightforward. The data indicate that present subsonic theory will provide reasonable upwash corrections and pitching-moment corrections (provided one knows the "right" value of the porosity parameter) if the flow is everywhere subsonic. However, at $M_\infty < 1$ with moderate to large regions of supercritical flow over the model, the interference is

characterized by an apparent distortion of the supercritical portion of the flow field. There is no value of porosity with the present wall configurations which will yield interference-free pressure distributions for mixed-flow conditions with reasonable size models. The extent of the interference is thought to be a function of the size of the supercritical region with respect to the tunnel semiheight. However, there are hints that the interference may also be a function of some other flow field property, possibly the pressure gradient. Sufficient information is not yet available to establish definitive guidelines for predicting the interference at supercritical conditions. The results of the present study do provide, however, an insight into the magnitude of the problem.

At Mach numbers above unity, the wall interference which exists is, of course, characterized by wave reflections. While the variable porosity walls alleviate wave reflections in many instances, they are far from perfect, particularly in the low supersonic speed range.

The data analysis has been undertaken with a purist attitude in that many of the data differences noted between the two tunnel tests have little effect on many routine wind tunnel programs. In those instances, it is recommended that the porosity schedule shown in Fig. 24 be used in the Tunnel 4T facility with the recognition that a distortion of the supercritical flow field will occur depending on the model and test conditions. In cases where exact data are required, it is evident that great care must be exercised during tests in the transonic speed range and that the experimenter must have a greater knowledge of the tunnel than he now, in general, possesses.

REFERENCES

1. Couch, L. M. and Brooks, C. W., Jr. "Effect of Blockage Ratio on Drag and Pressure Distribution for Bodies of Revolution at Transonic Speeds." NASA TND-7331, November 1973.

2. Binion, T. W. and Lo, C. F. "Application of Wall Corrections to Transonic Wind Tunnel Data." AIAA Paper No. 72-1009, presented at the AIAA 7th Aerodynamic Testing Conference, Palo Alto, California, September 13-15, 1972.

3. Lo, C. F. and Oliver, R. H. "Boundary Interference in a Rectangular Wind Tunnel with Perforated Walls." AEDC-TR-70-67 (AD704123), April 1970.

4. Lo, C. F. "Wind Tunnel Wall Interference Reduction by Streamwise Porosity Distribution." AIAA Journal, Vol. 10, No. 4, April 1972.

5. Kraft, E. M. "Upwash Interference on a Symmetrical Wing in a Rectangular Ventilated Wall Wind Tunnel: Part I - Development of Theory." AEDC-TR-72-187 (AD757197), March 1973.

6. Jacocks, J. L. "Evaluation of Interference Effects on a Lifting Model in the AEDC-PWT 4-ft Transonic Tunnel." AEDC-TR-70-72 (AD868290), April 1970.

7. Smith, A. M. O. and Pierce, J. "Exact Solution of the Neumann Problem Calculation of Non-Circulatory Plane and Axially Symmetric Flows about or within Arbitrary Boundaries." Report No. S26988, Douglas Aircraft Company.

8. Jacocks, J. L. and Hartley, M. S. "Calibration of the AEDC-PWT 4-ft Transonic Tunnel with Modified Walls." AEDC-TR-69-134 (AD853841), June 1969.

9. Estabrooks, Bruce B. "Wall-Interference Effects on Axisymmetric Bodies in Transonic Wind Tunnels with Perforated Wall Test Sections." AEDC-TR-59-12 (AD216698), June 1959.

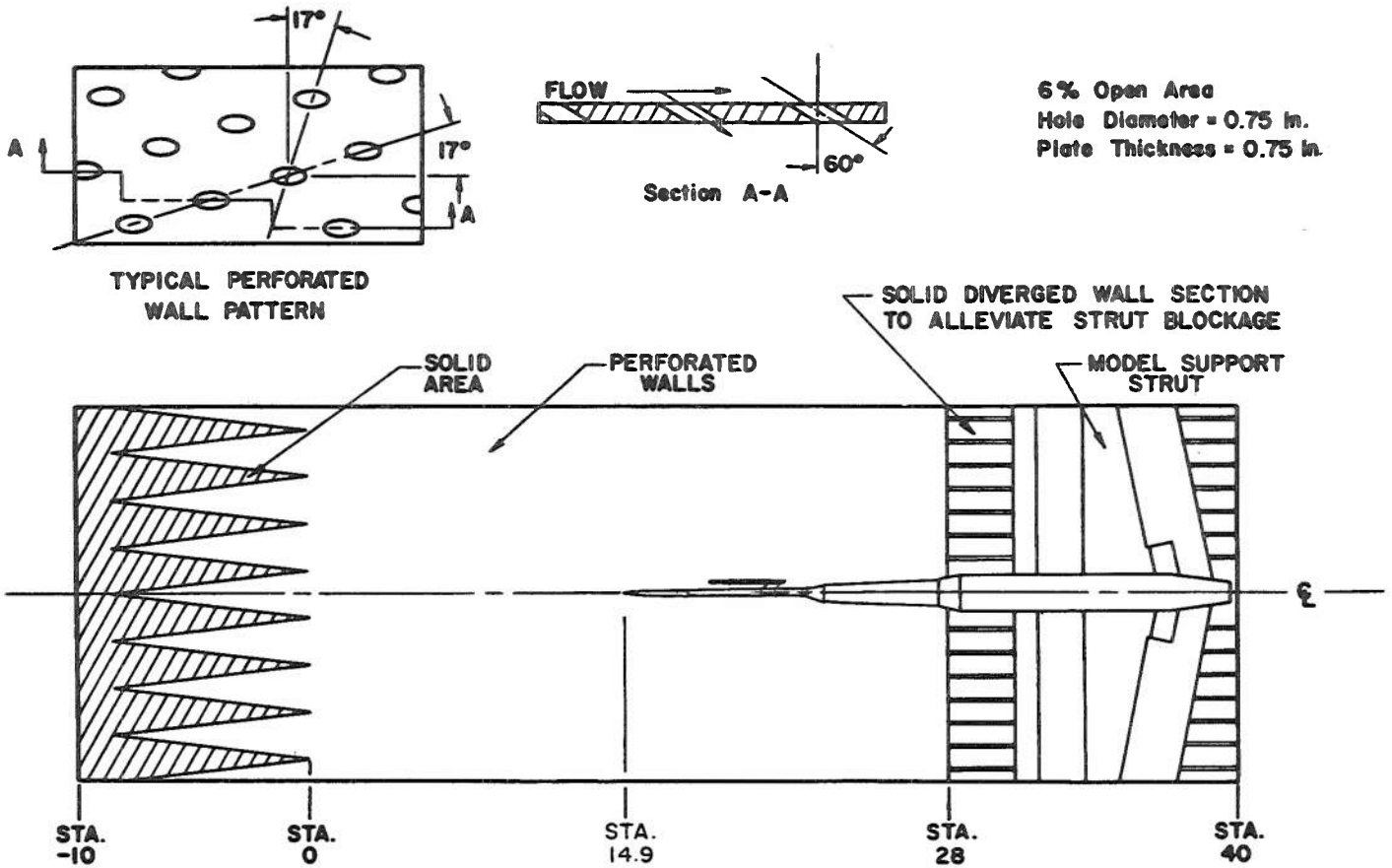

a. Tunnel 16T

Figure 1. Location of the model in the tunnel.

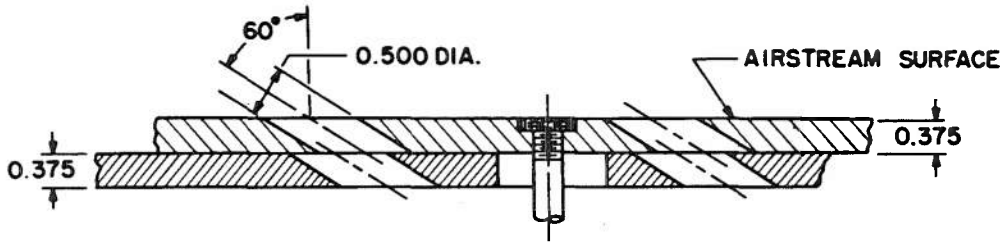

TYPICAL PERFORATED WALL CROSS SECTION

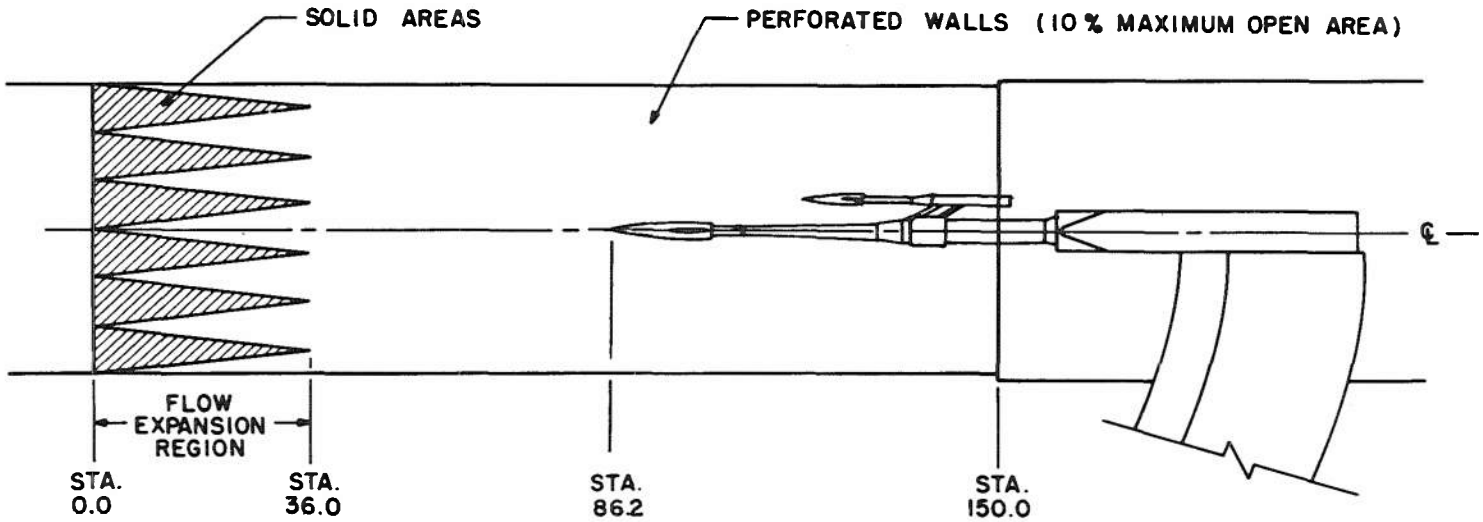

b. Tunnel 4T

Figure 1. Concluded.

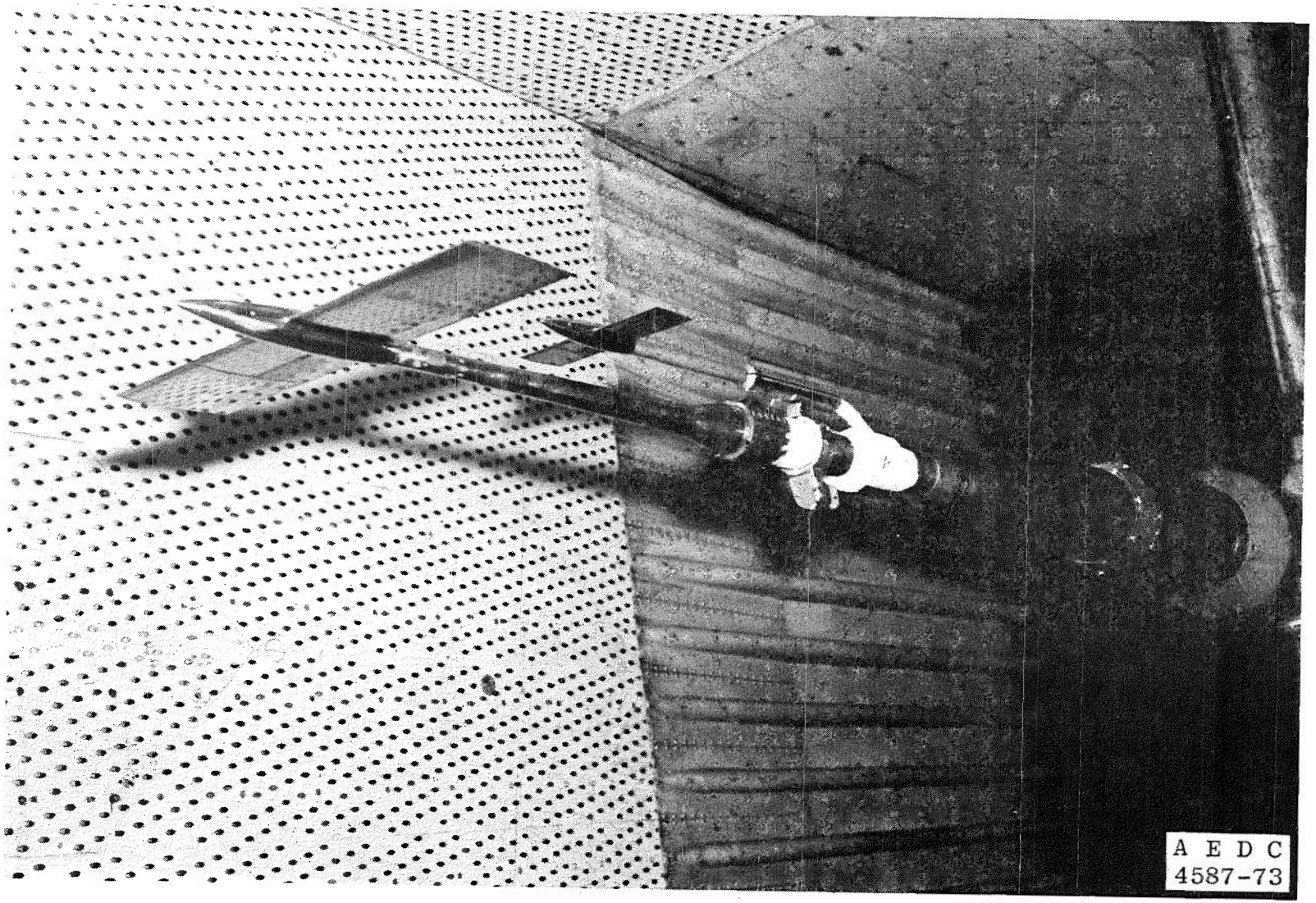

a. Model with tail aft in Tunnel 16T
Figure 2. Model installation.

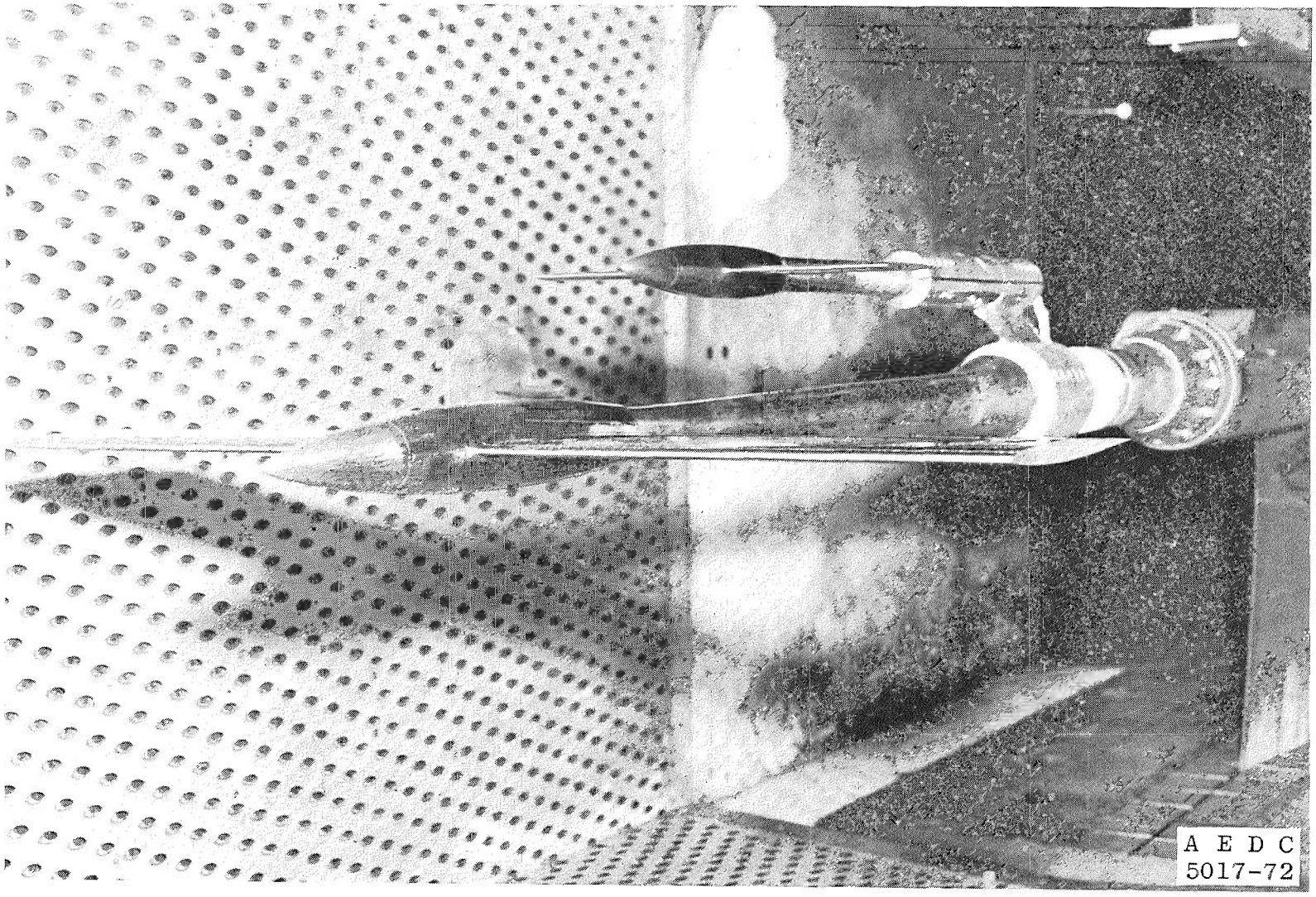

b. Model with tail forward in Tunnel 4T
Figure 2. Continued.

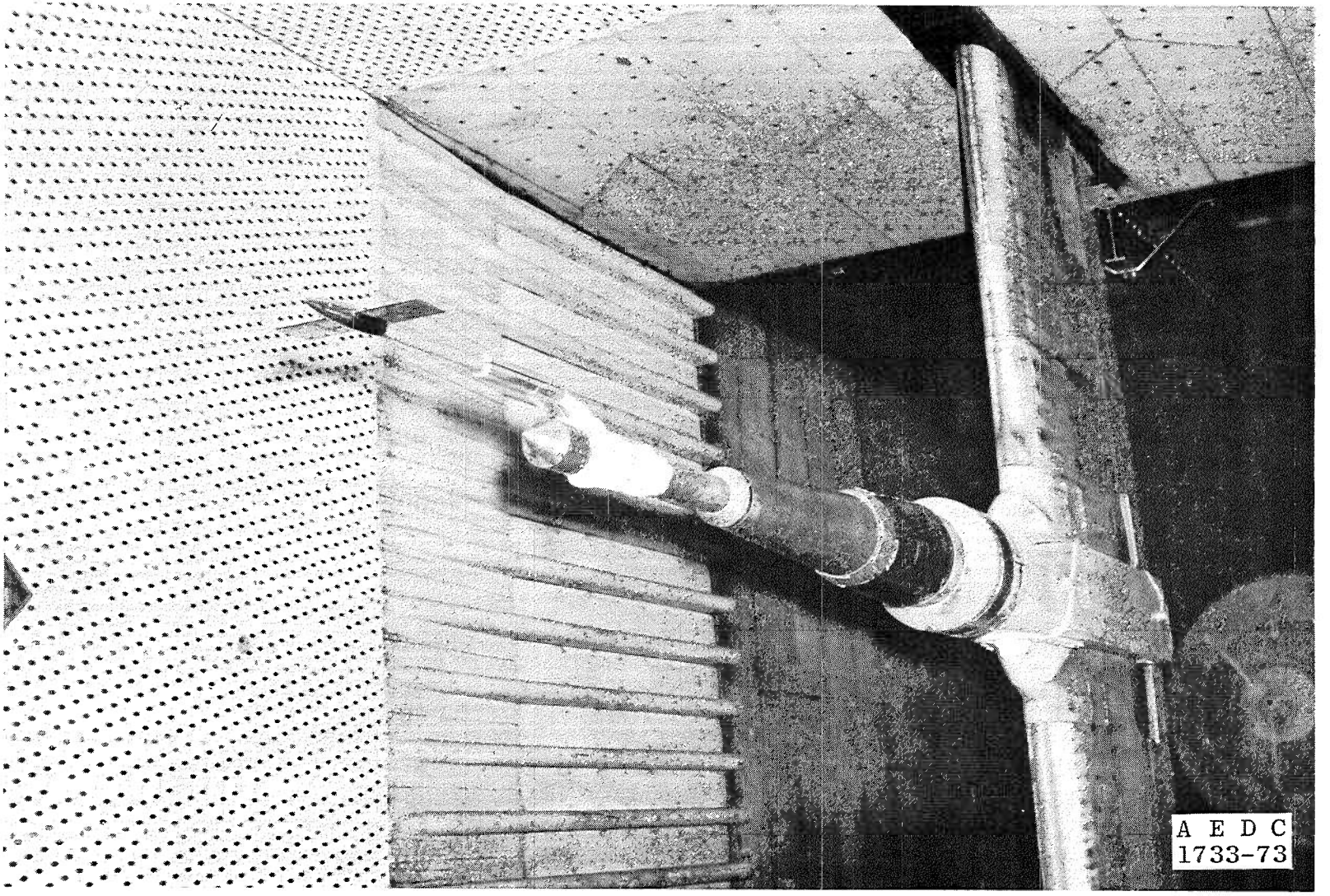

c. Tail alone in Tunnel 16T
Figure 2. Concluded.

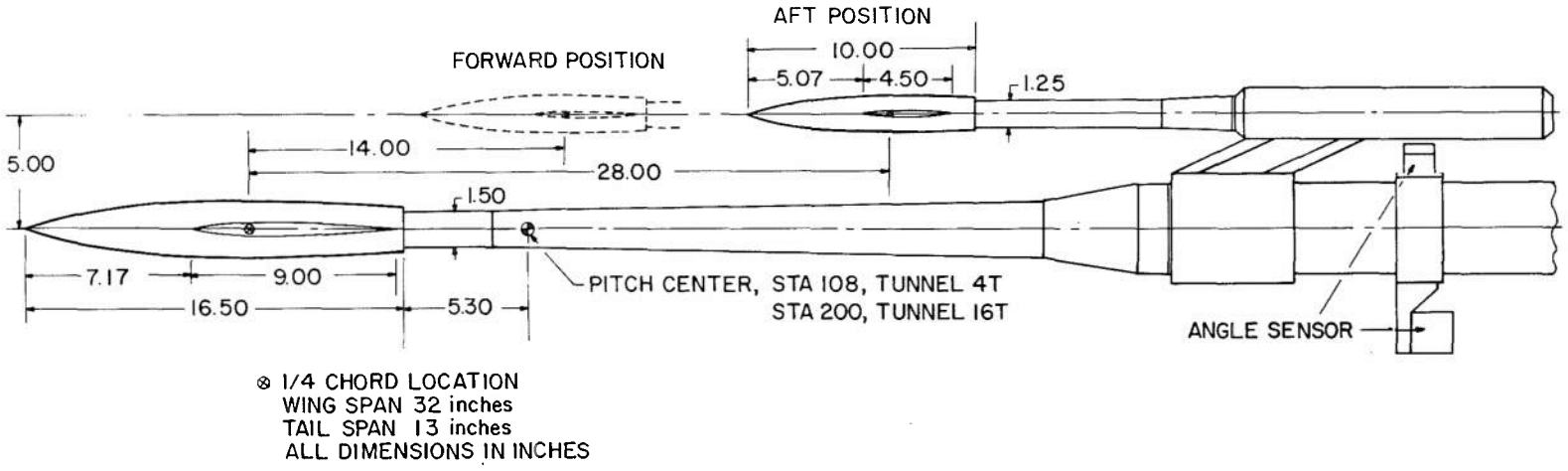

Figure 3. Model dimensions.

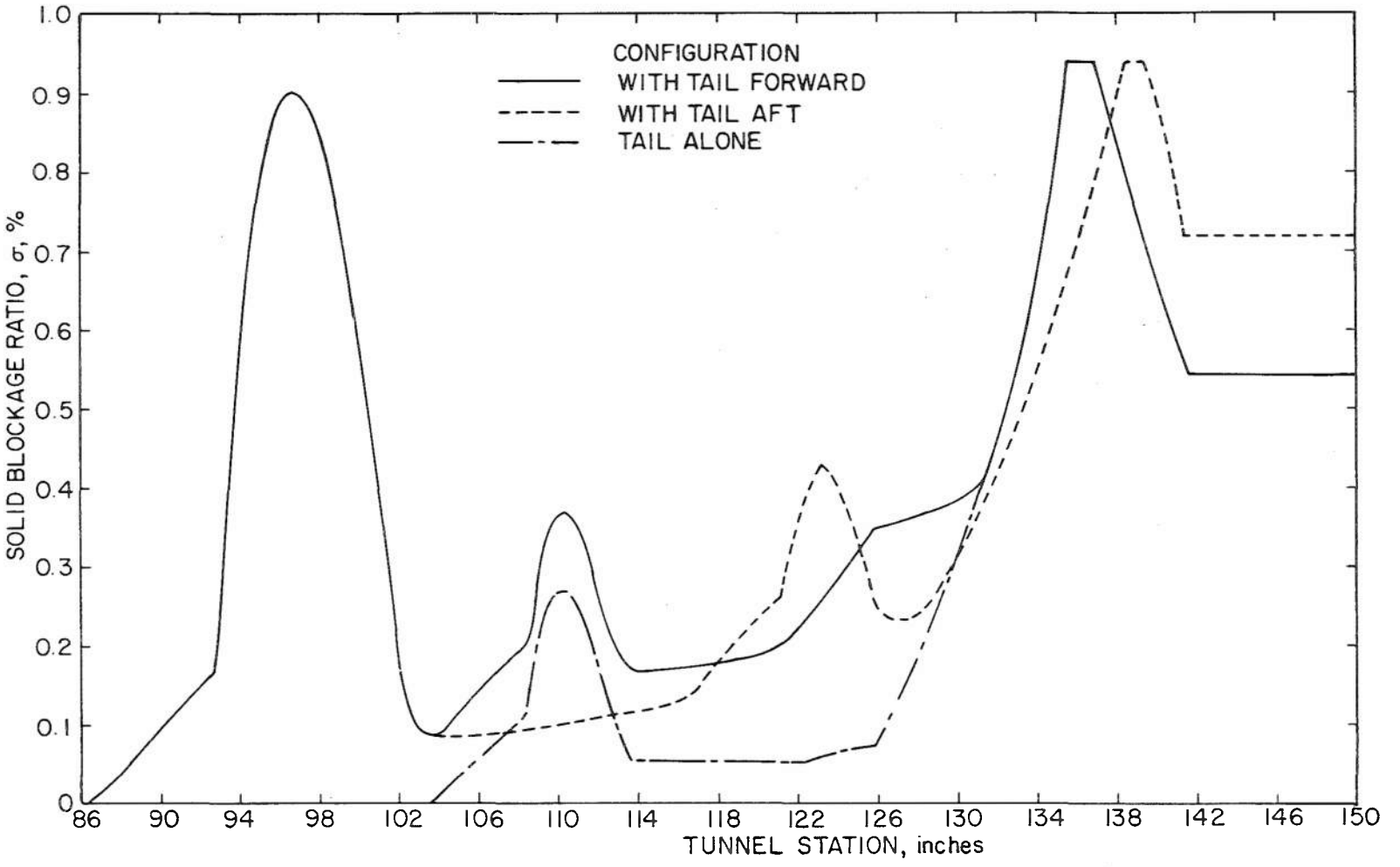

Figure 4. Solid blockage distribution in Tunnel 4T.

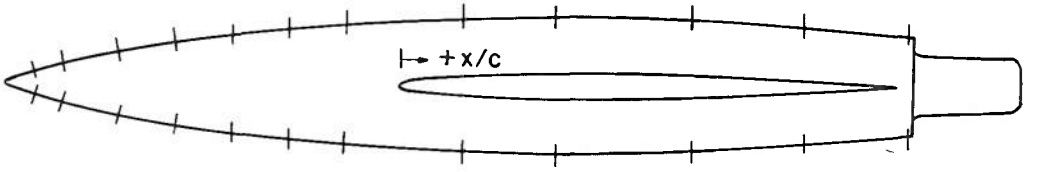

WING CENTERBODY

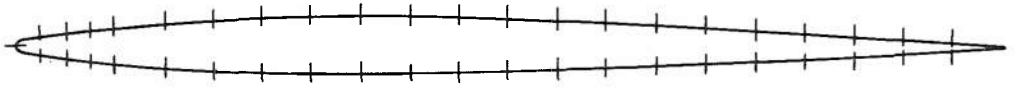

WING AIRFOIL AT MID-SEMISPAN

NOMINAL ORIFICE LOCATIONS

CENTERBODY $(x/c)_W$	AIRFOIL $(x/c)_W$
-0.738	0.000
-0.680	0.025
-0.564	0.050
-0.448	0.075
-0.332	0.100
-0.216	0.150
-0.100	0.200
0.131	0.250
0.315	0.300
0.572	0.350
0.826	0.400
1.025	0.450
	0.500
	0.550
	0.600
	0.650
	0.700
	0.750
	0.800
	0.850
	0.900
	0.950

a. Wing

Figure 5. Pressure orifice location.

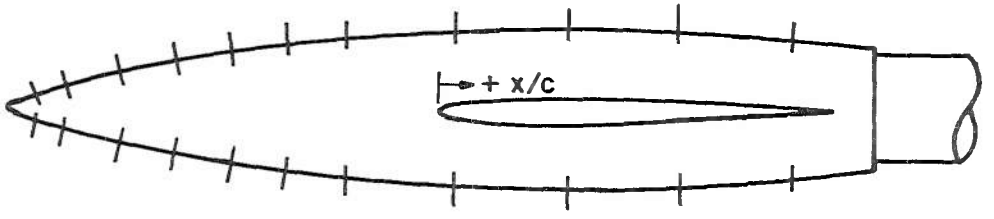

TAIL CENTERBODY

TAIL AIRFOIL AT MID-SEMISPAN

NOMINAL ORIFICE LOCATIONS

CENTERBODY $(x/c)_T$	AIRFOIL $(x/c)_T$
-1.057	0.000
-0.985	0.025
-0.847	0.050
-0.697	0.075
-0.553	0.100
-0.408	0.150
-0.265	0.200
-0.024	0.250
0.313	0.300
0.601	0.350
0.890	0.400
	0.450
	0.500
	0.550
	0.600
	0.650
	0.700
	0.750
	0.800
	0.850
	0.900

b. Tail
Figure 5. Concluded.

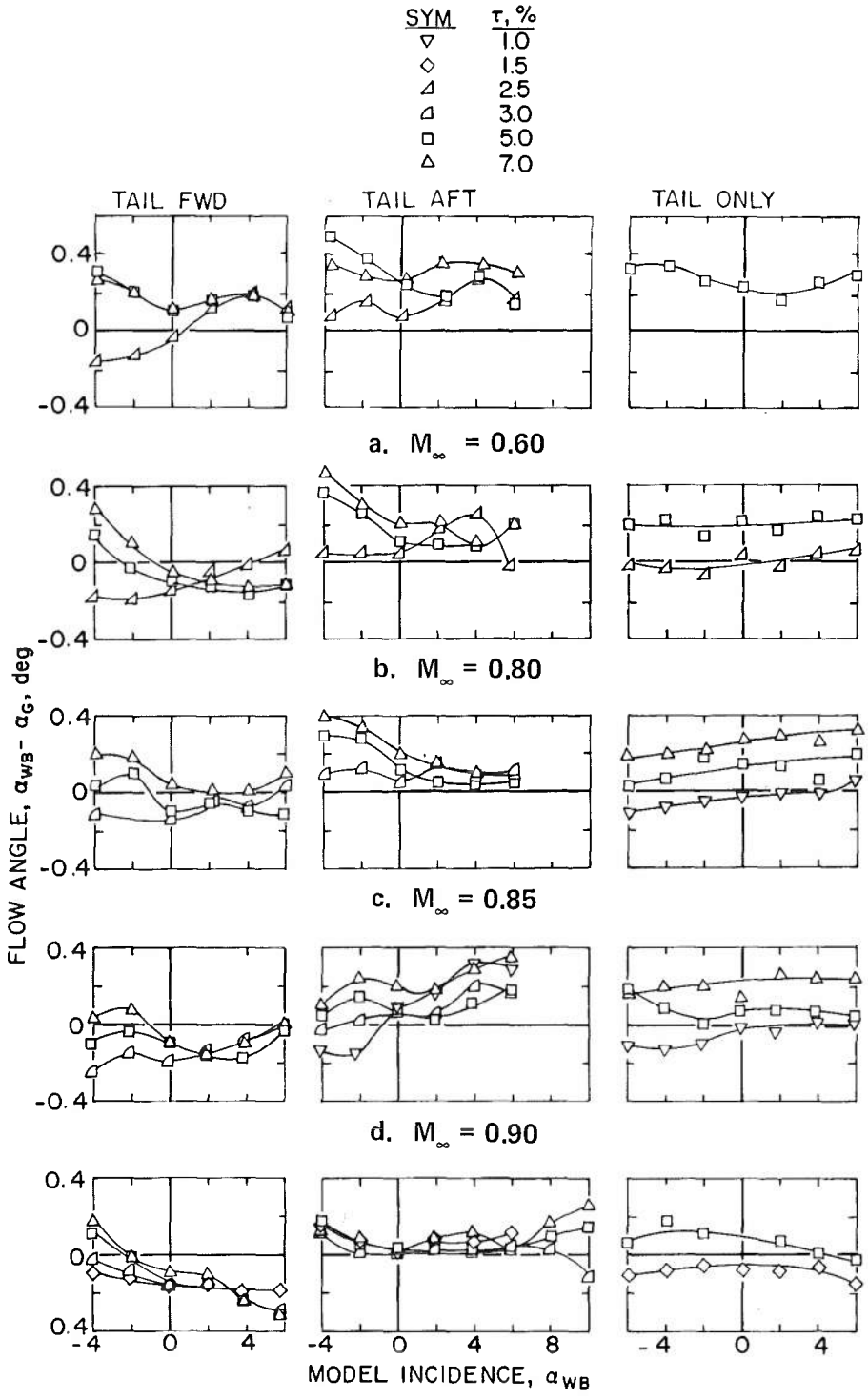

Figure 6. Flow angularity in Tunnel 4T.

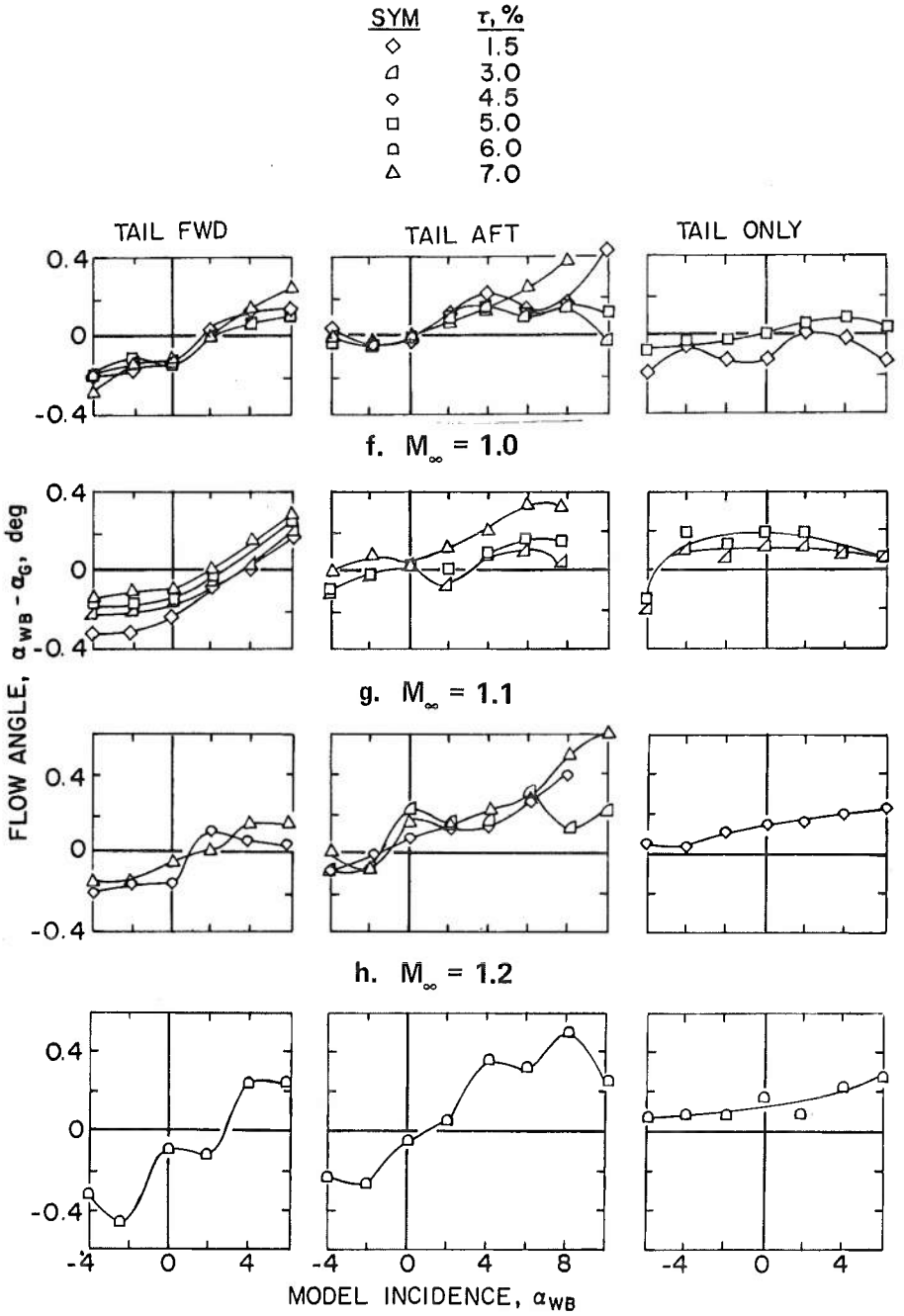

i. $M_\infty = 1.3$

Figure 6. Concluded.

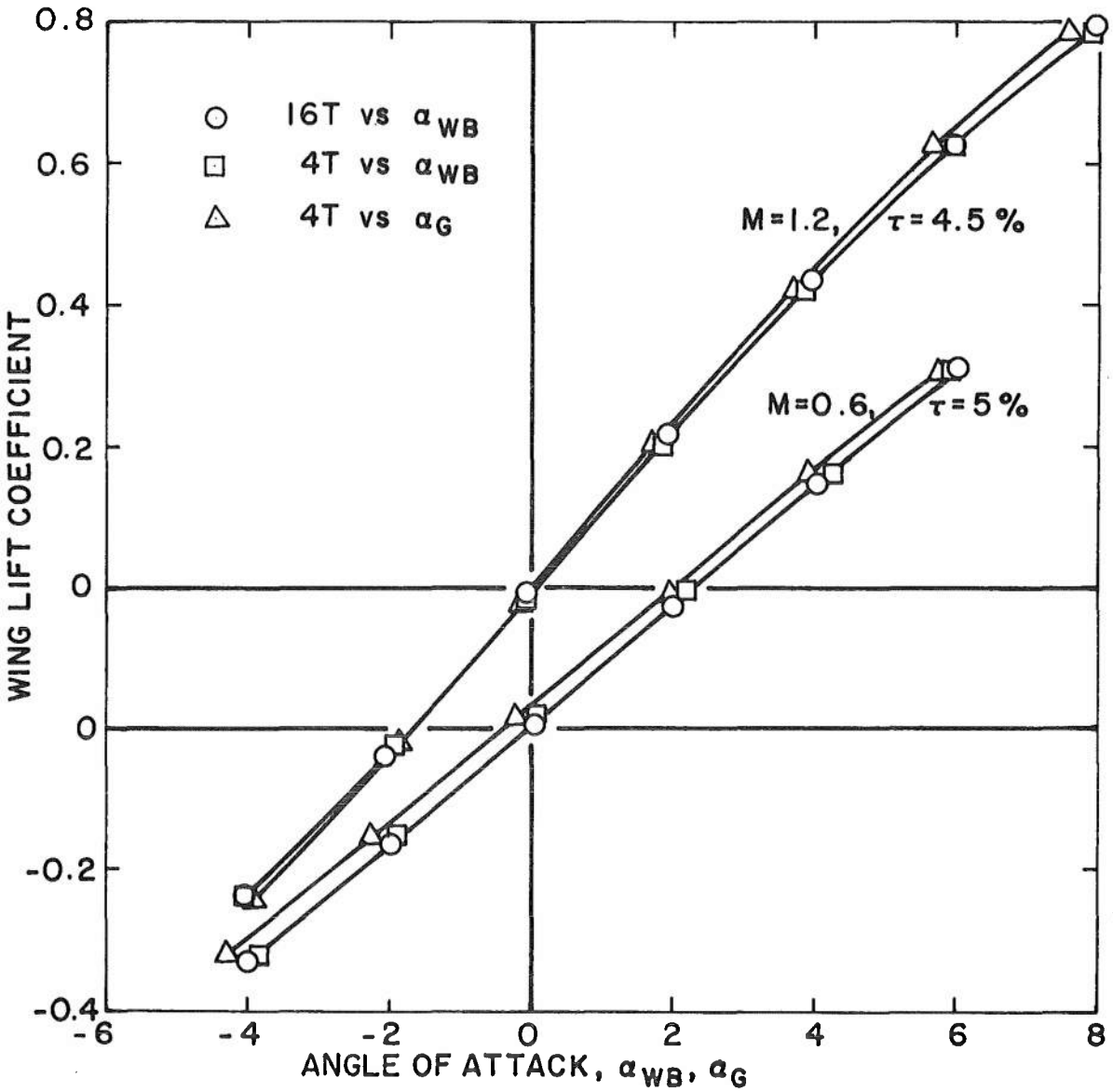

Figure 7. Effect of flow angularity on correlation of lift data.

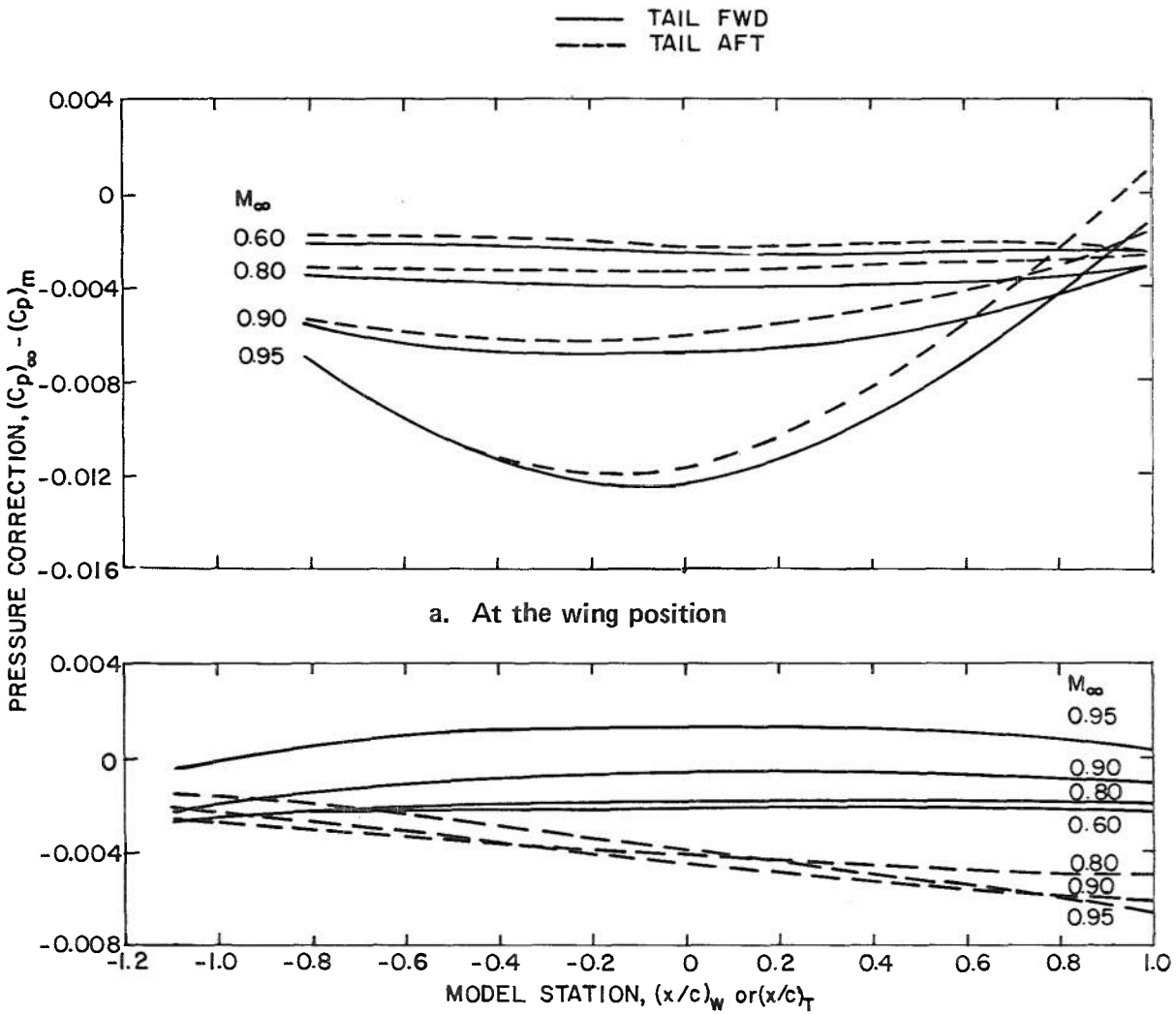

b. At the tail position

Figure 8. Theoretical blockage corrections in Tunnel 4T.

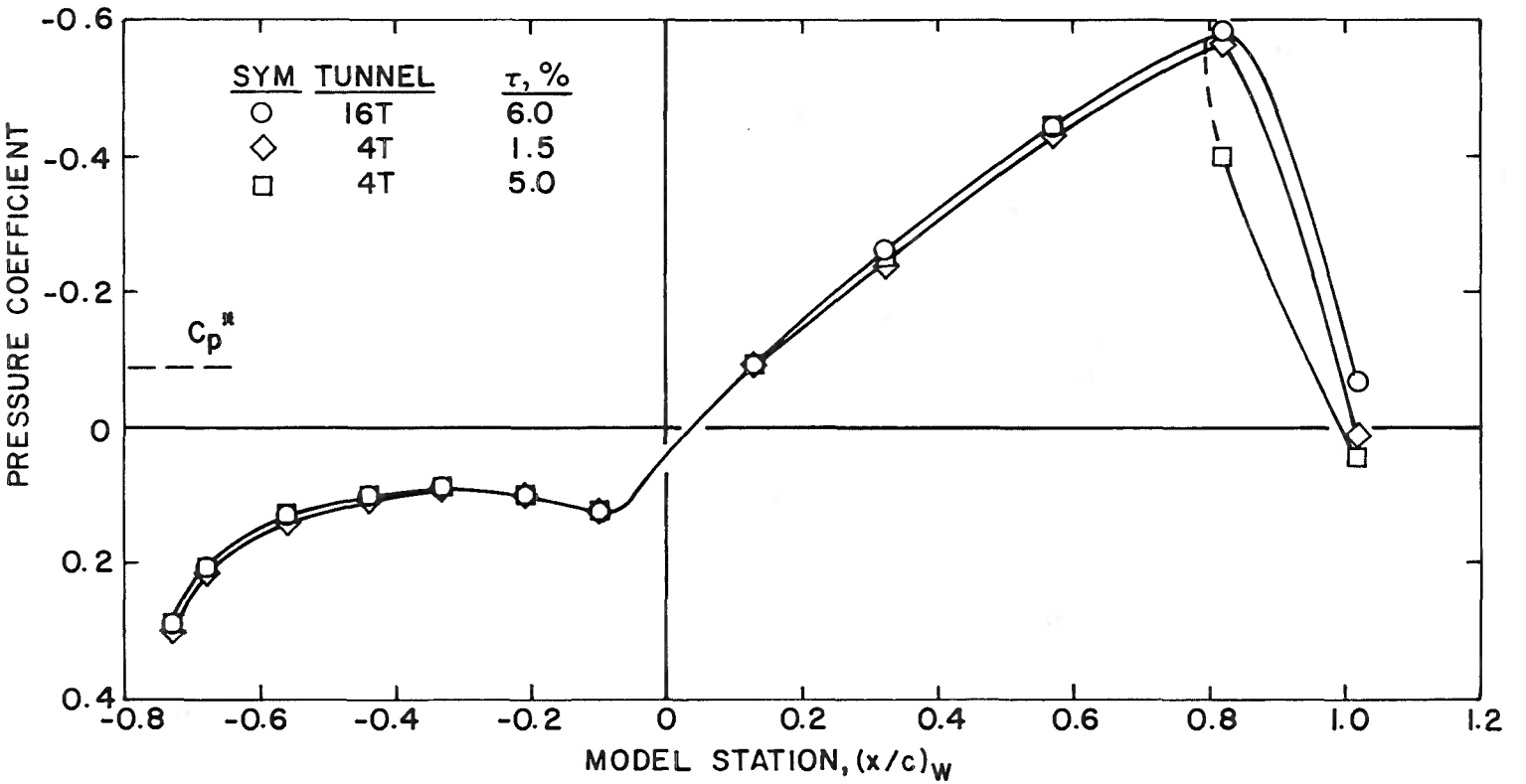

Figure 9. Pressure distribution on the wing centerbody, $M_\infty = 0.95$.

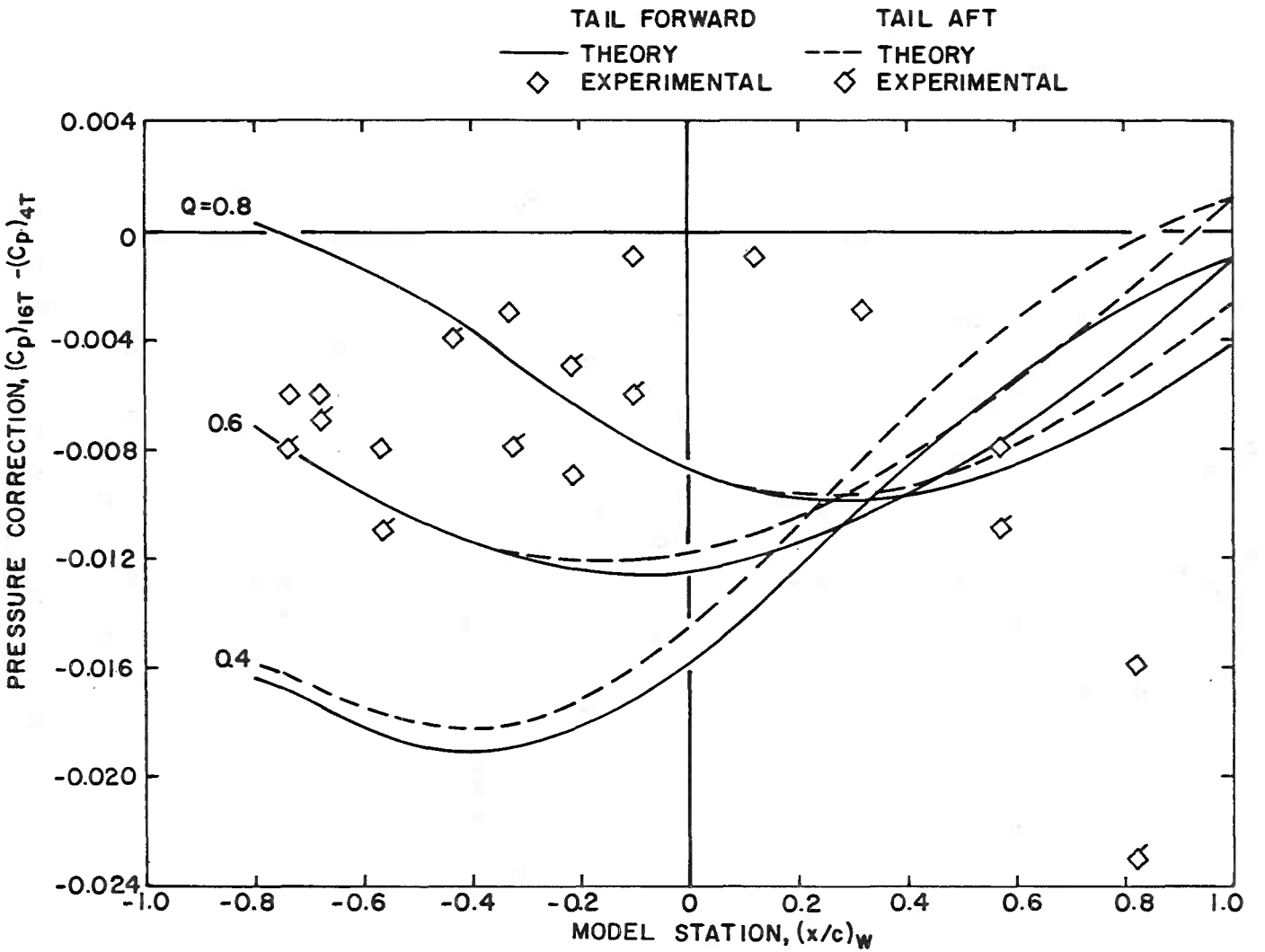

Figure 10. Comparison of experimental and theoretical blockage corrections, $M_\infty = 0.95$.

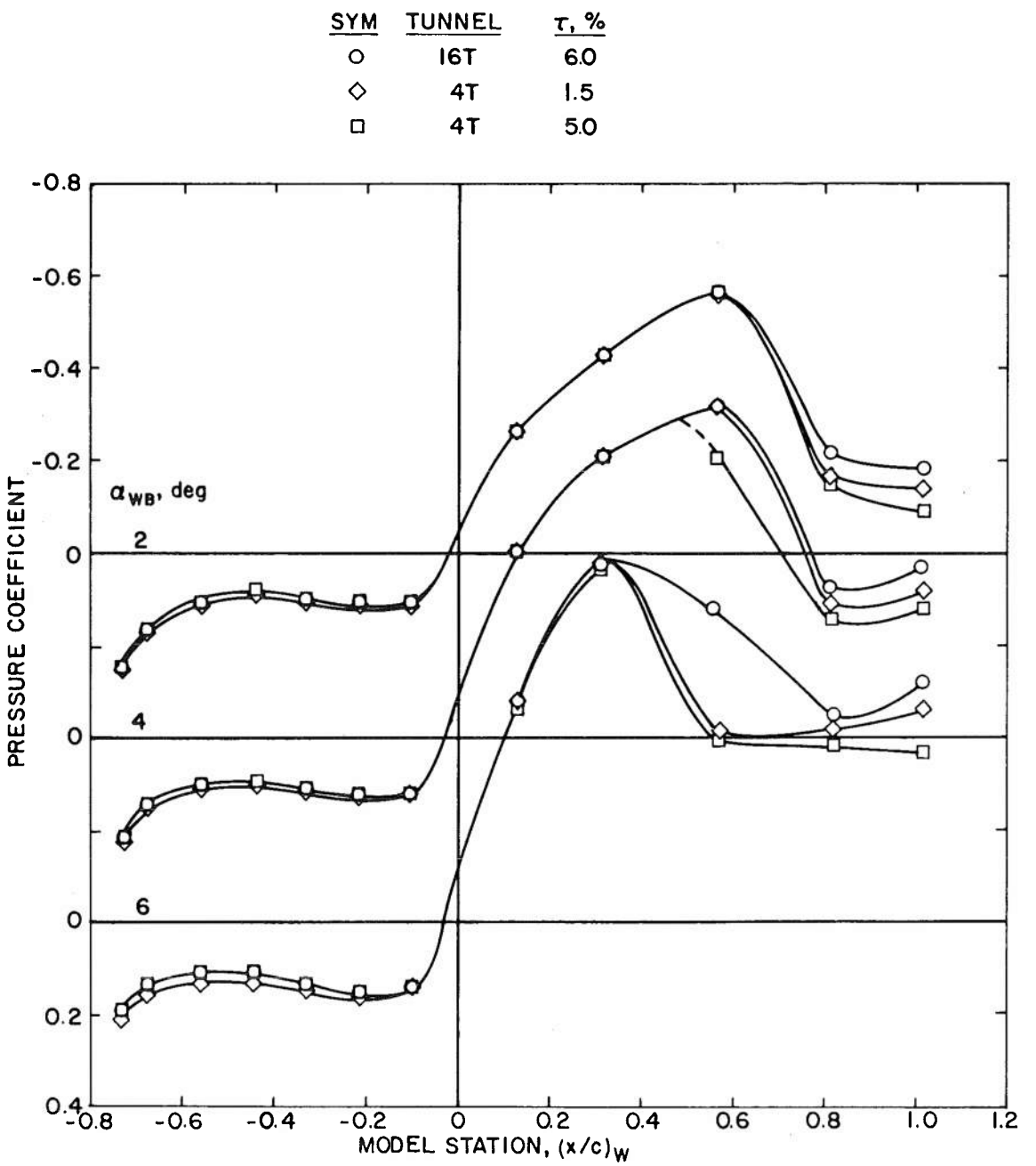

Figure 11. Pressure distributions on the wing centerbody at angle of attack, $M_\infty = 0.95$.

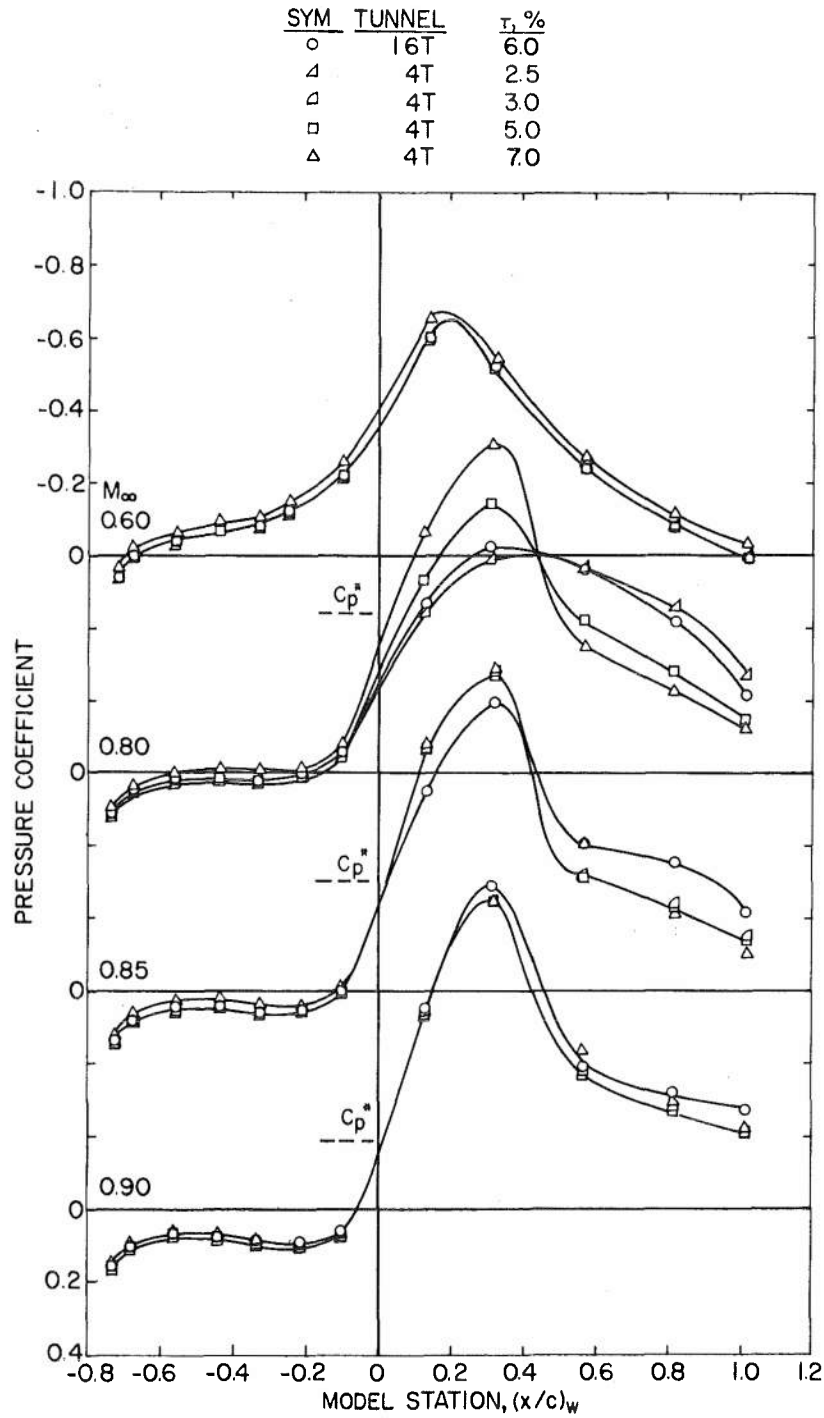

a. Subsonic Mach numbers

Figure 12. Wing centerbody pressure distributions, α_{WB} = 6 deg.

SYM	TUNNEL	τ, %
○	16T	6.0
◇	4T	1.5
◿	4T	2.5
◇	4T	4.5
□	4T	5.0
⌂	4T	6.0
⌂	4T	6.0 (CORRECTED FOR MACH NUMBER GRADIENT)

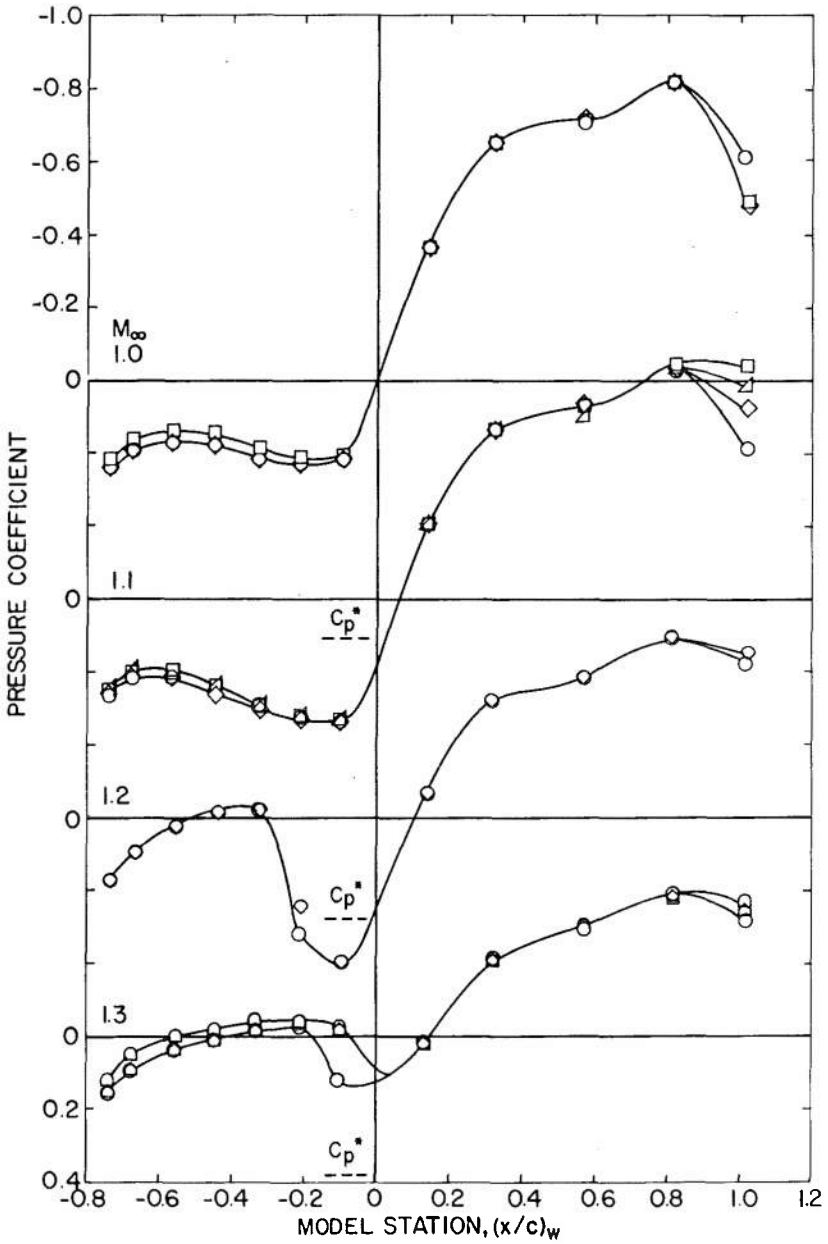

b. Supersonic Mach number
Figure 12. Concluded.

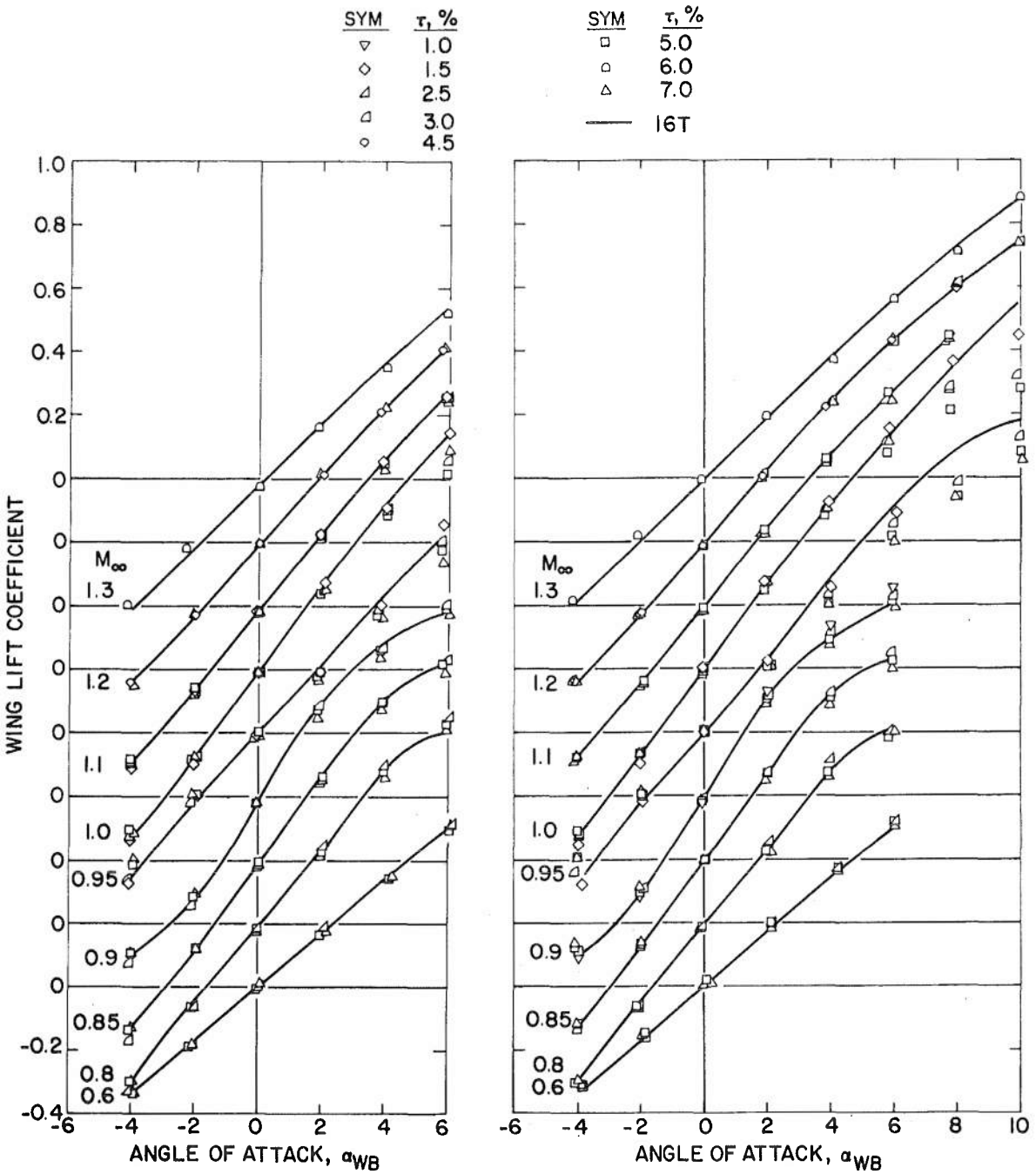

a. Tail forward

b. Tail aft

Figure 13. Wing lift coefficient.

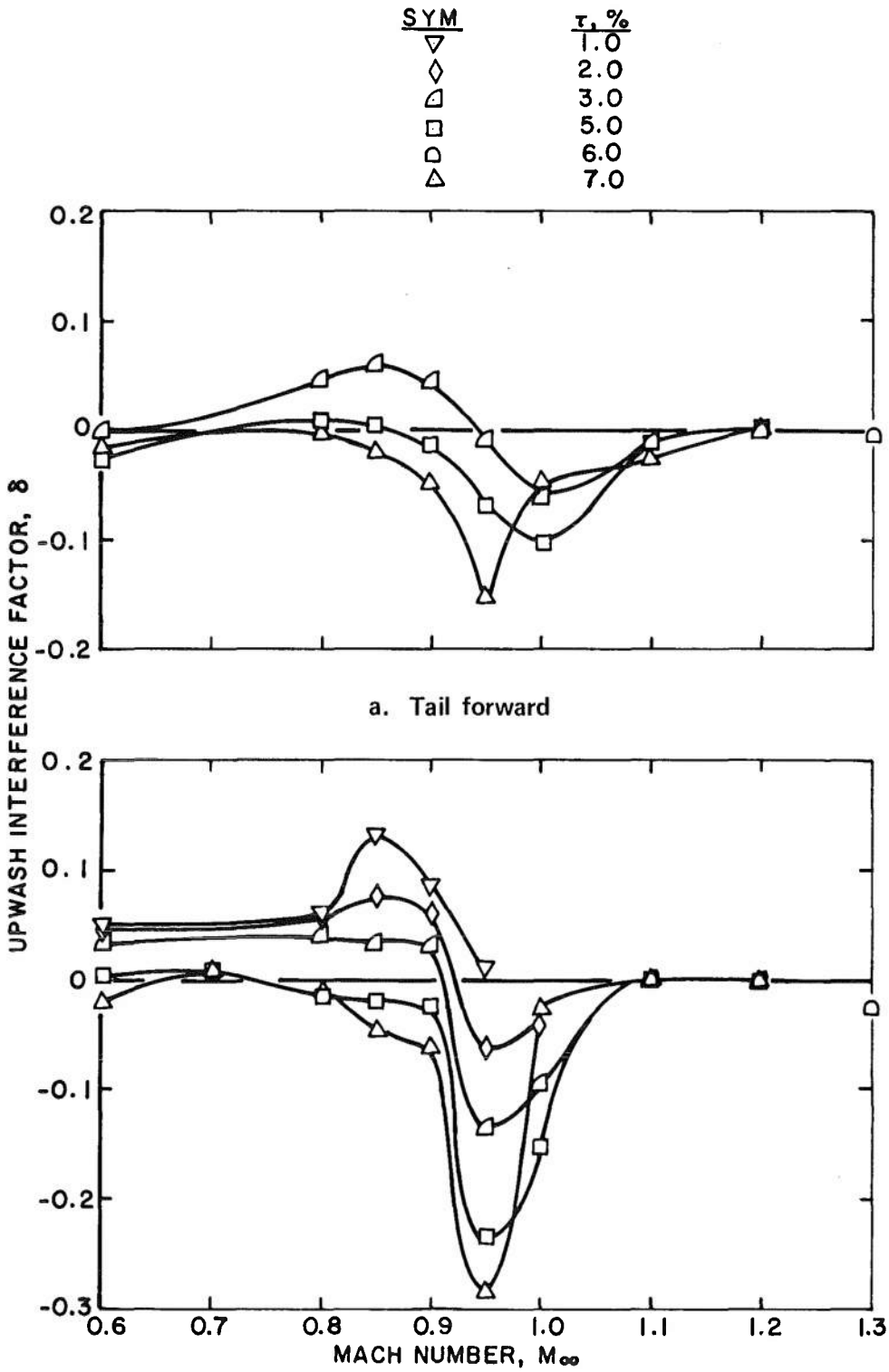

b. Tail aft

Figure 14. Experimentally determined upwash interference factor.

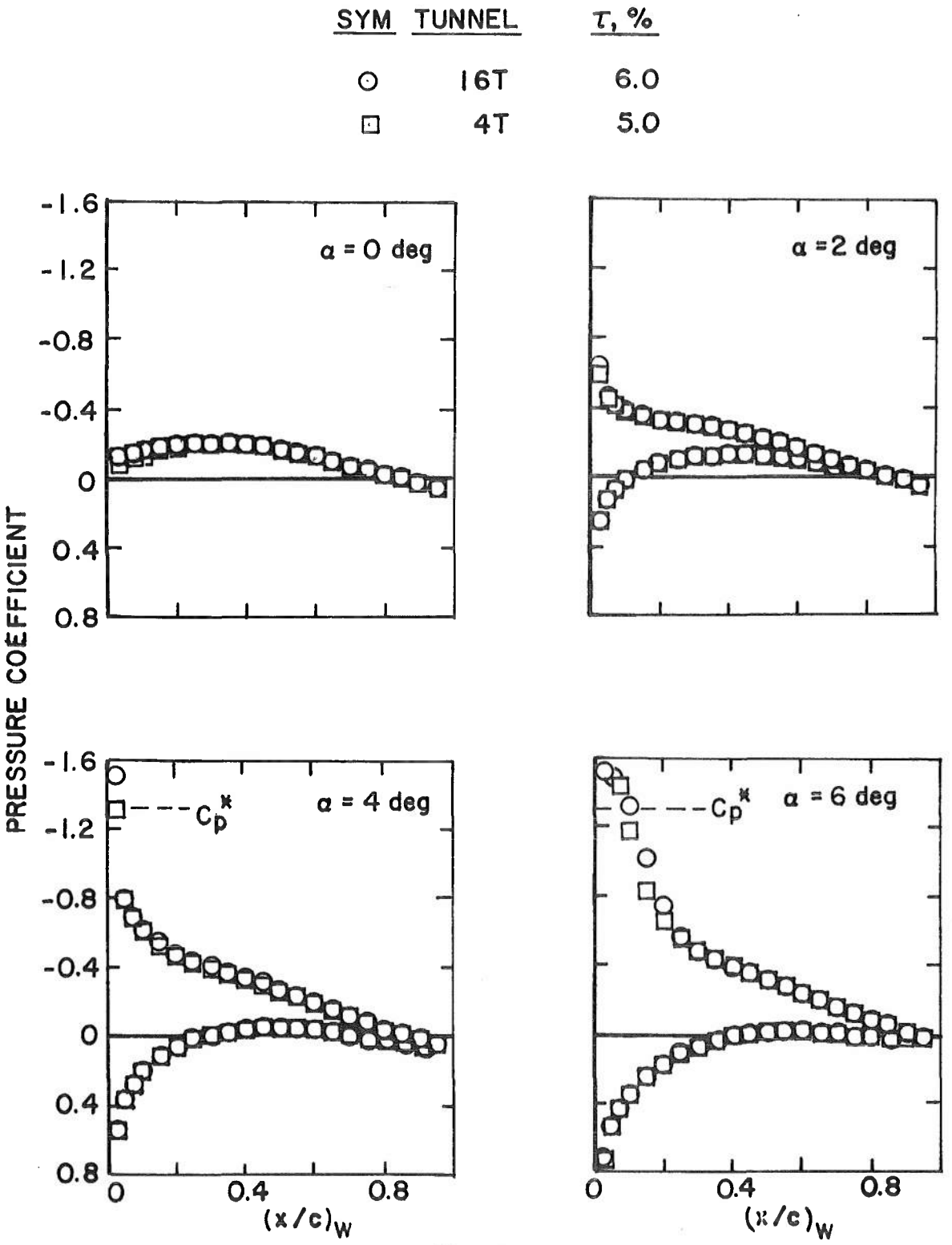

a. $M_\infty = 0.6$

Figure 15. Wing pressure distributions, tail forward.

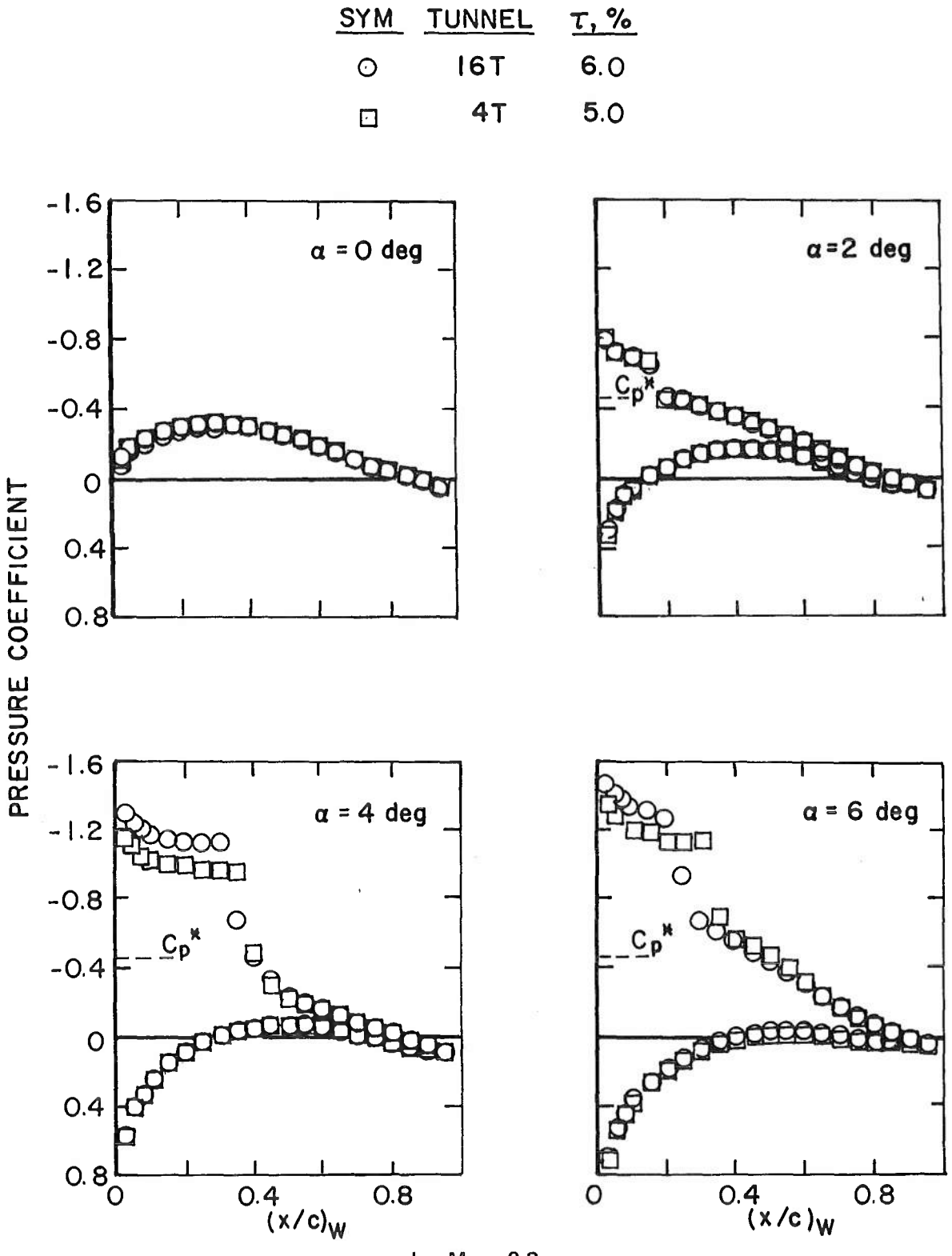

b. $M_\infty = 0.8$

Figure 15. Continued.

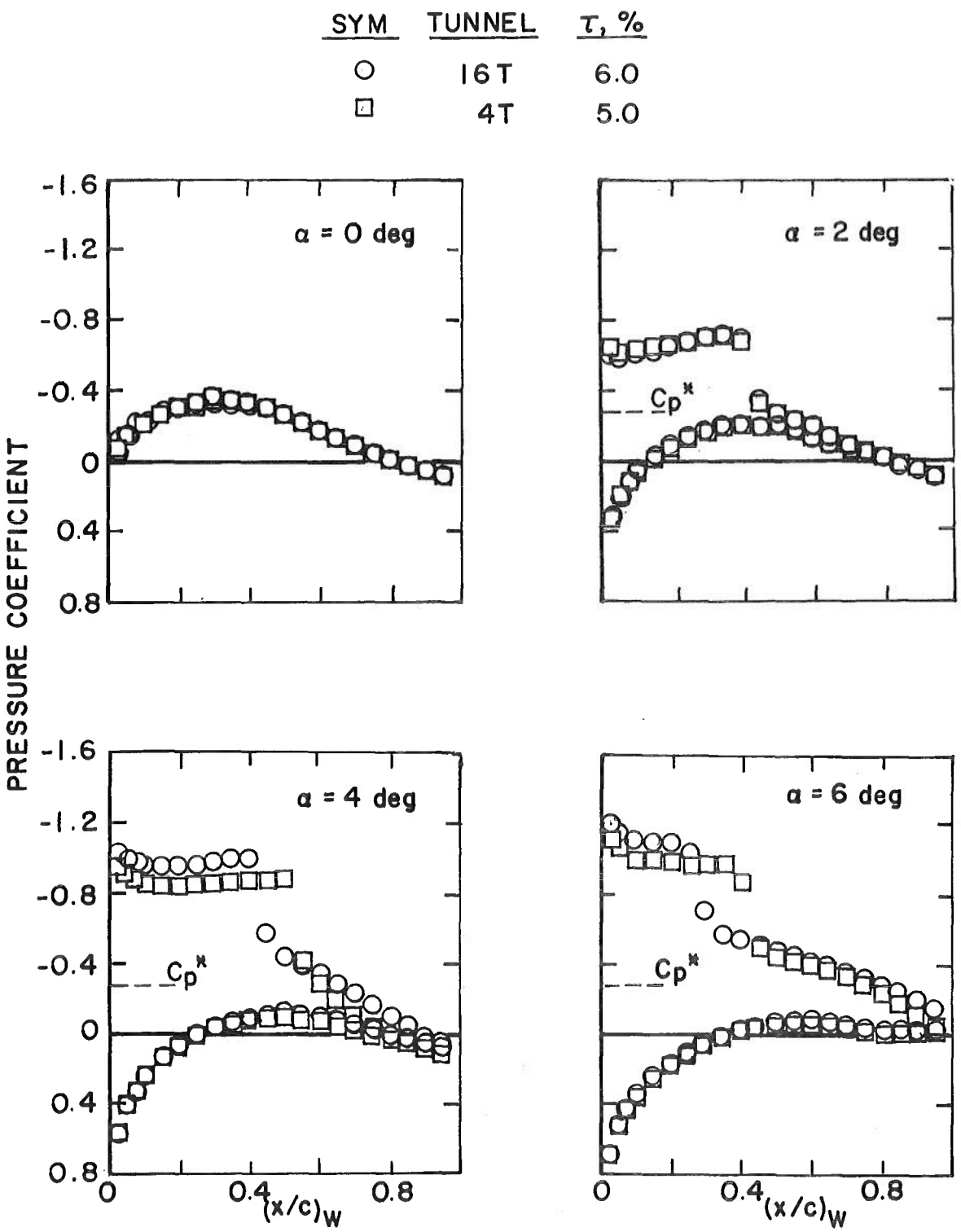

c. $M_\infty = 0.85$
Figure 15. Continued.

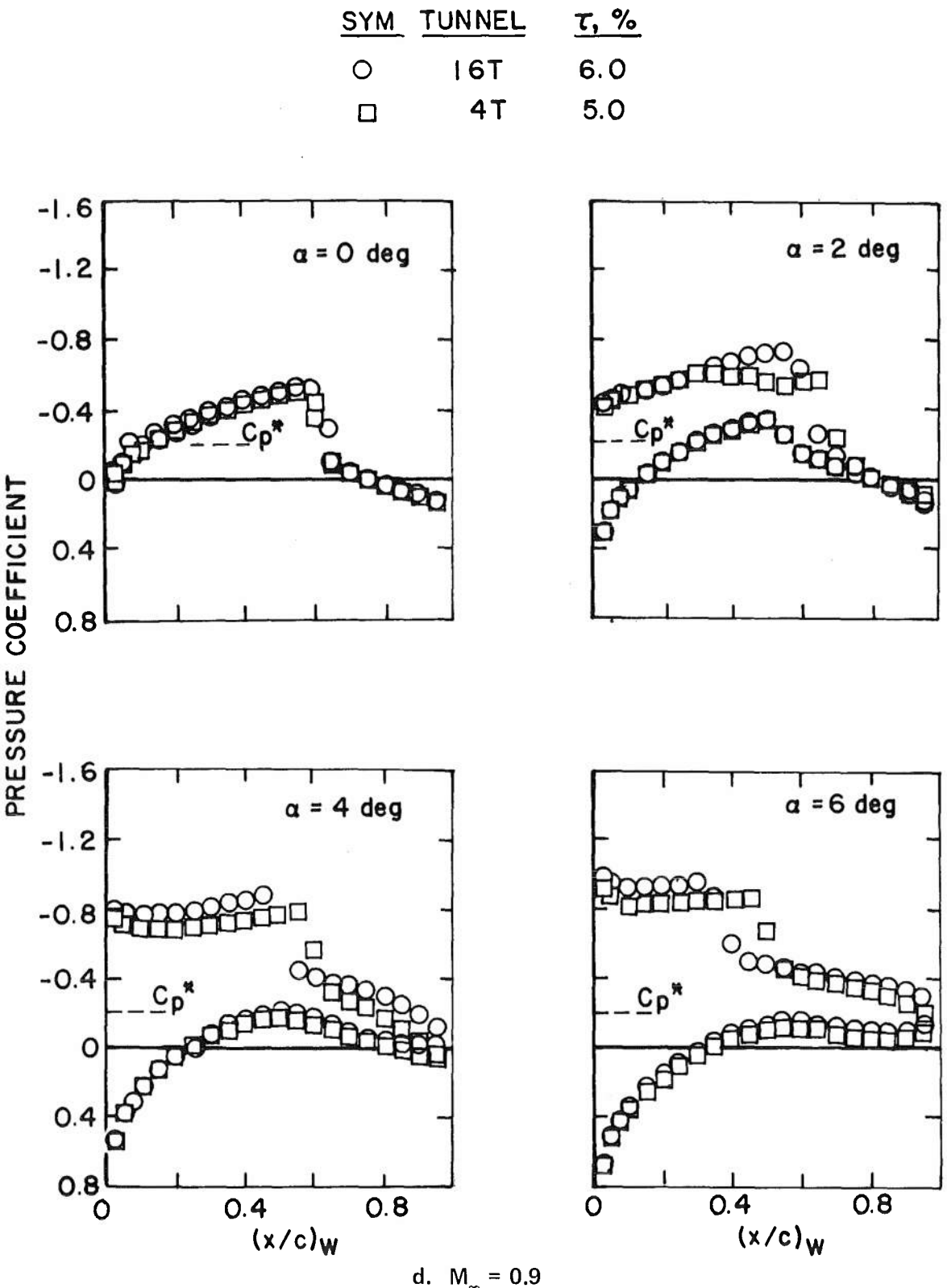

d. $M_\infty = 0.9$

Figure 15. Continued.

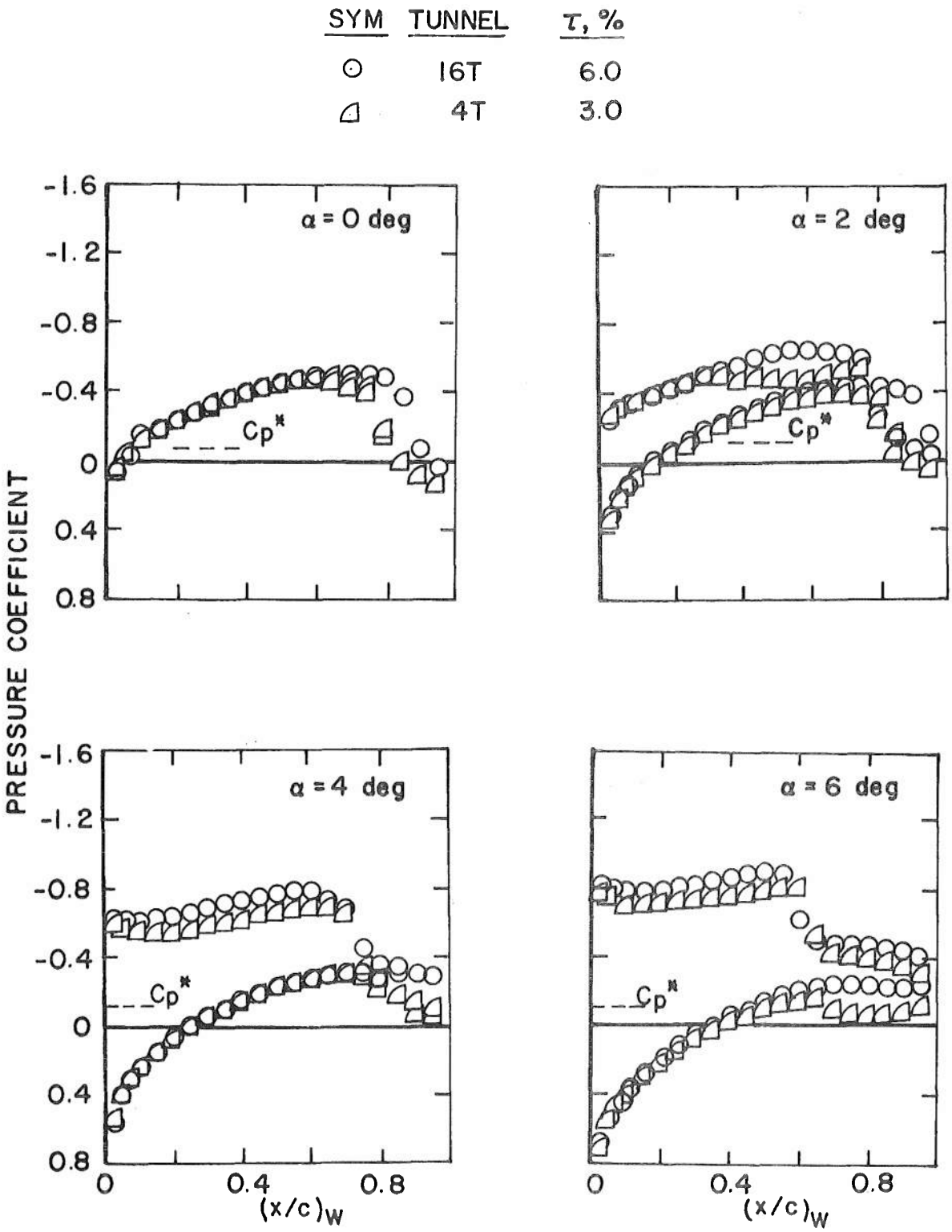

e. $M_\infty = 0.95$

Figure 15. Continued.

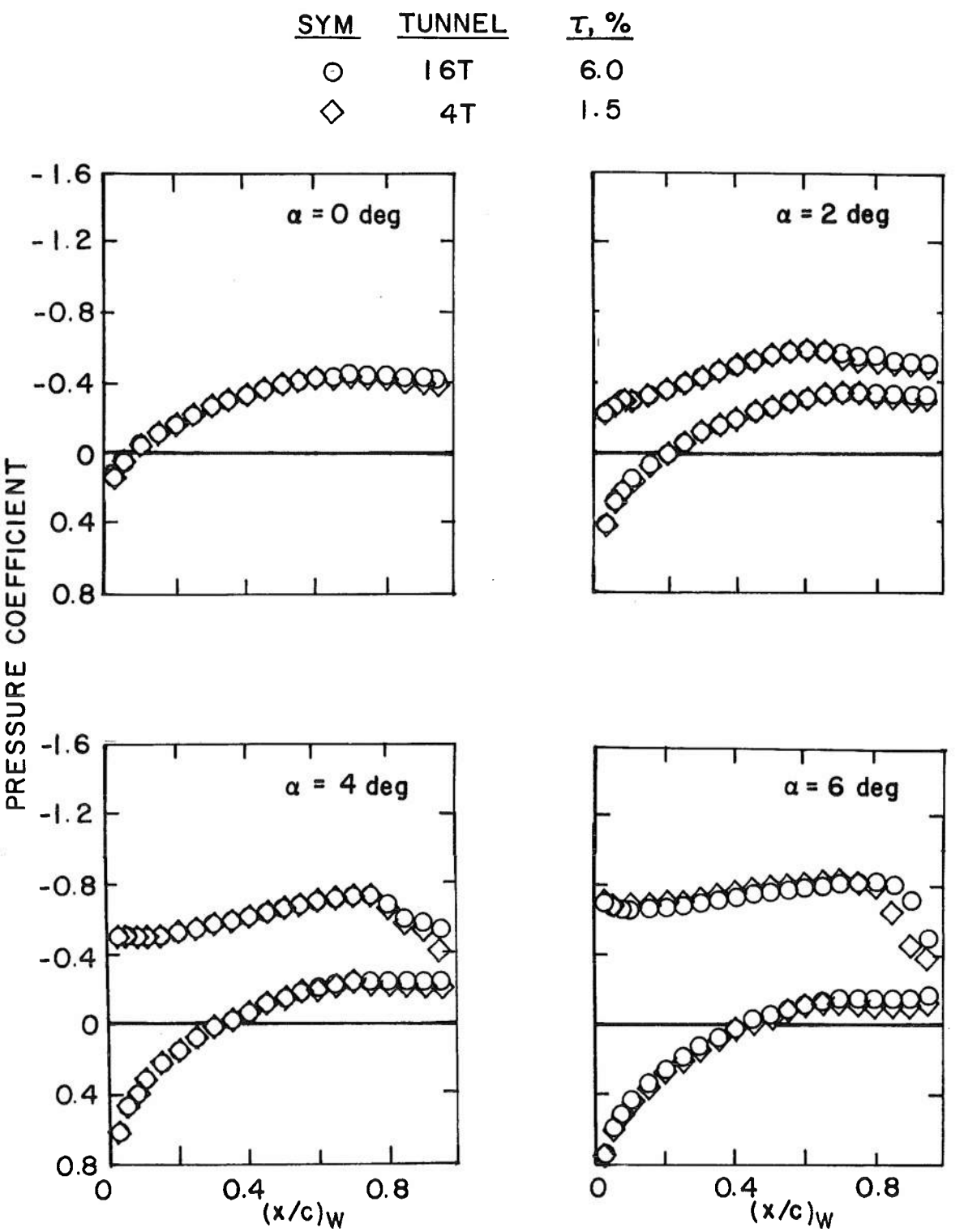

f. $M_\infty = 1.0$

Figure 15. Continued.

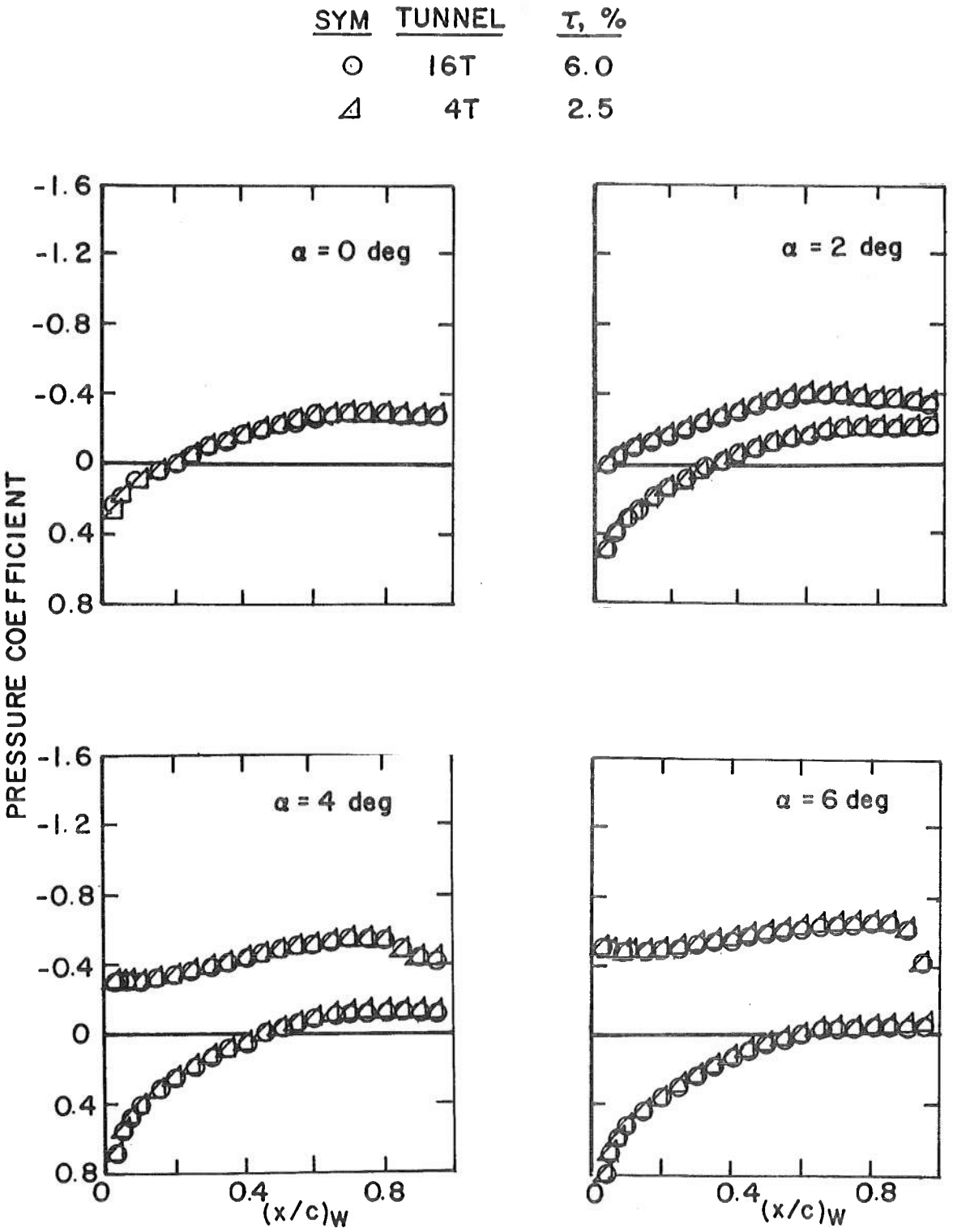

g. $M_\infty = 1.1$

Figure 15. Continued.

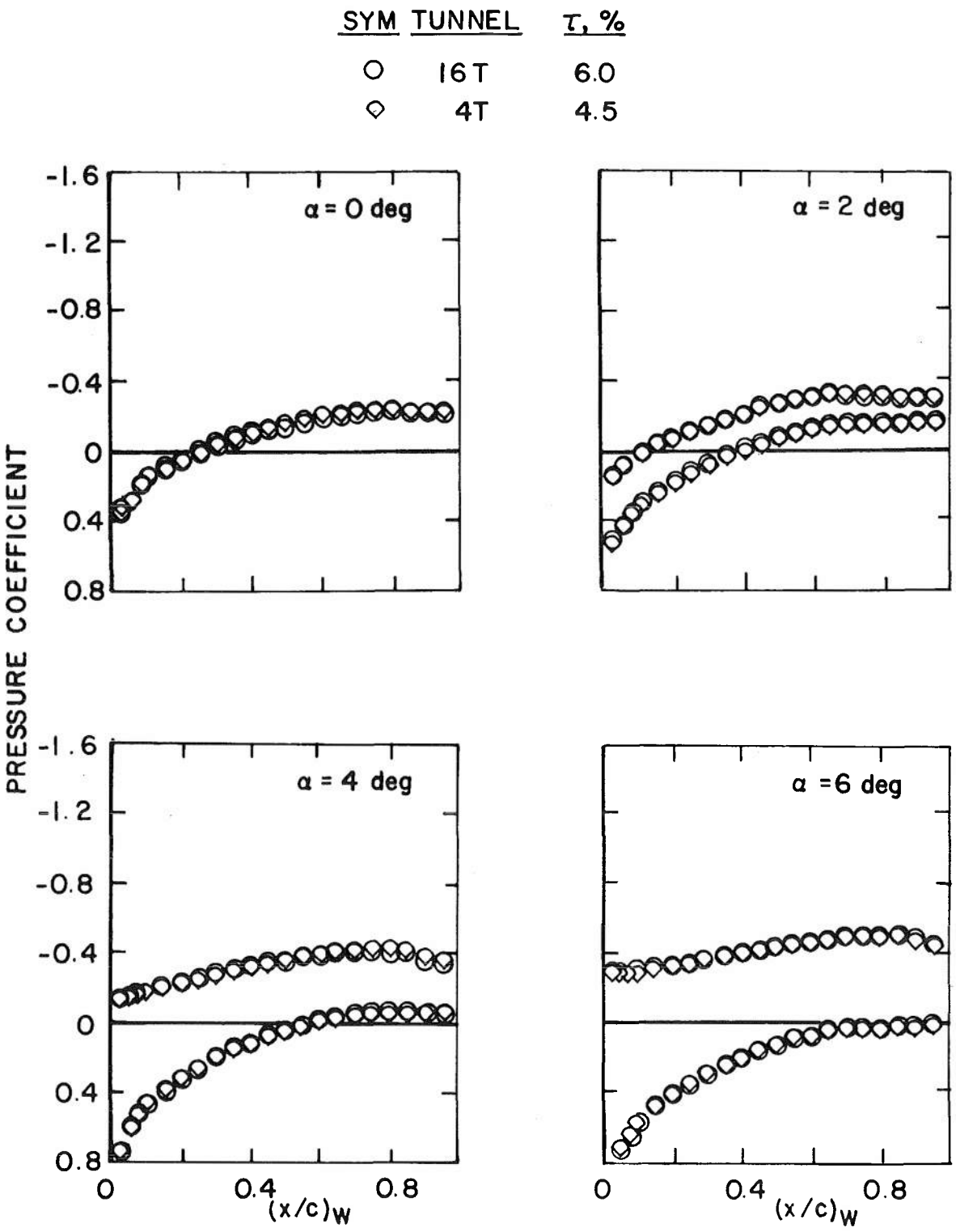

h. $M_\infty = 1.2$
Figure 15. Continued.

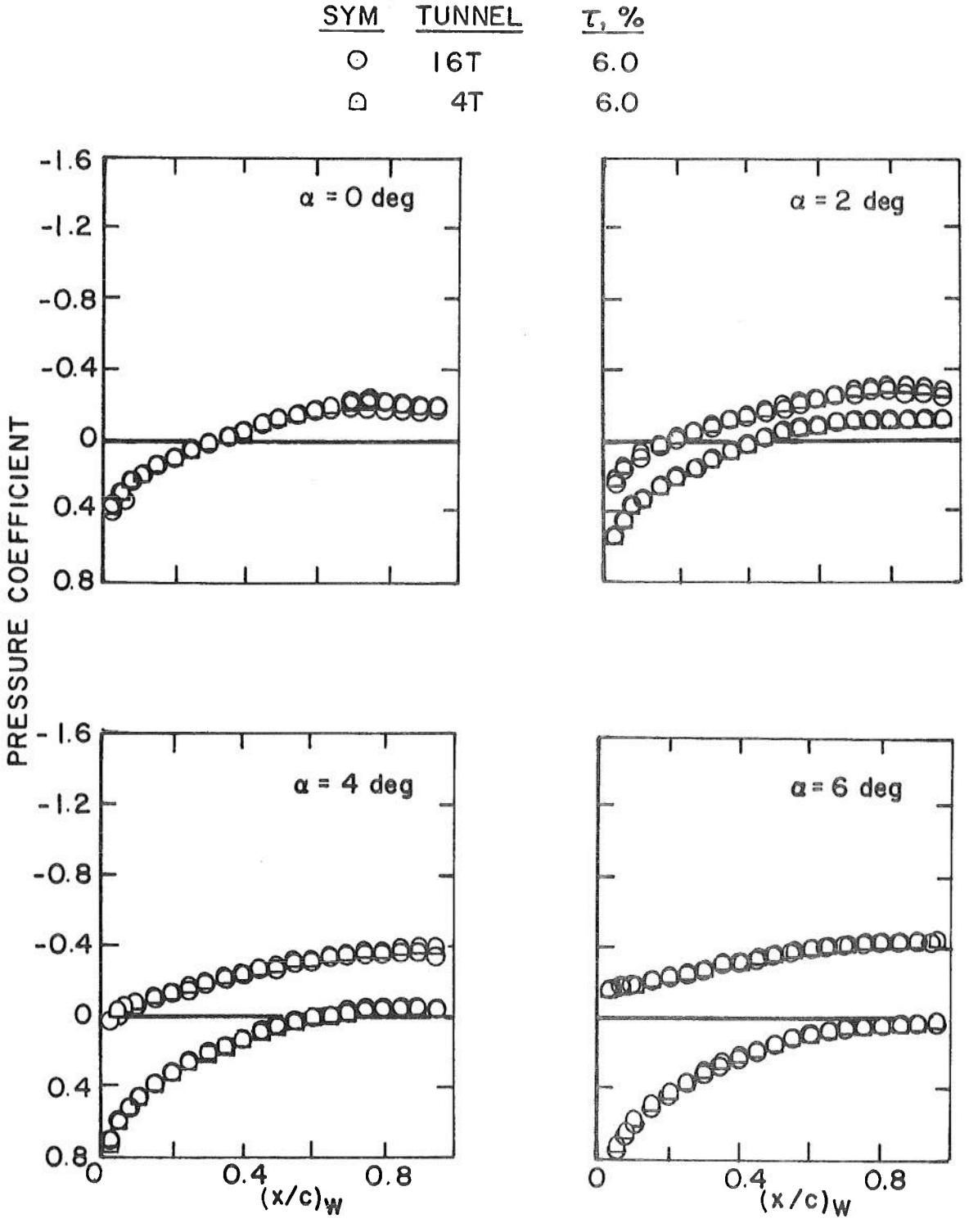

i. $M_\infty = 1.3$

Figure 15. Concluded.

SYM	TUNNEL	τ, %
○	16T	6.0
▽	4T	1.0
◿	4T	3.0
□	4T	5.0
△	4T	7.0

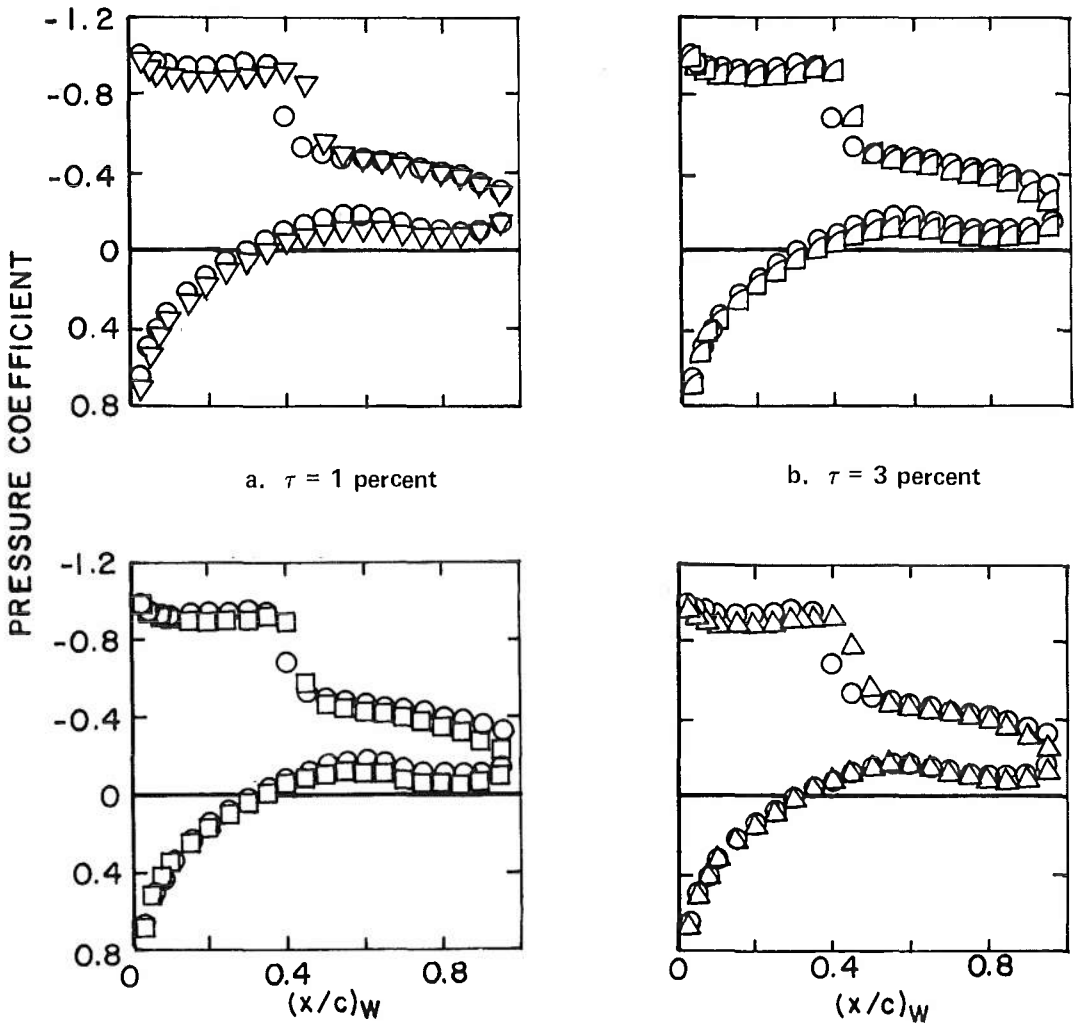

a. τ = 1 percent

b. τ = 3 percent

c. τ = 5 percent

d. τ = 7 percent

Figure 16. Effect of porosity on the wing pressure distribution, tail aft, M_∞ = 0.9, α_{WB} = 6 deg.

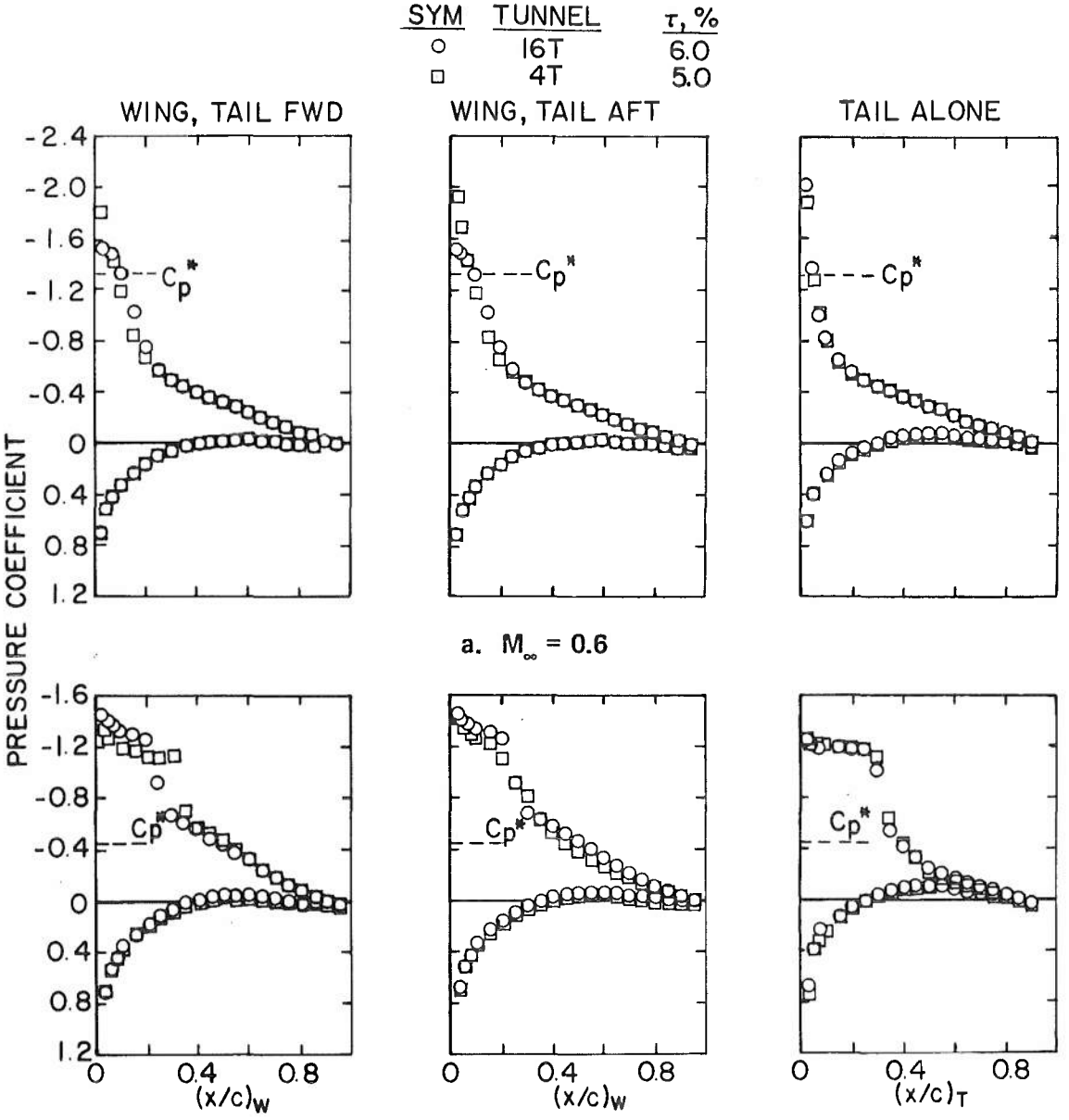

a. $M_\infty = 0.6$

b. $M_\infty = 0.8$

Figure 17. Wall interference on the three configurations at supercritical flow conditions, $\alpha_{WB} \approx \alpha_{TB} \approx 6$ deg.

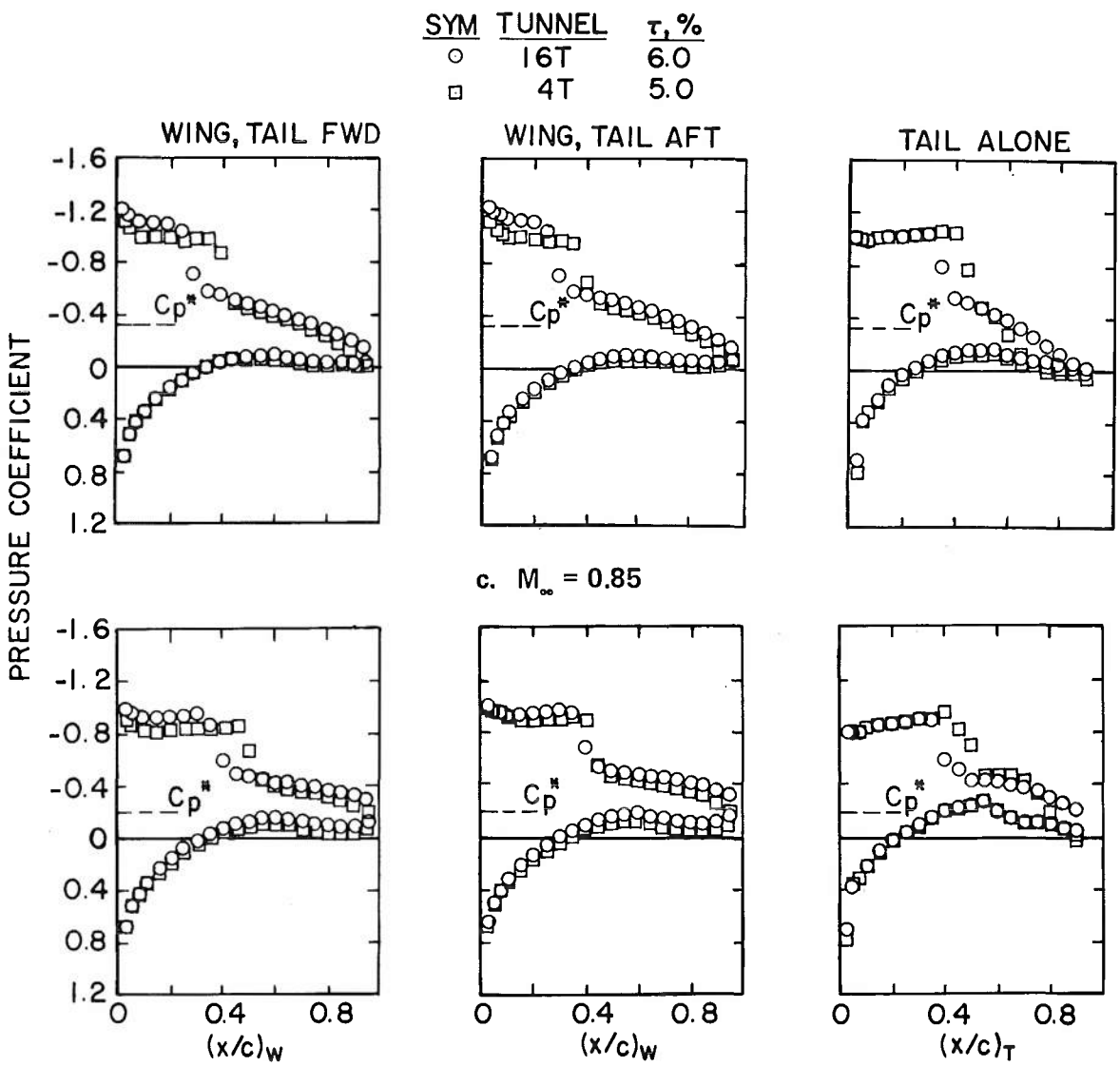

c. $M_\infty = 0.85$

d. $M_\infty = 0.90$

Figure 17. Continued.

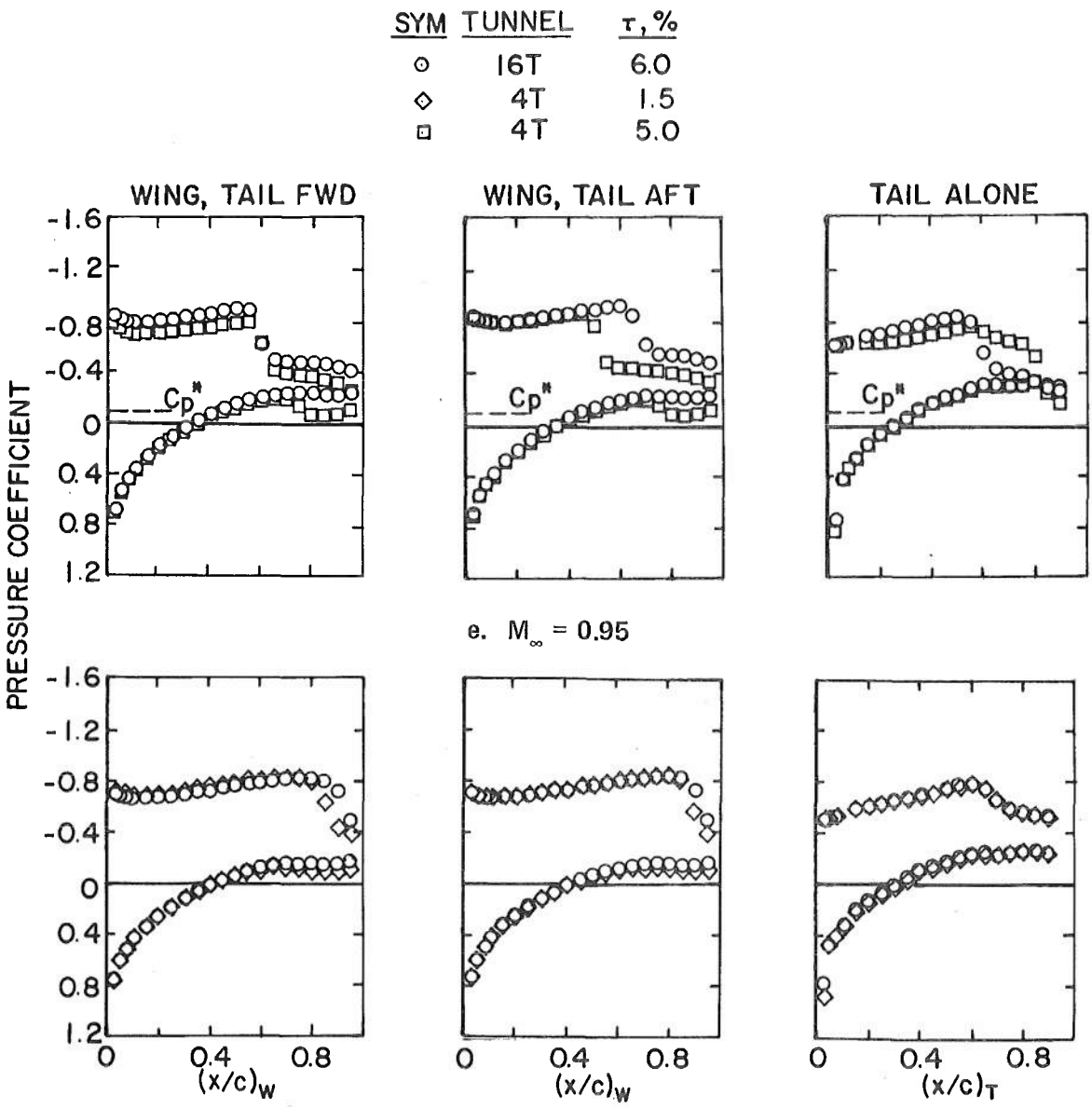

e. $M_\infty = 0.95$

f. $M_\infty = 1.00$

Figure 17. Concluded.

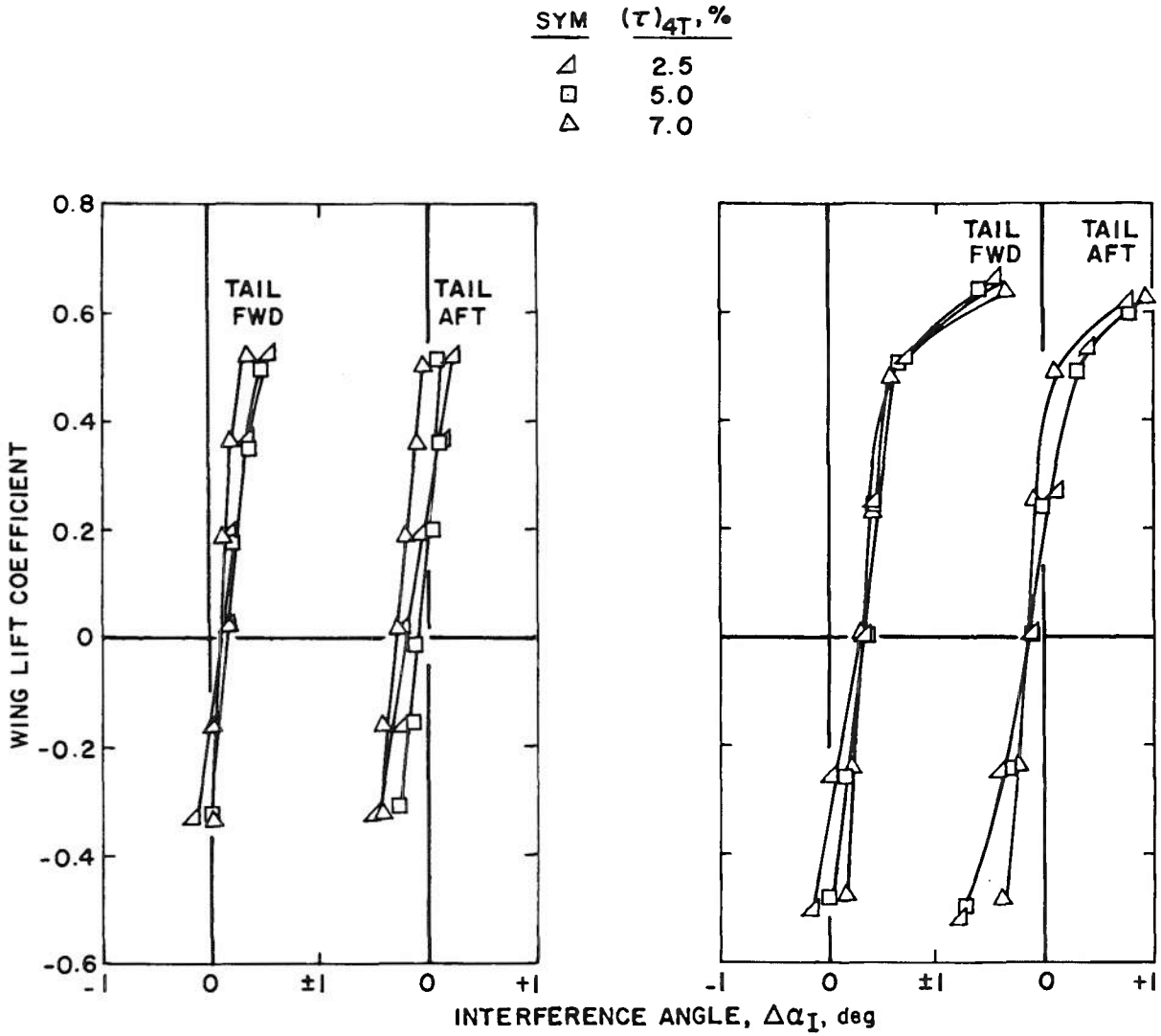

a. $M_\infty = 0.6$

b. $M_\infty = 0.8$

Figure 18. Interference angle at the tail centerbody position.

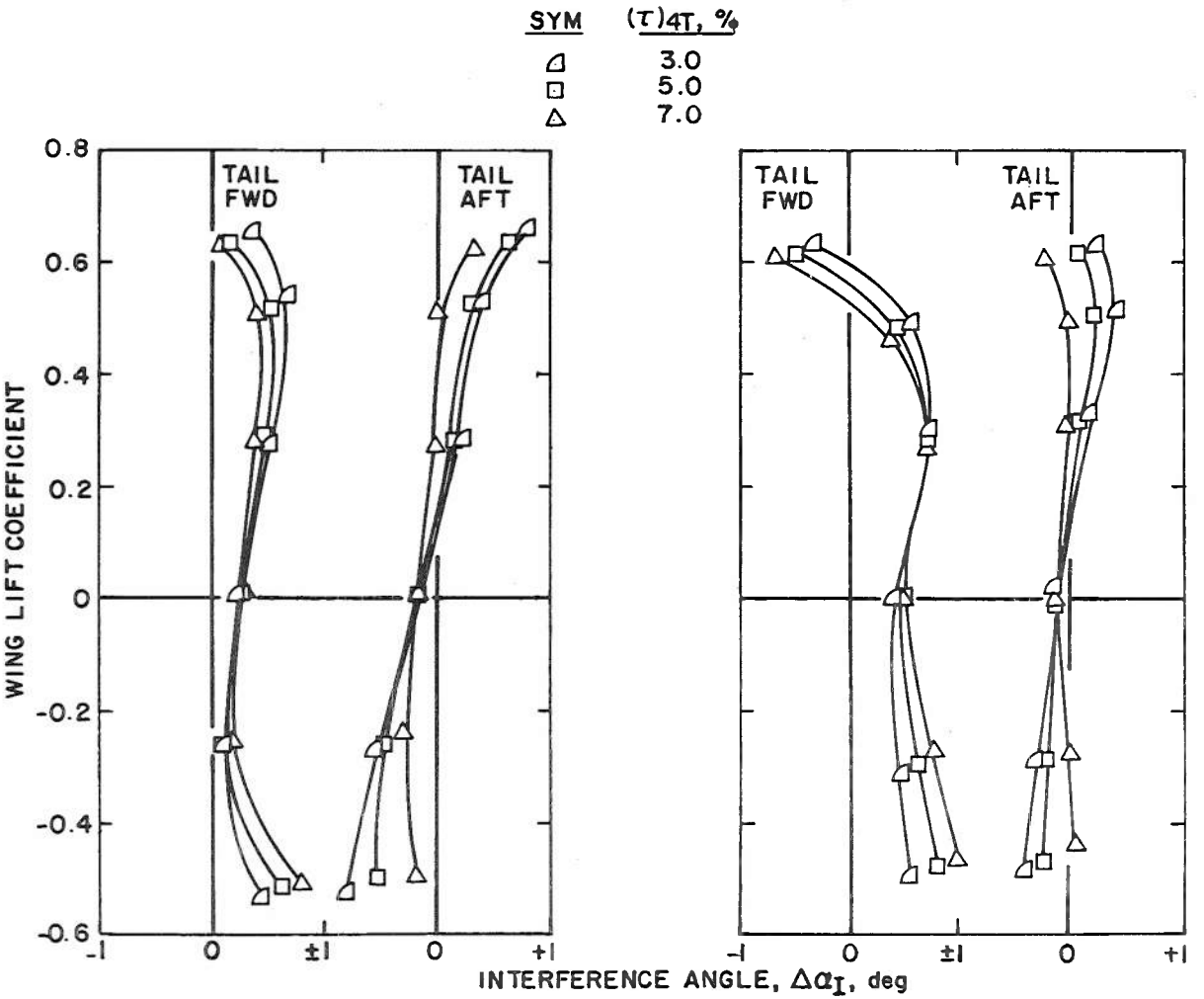

c. $M_\infty = 0.85$

d. $M_\infty = 0.90$

Figure 18. Continued.

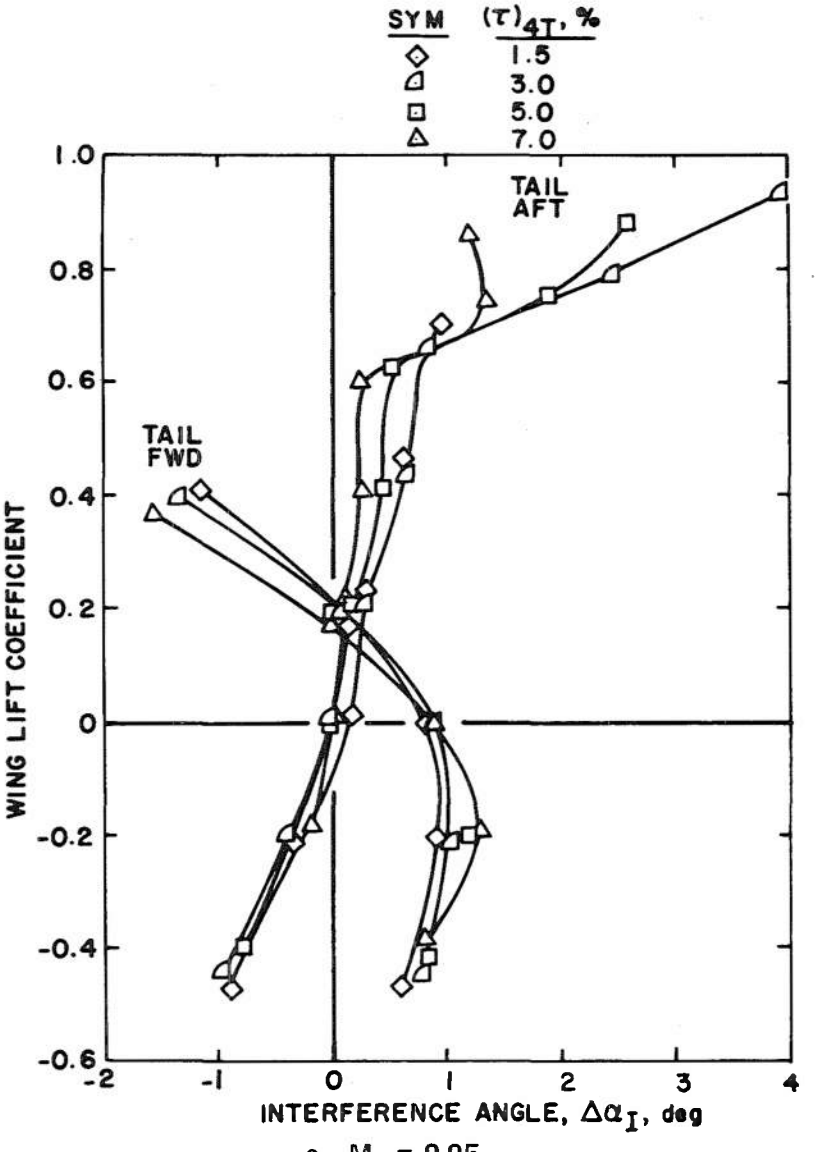

e. $M_\infty = 0.95$

Figure 18. Continued.

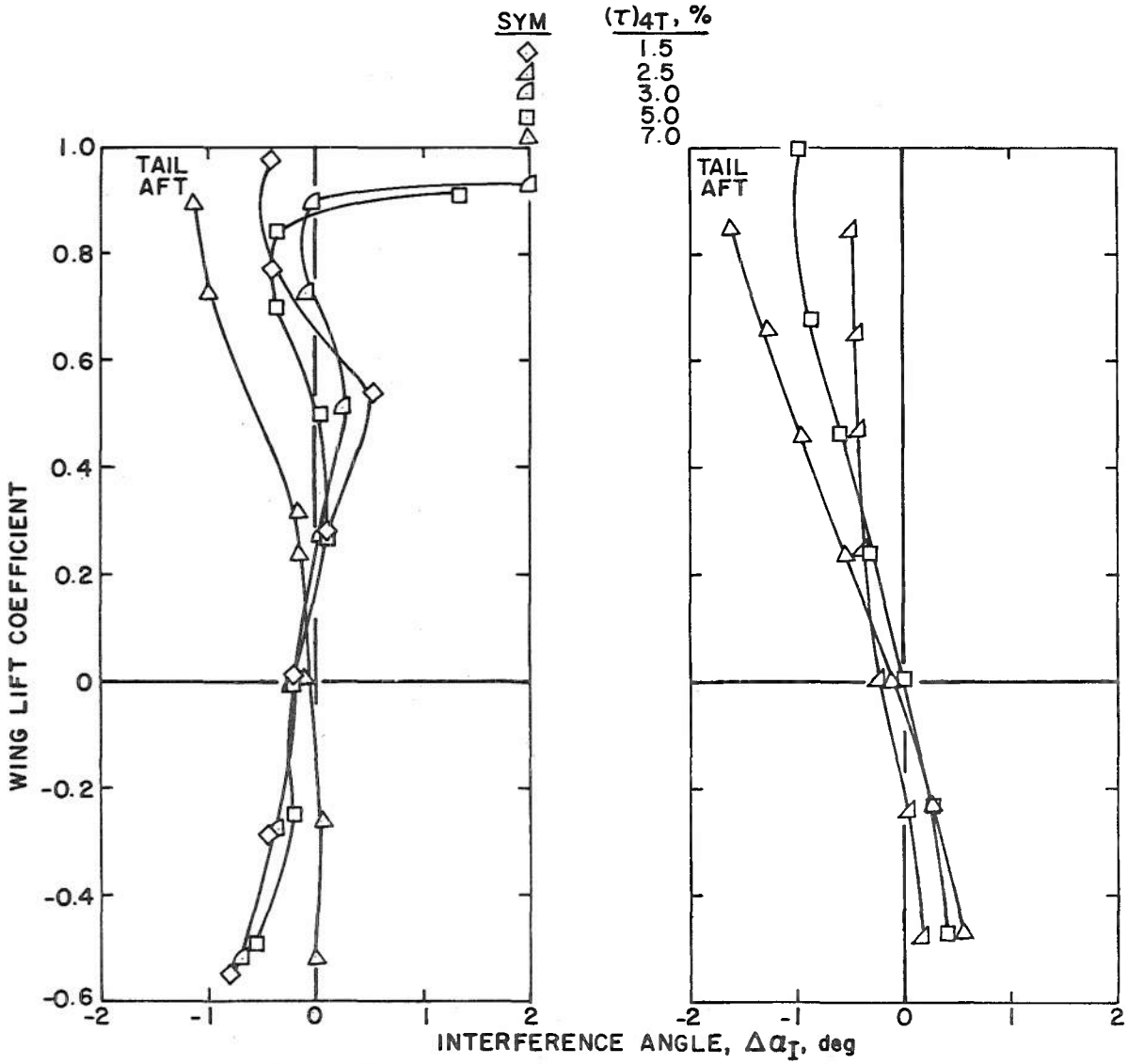

f. $M_\infty = 1.00$

g. $M_\infty = 1.10$

Figure 18. Continued.

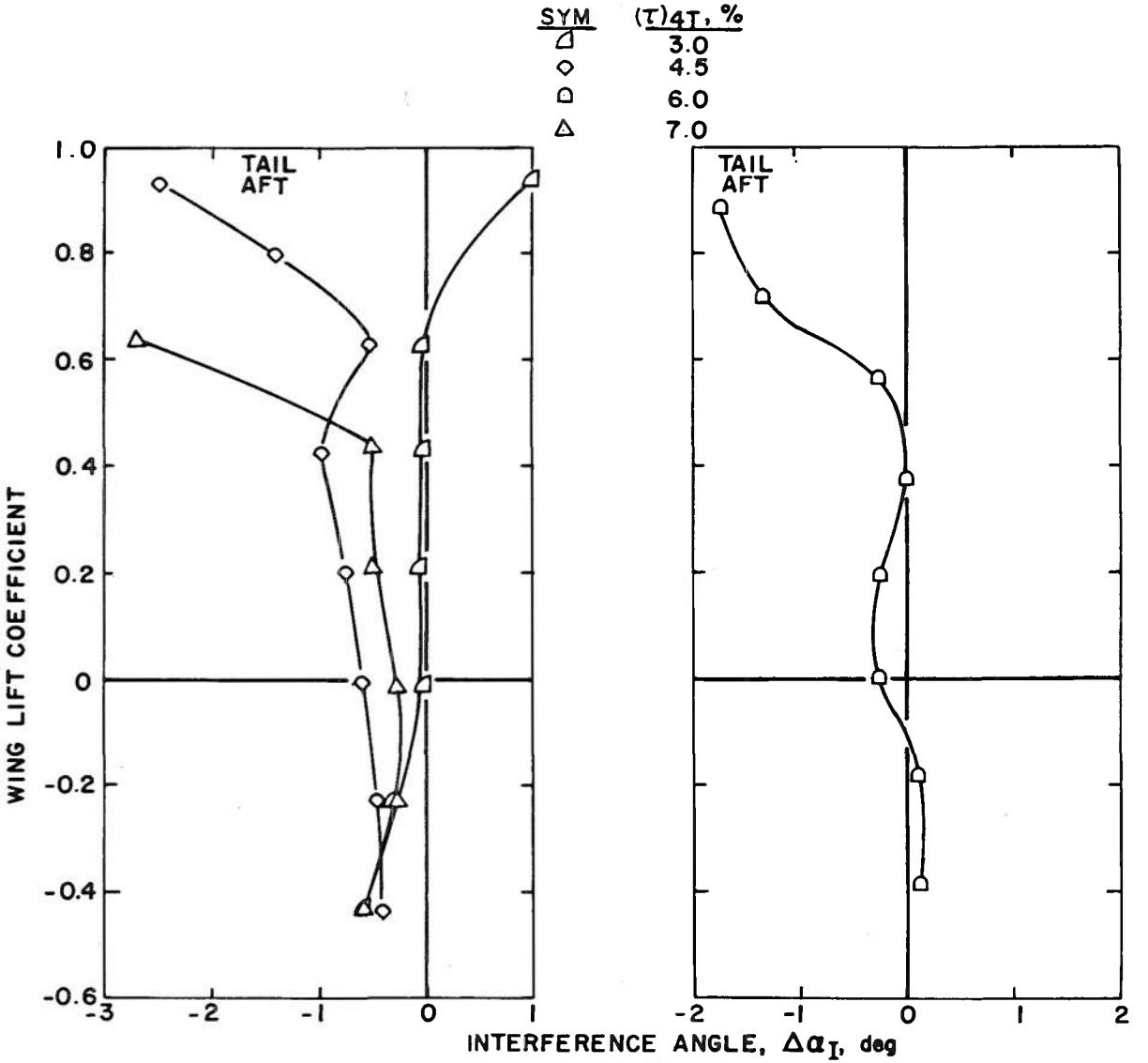

h. $M_\infty = 1.20$ i. $M_\infty = 1.30$

Figure 18. Concluded.

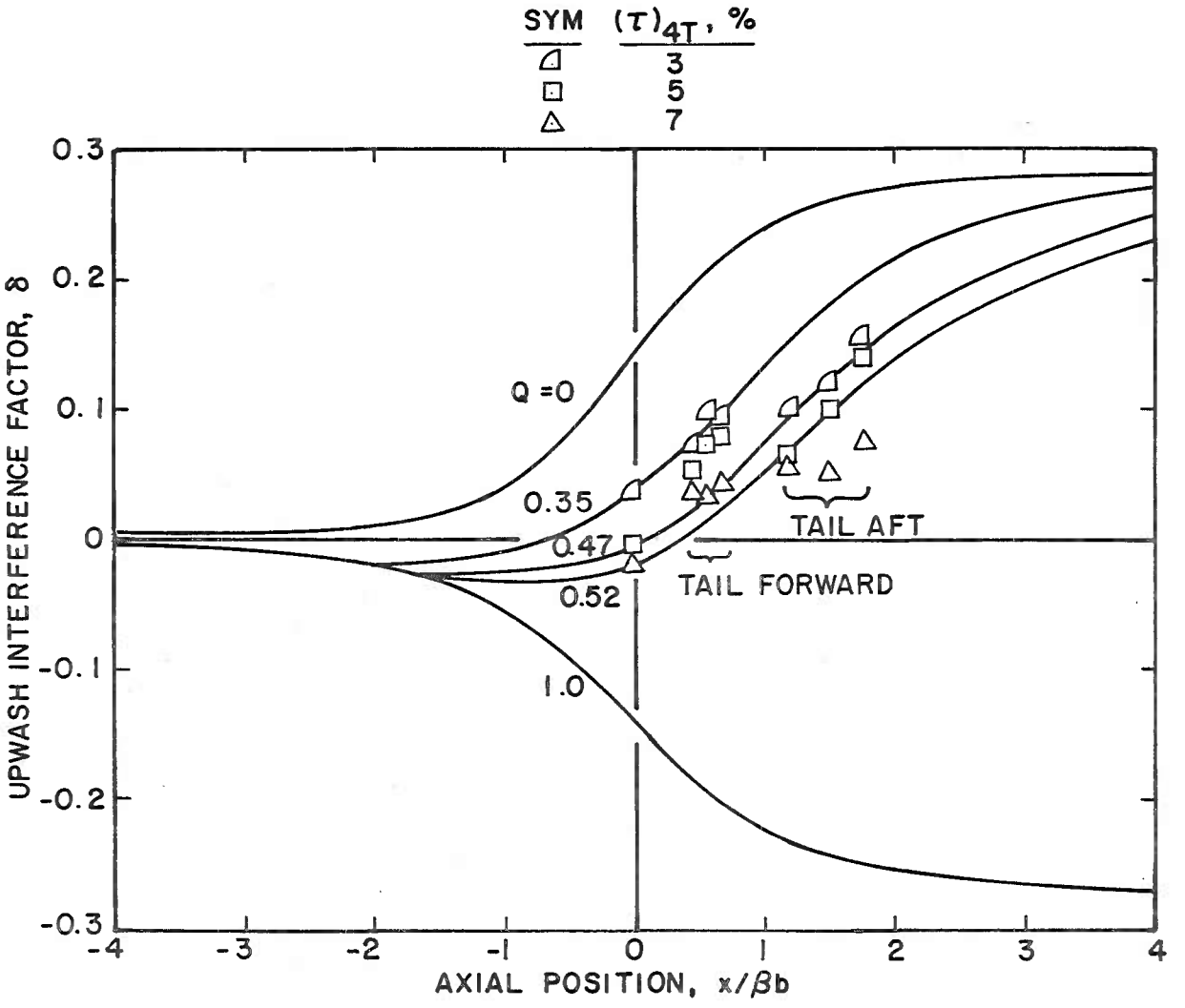

Figure 19. Comparison of theoretical and experimental upwash interference factors.

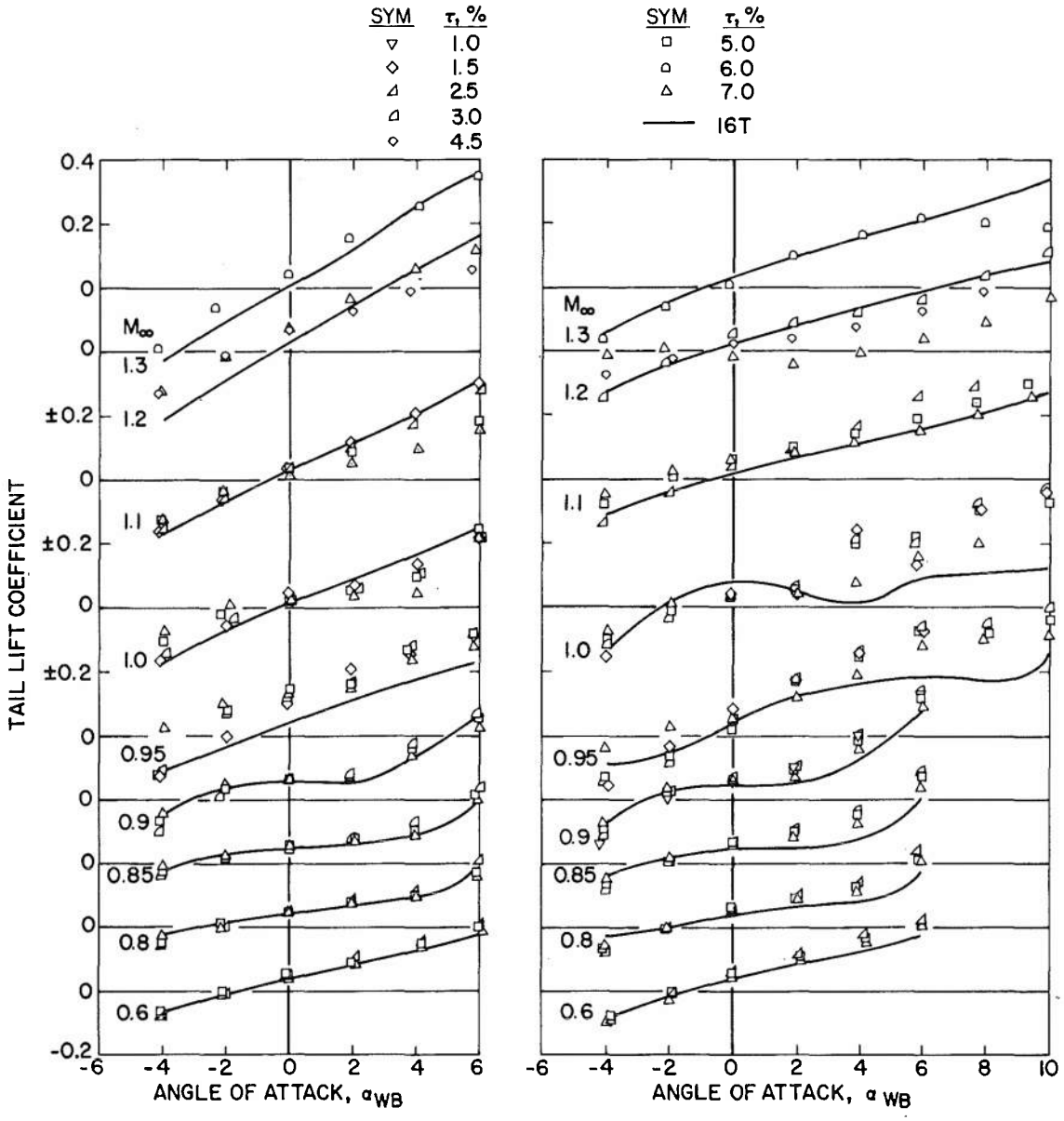

a. Tail forward

b. Tail aft

Figure 20. Effect of porosity on tail lift coefficient.

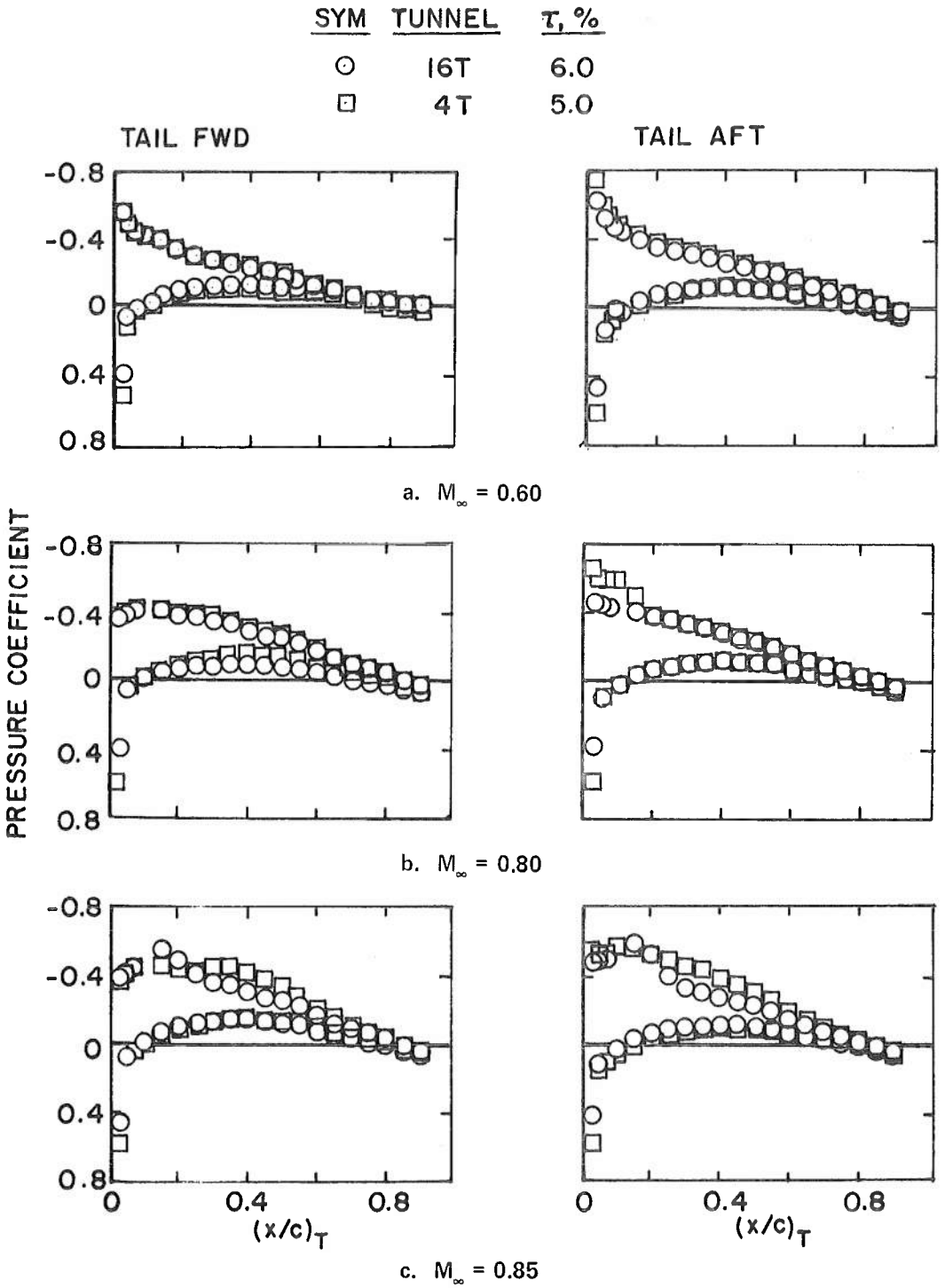

Figure 21. Tail pressure distributions, α_{WB} = 6 deg.

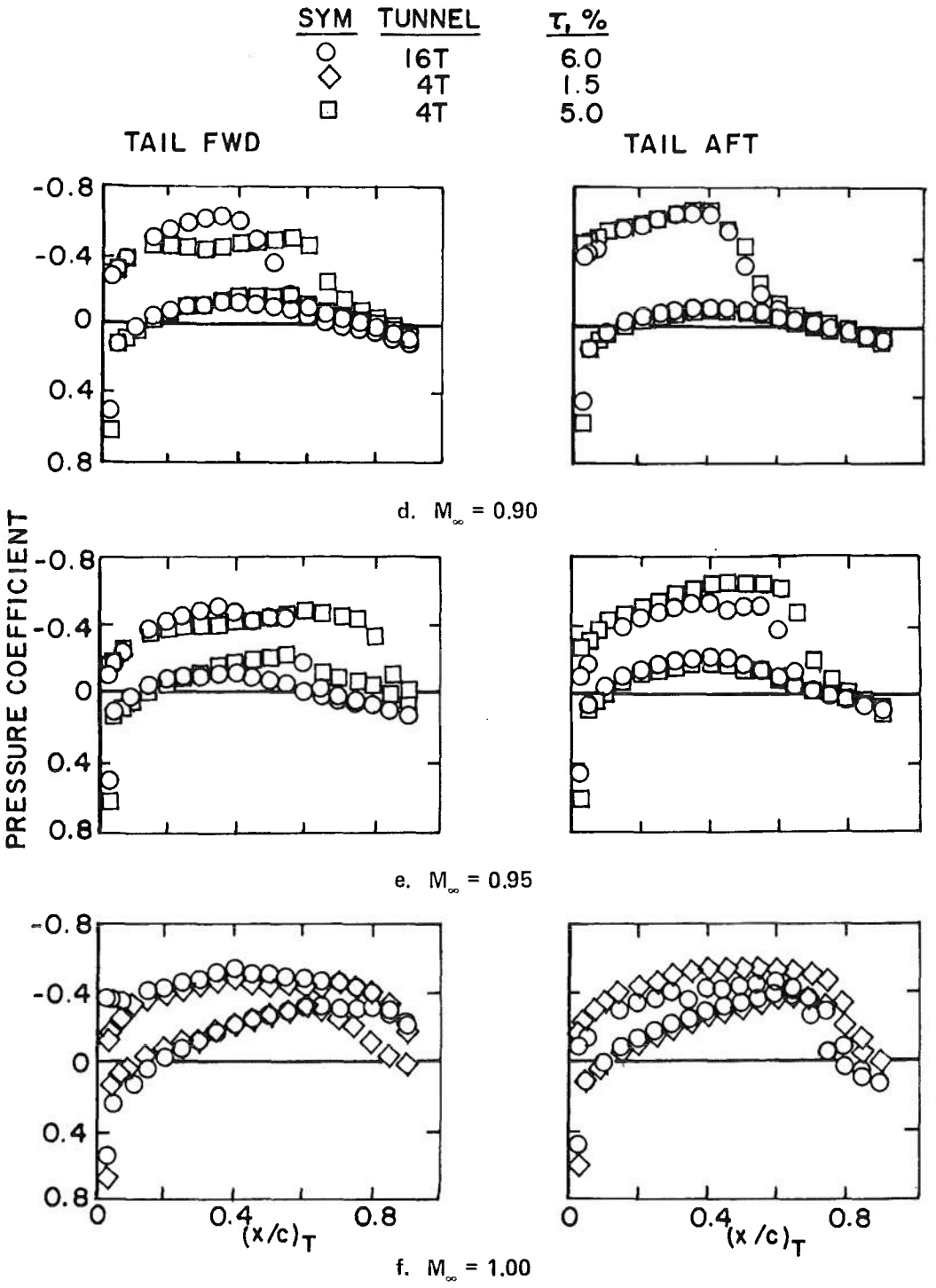

d. $M_\infty = 0.90$

e. $M_\infty = 0.95$

f. $M_\infty = 1.00$

Figure 21. Continued.

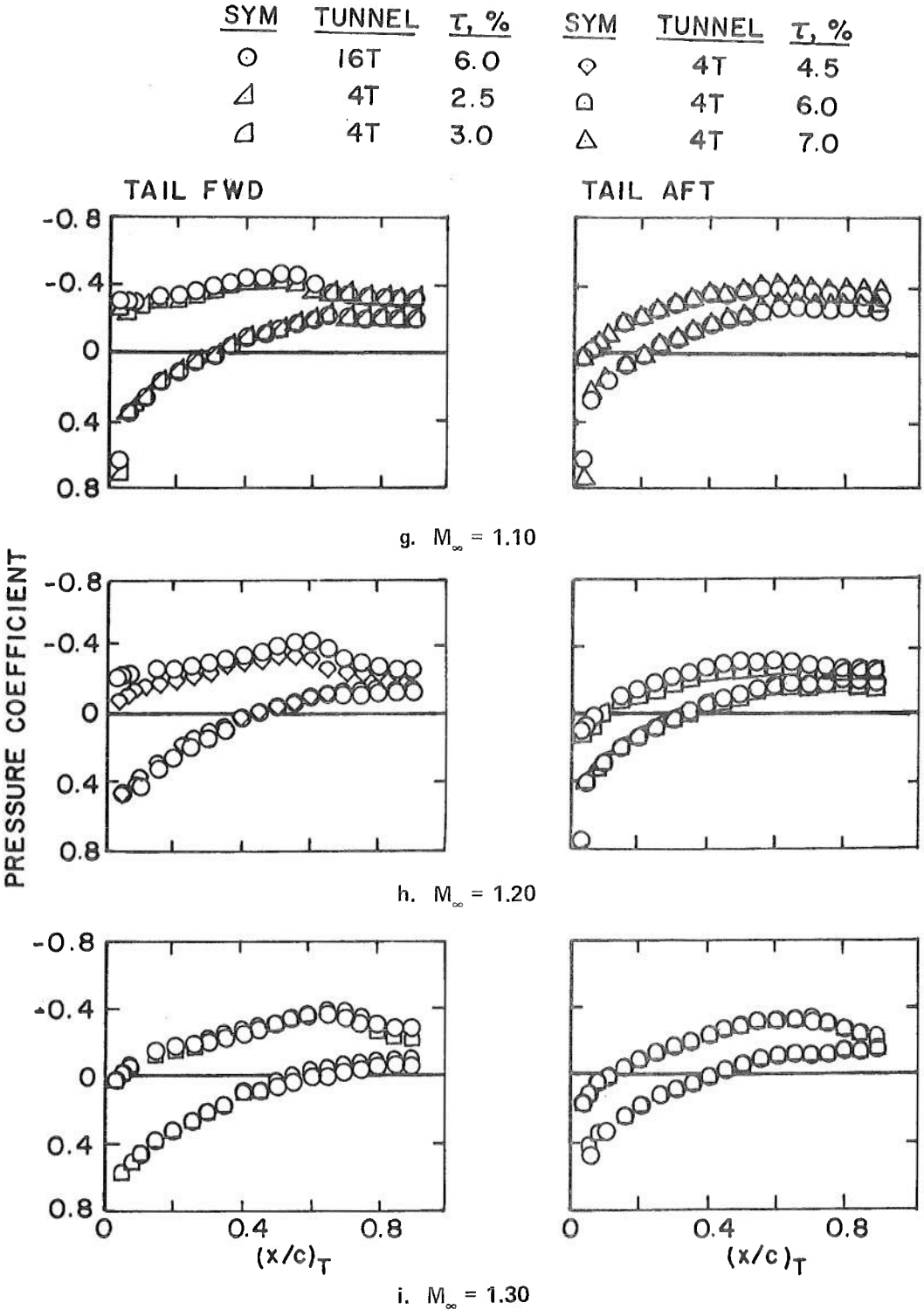

g. $M_\infty = 1.10$

h. $M_\infty = 1.20$

i. $M_\infty = 1.30$

Figure 21. Concluded.

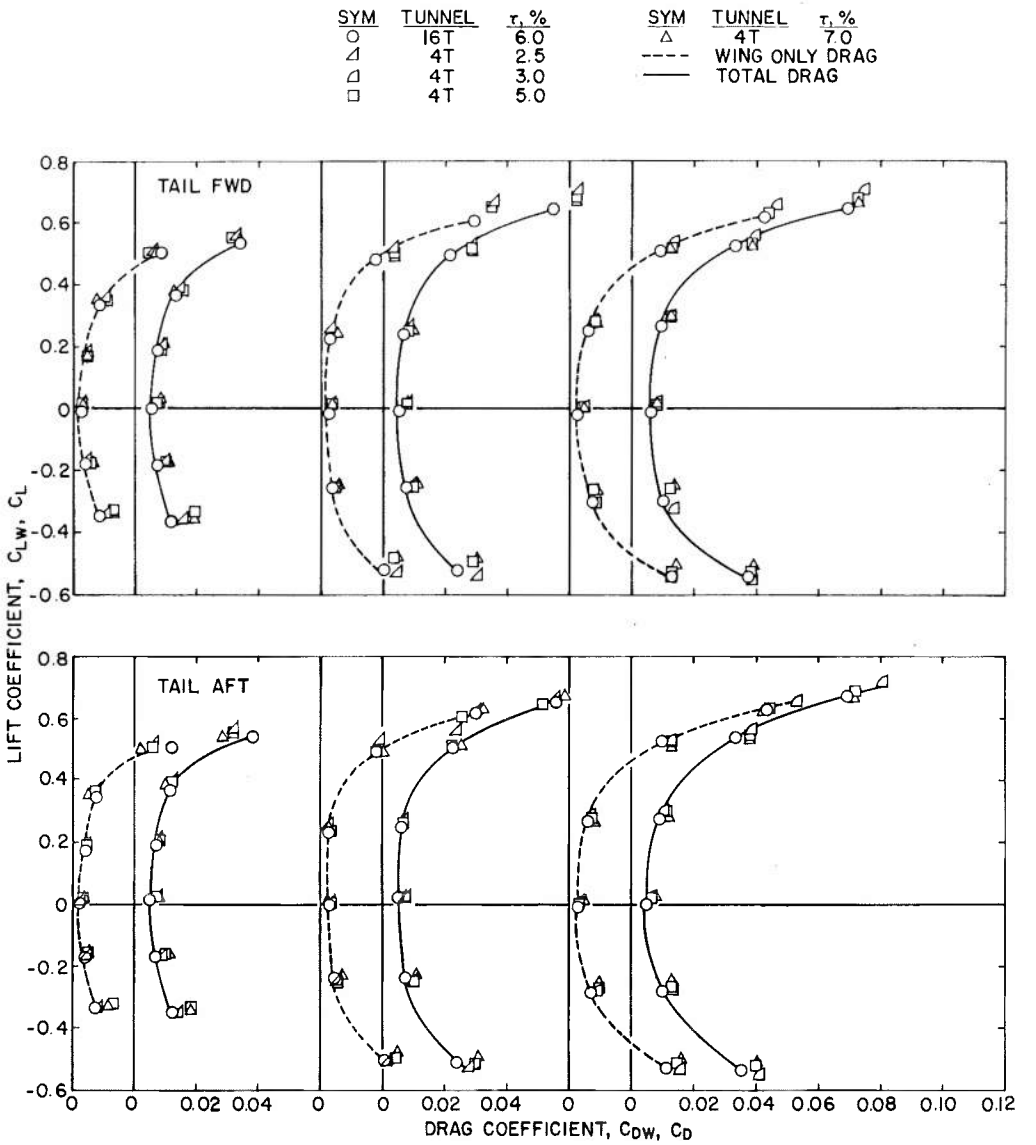

a. $M_\infty = 0.60$ b. $M_\infty = 0.80$ c. $M_\infty = 0.85$

Figure 22. Effect of porosity on pressure drag.

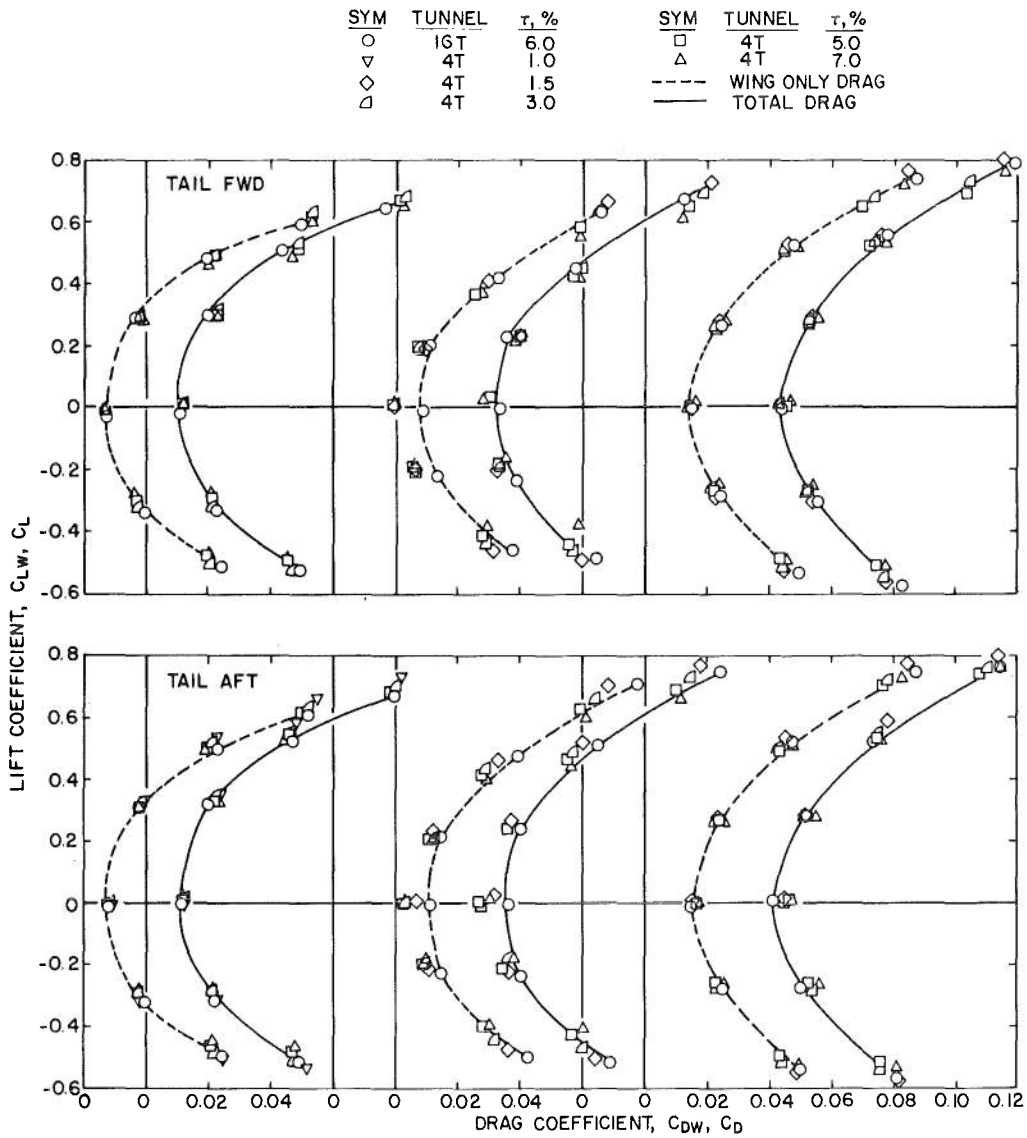

d. M_∞ = 0.90 e. M_∞ = 0.95 f. M_∞ = 1.00

Figure 22. Continued.

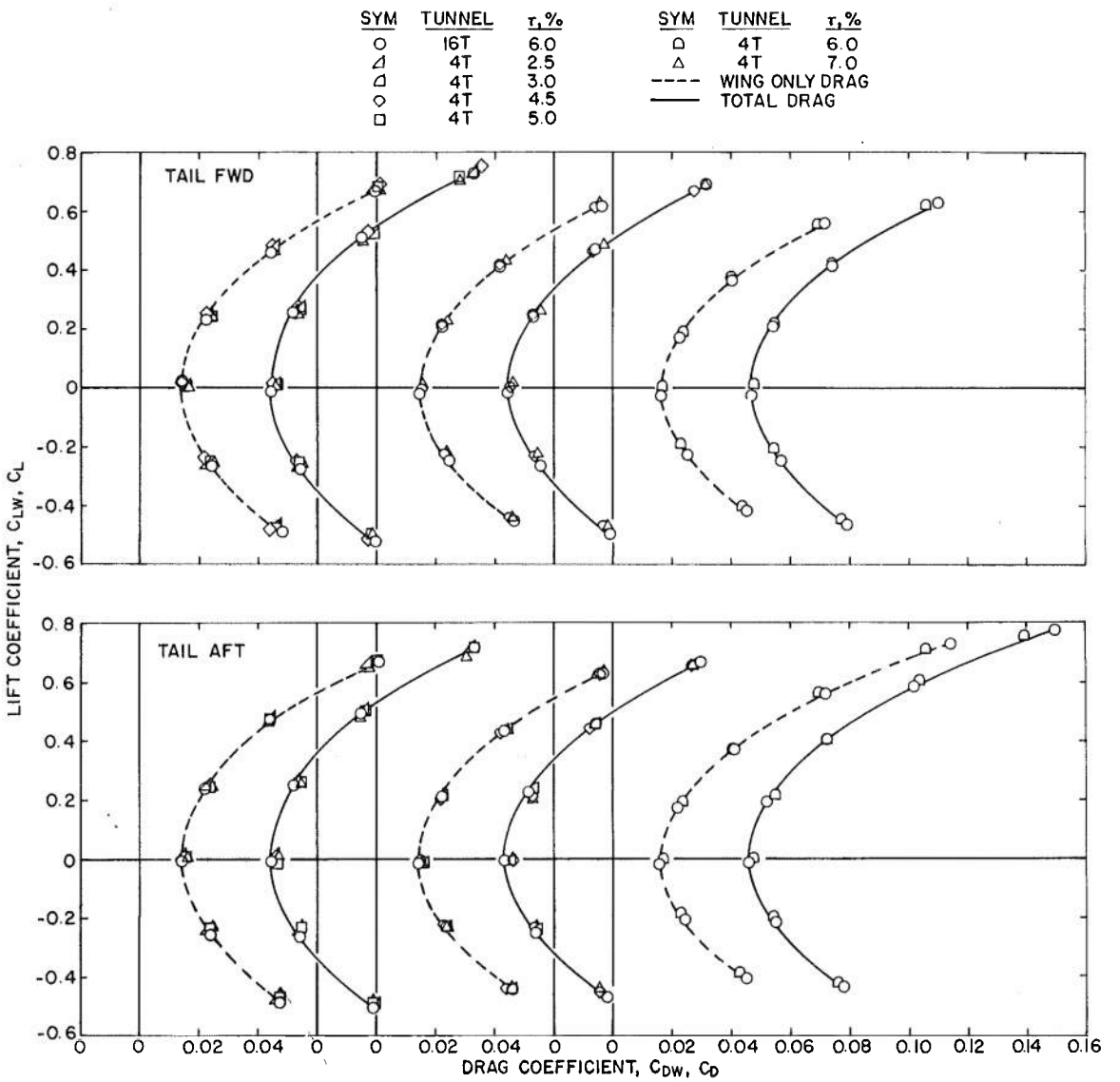

g. $M_\infty = 1.10$ h. $M_\infty = 1.20$ i. $M_\infty = 1.30$

Figure 22. Concluded.

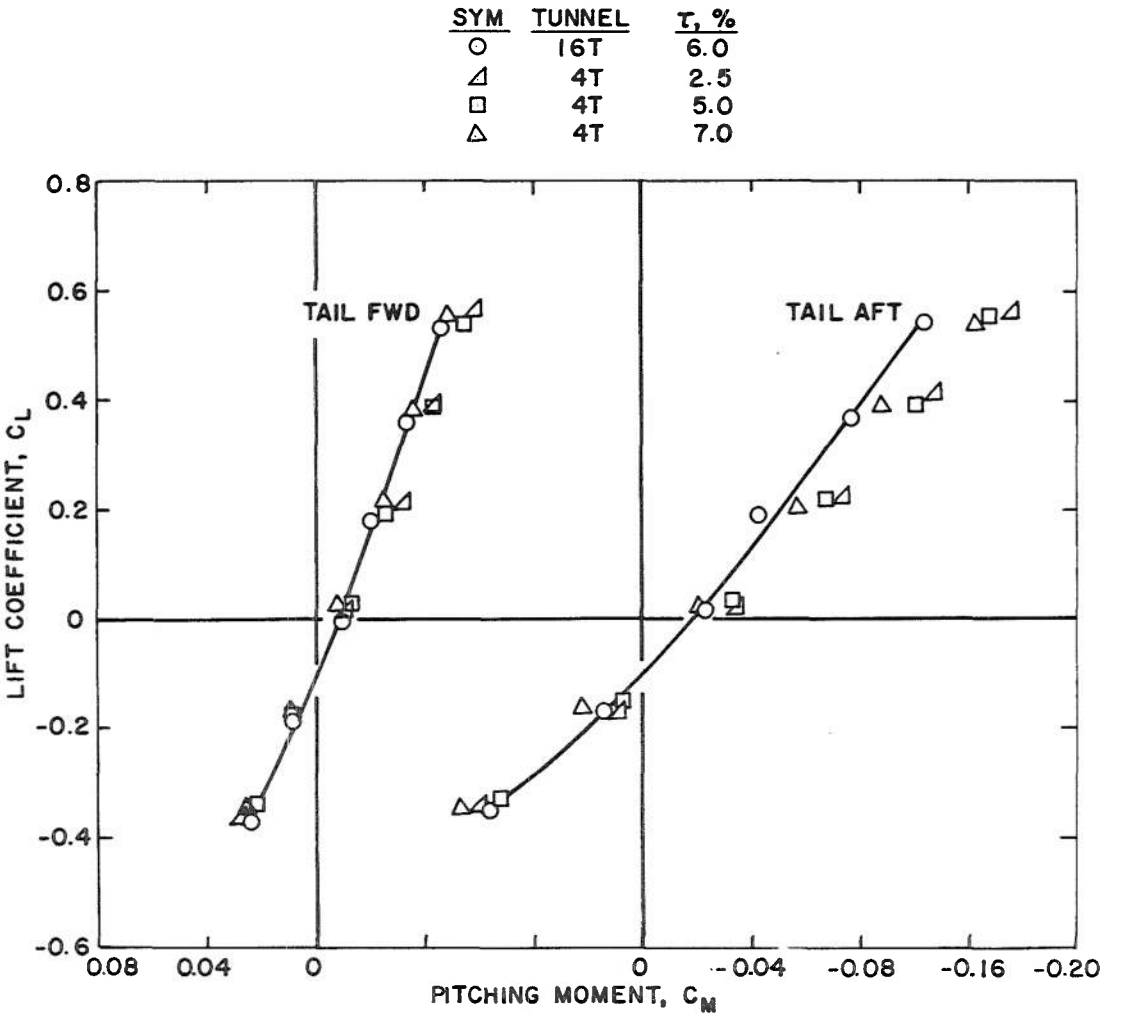

a. $M_\infty = 0.6$

Figure 23. Effect of porosity on pitching moment.

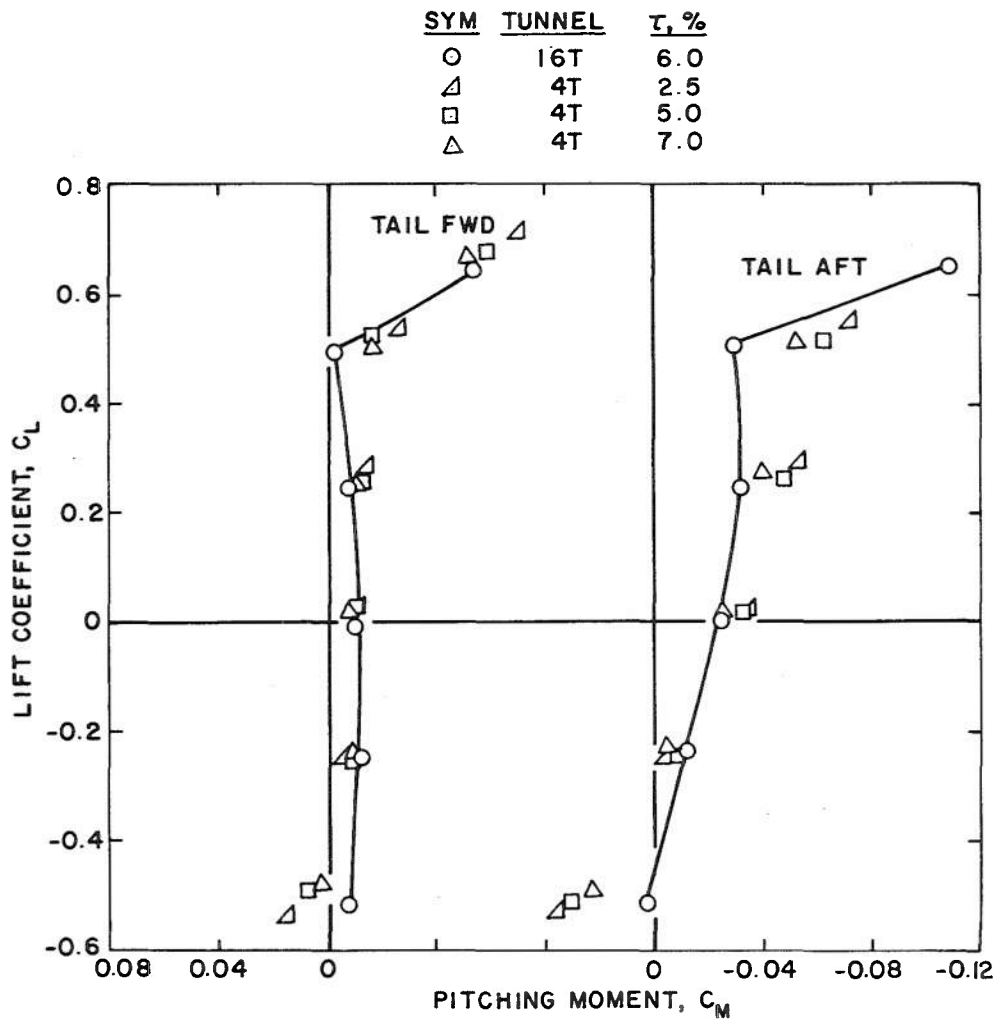

b. $M_\infty = 0.80$

Figure 23. Continued.

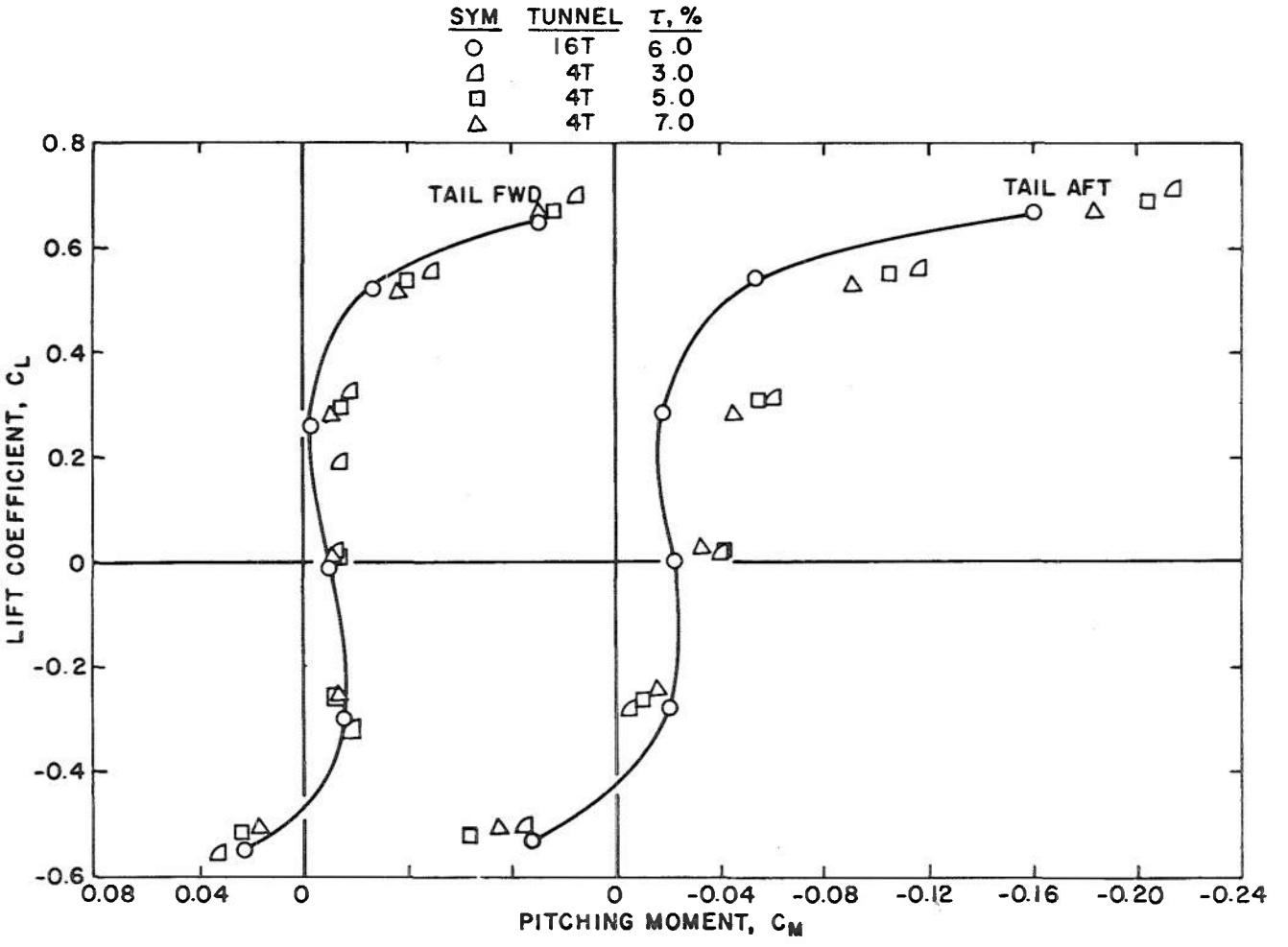

c. $M_\infty = 0.85$

Figure 23. Continued.

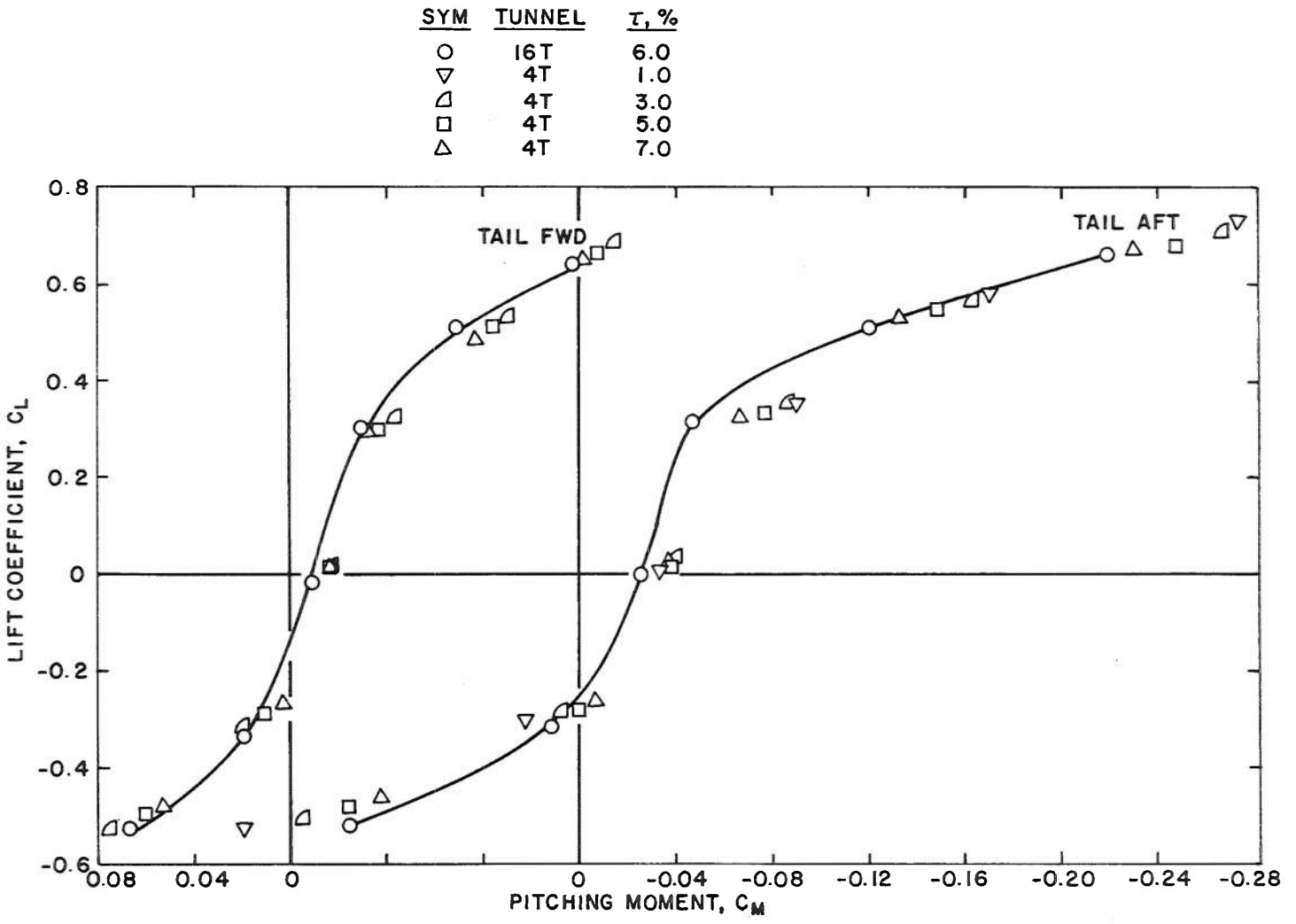

d. $M_\infty = 0.90$

Figure 23. Continued.

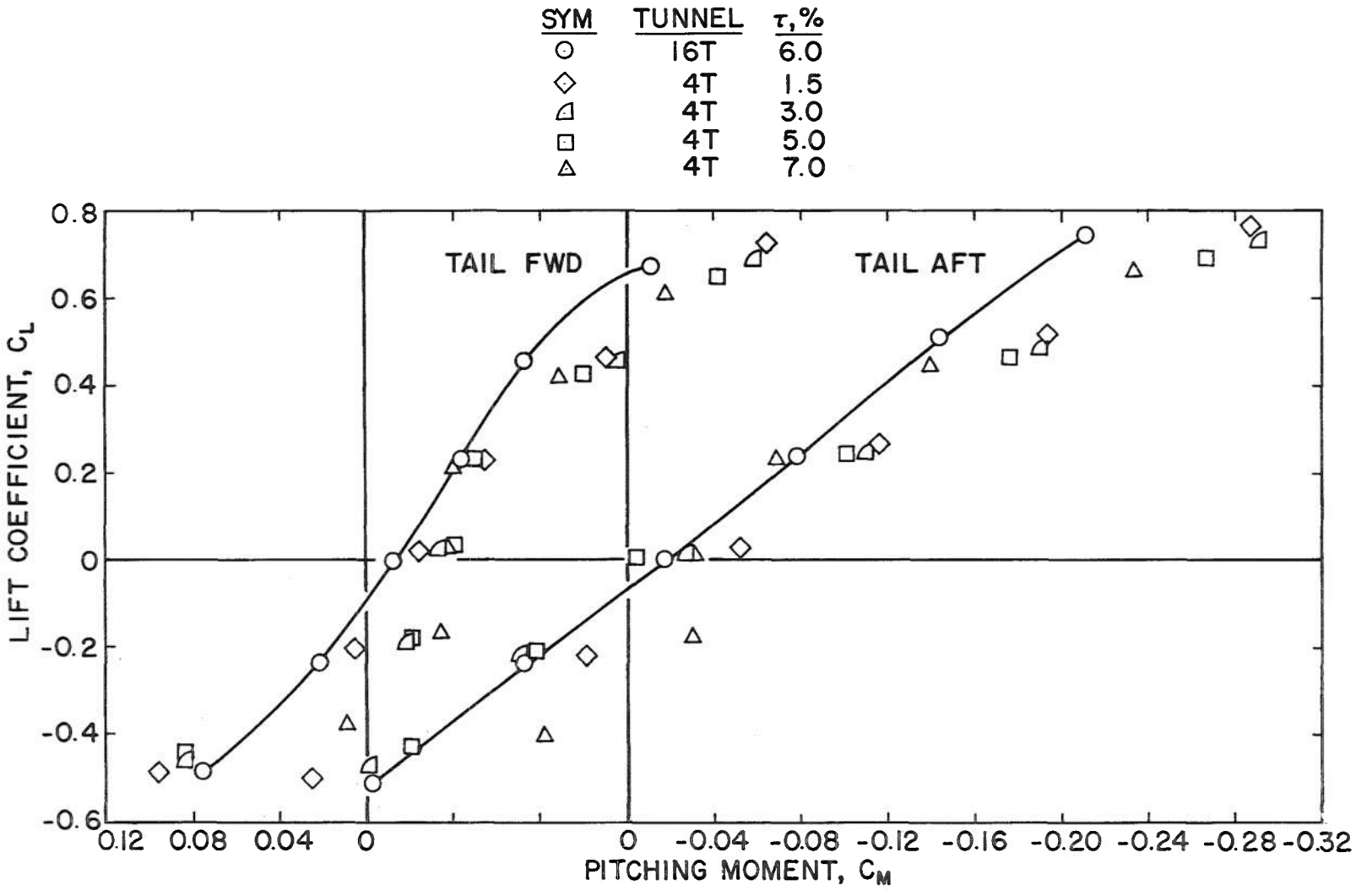

e. $M_\infty = 0.95$

Figure 23. Continued.

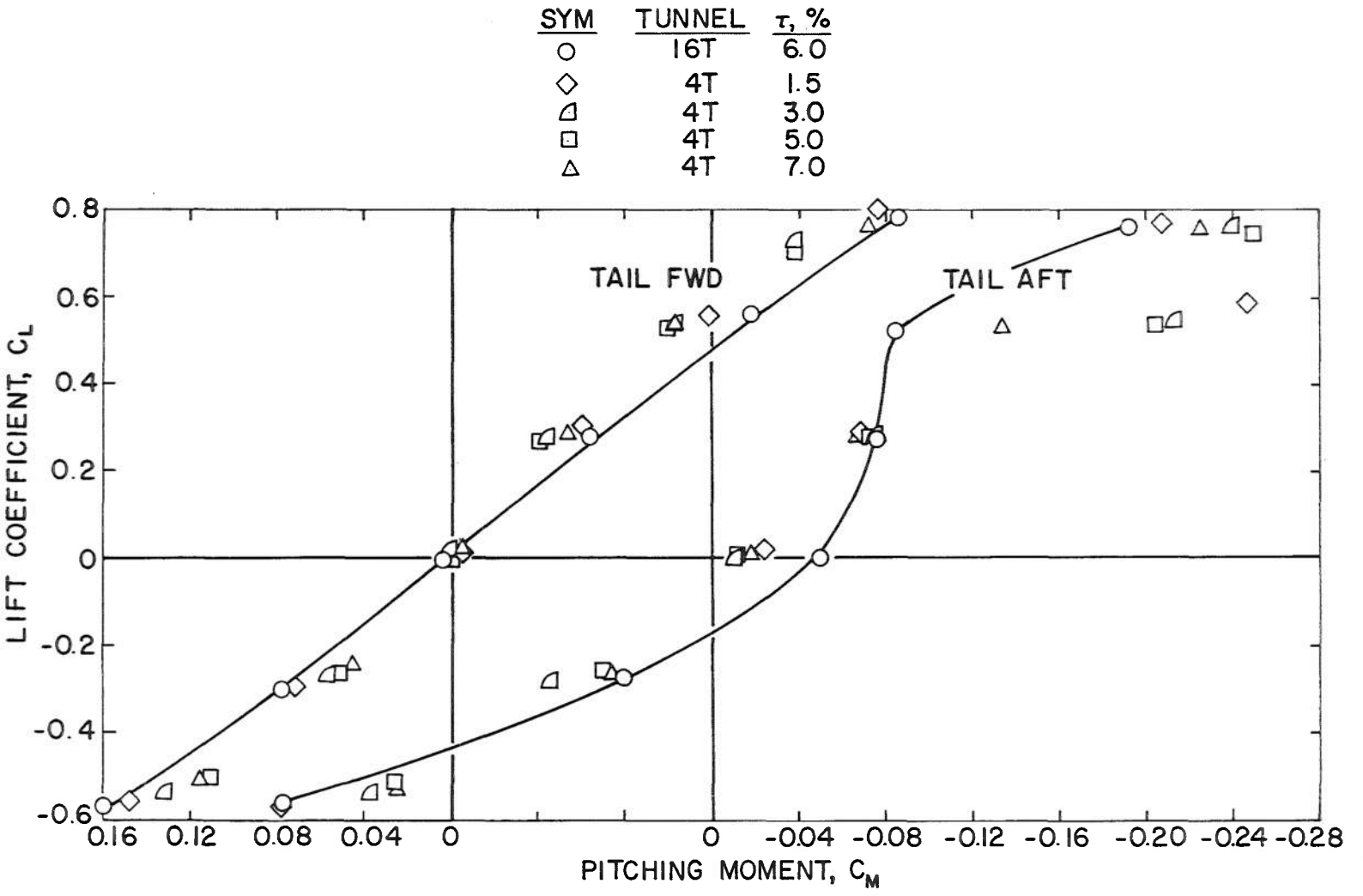

f. $M_\infty = 1.00$

Figure 23. Continued.

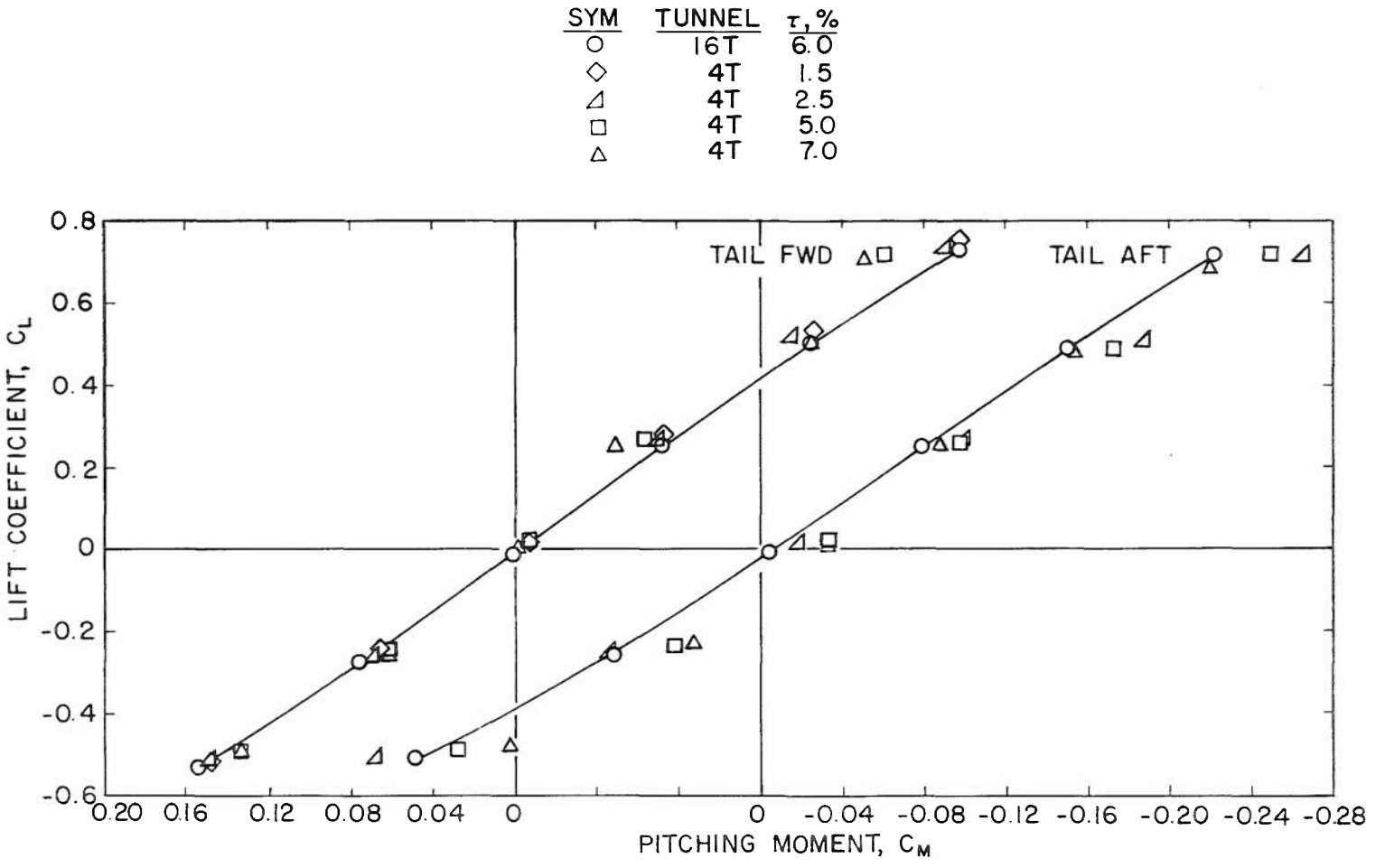

g. $M_\infty = 1.10$

Figure 23. Continued.

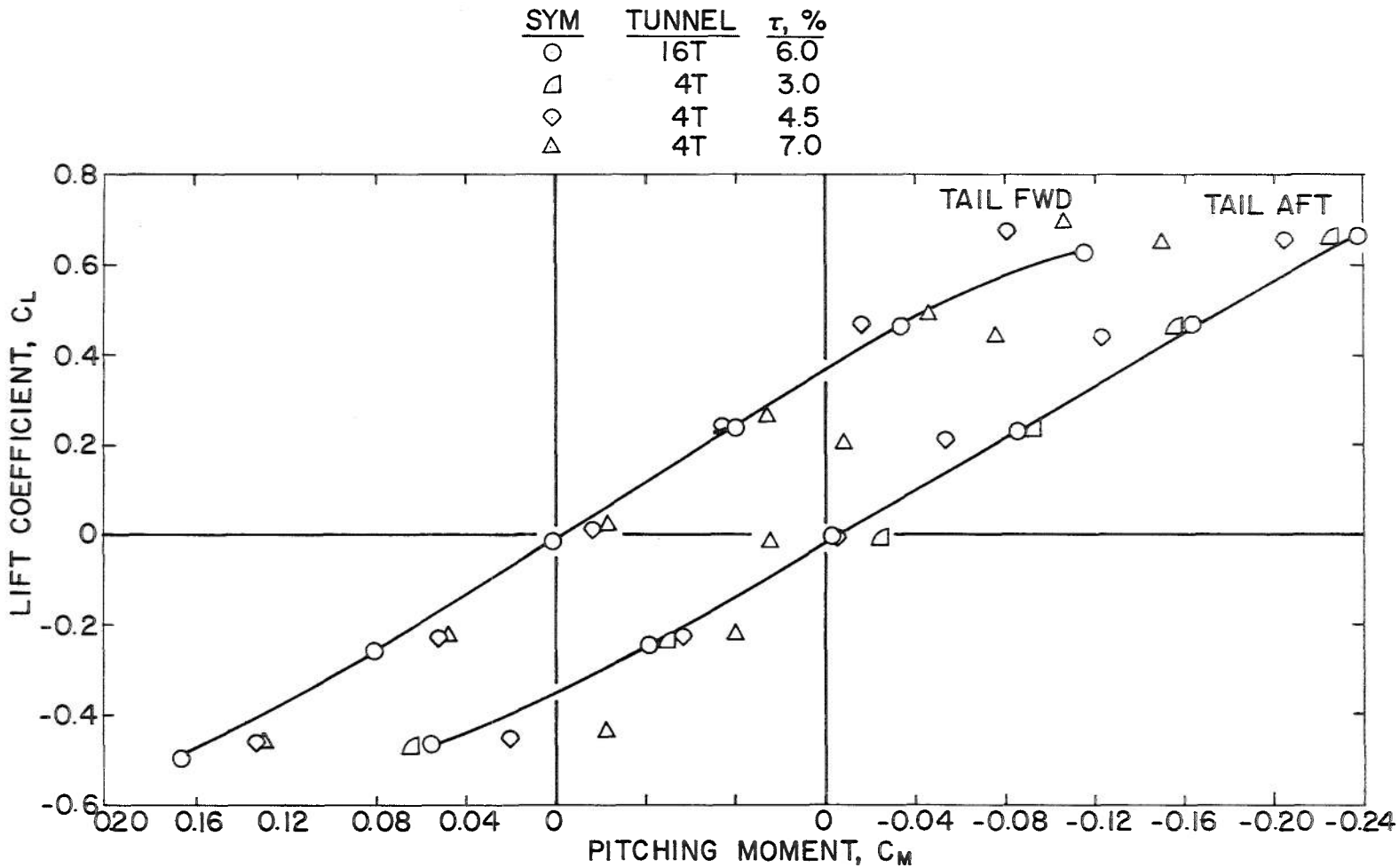

h. $M_\infty = 1.20$
Figure 23. Continued.

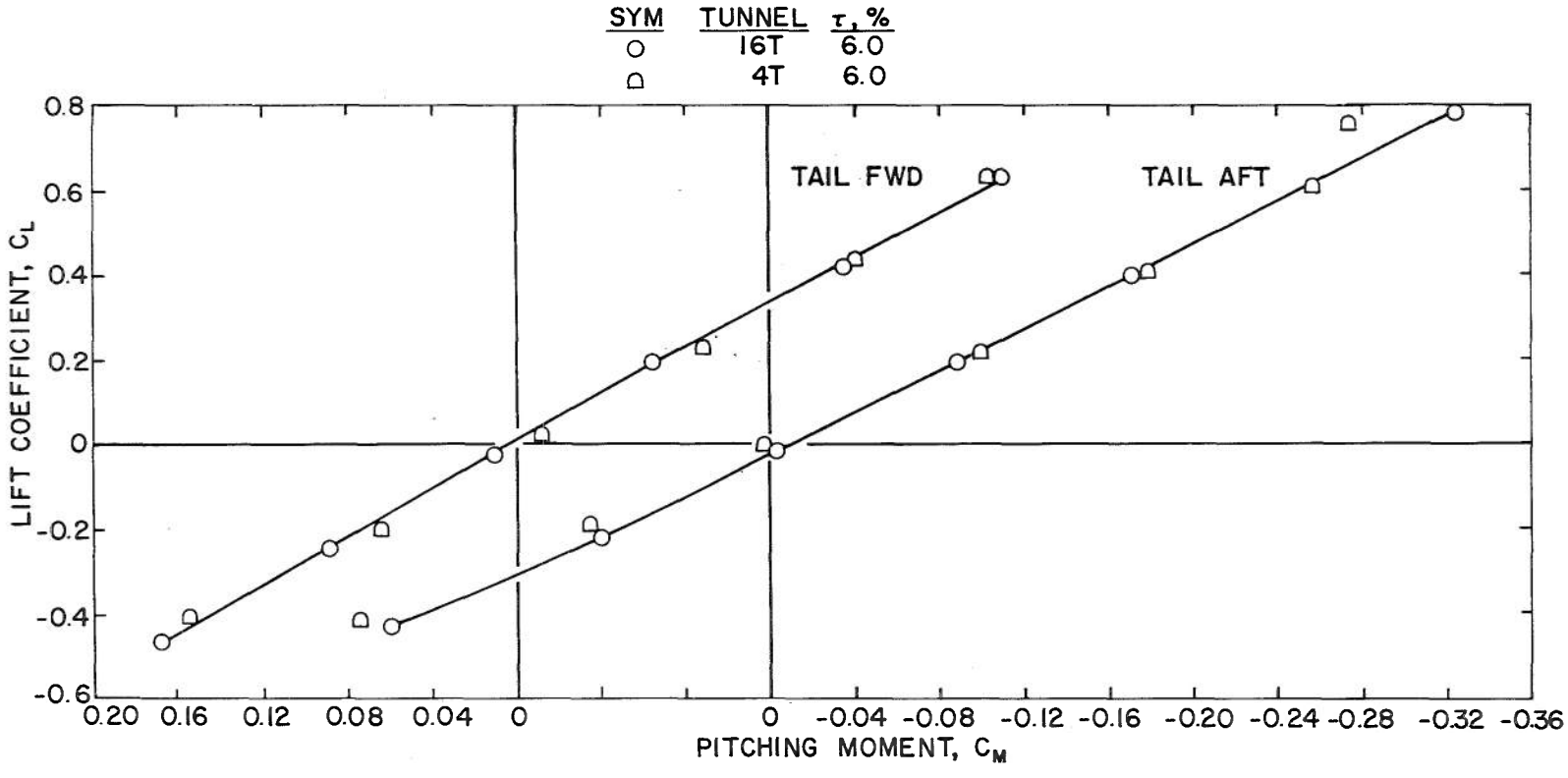

i. $M_\infty = 1.30$

Figure 23. Concluded.

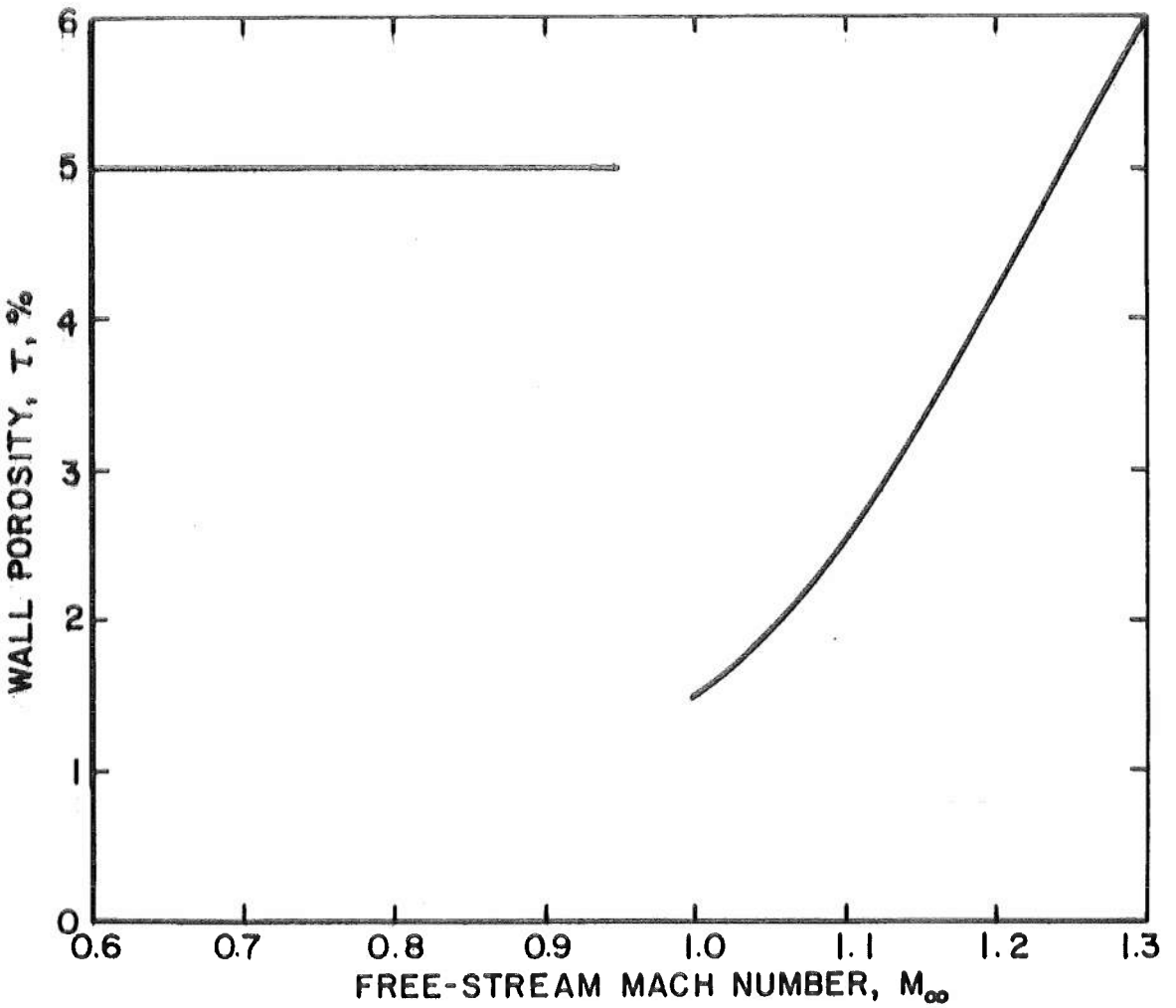

Figure 24. Porosity schedule for zero blockage correction.

NOMENCLATURE

A	Coefficient
b	Tunnel semiwidth
C	Tunnel cross-sectional area
C_D	Drag coefficient
C_L	Lift coefficient
C_M	Pitching-moment coefficient
C_P	Pressure coefficient
C_P^*	Value of C_P at local sonic conditions
c	Airfoil chord
L	Reference body length
M	Mach number
P	Pressure
P_t	Total pressure
Q	Porosity parameter as defined in Ref. 3
R	Radius
S	Area of lifting surfaces
x	Axial coordinate
z	Vertical coordinate
α	Angle of attack
α_G	Gravimetric angle of attack
α_{WB}	Wing incidence determined from wing centerbody pressure measurements
β	Compressibility factor, $\sqrt{1 - M_\infty^2}$
γ	Specific heat ratio
$\Delta\alpha_I$	Interference angle, difference in flow angle at a point between the Tunnel 4T and 16T flow fields
δ	Upwash interference factor
ϵ	Blockage interference factor

σ	Solid blockage ratio, local model cross-sectional area to tunnel cross-sectional area
τ	Wall porosity

SUBSCRIPTS

m	Measured quantity
max	Maximum
T	Tail
W	Wing
WB	Wing centerbody
∞	Free stream
4T	Tunnel 4T
16T	Tunnel 16T